DIPLOMARBEIT

Titel der Diplomarbeit

Baculovirus-induced actin comet tails: Structure of the propulsion machinery

Verfasser

Jan Müller

angestrebter akademischer Grad

Magister der Naturwissenschaften (Mag.rer.nat.)

Wien, 2011

Baculovirus-induced Actin Comet Tails: Structure of the Propulsion Machinery

Jan Müller

This work aims to elucidate the structural organization of the pushing machineries based on actin filaments, to contribute to an understanding of how actin filament polymerization is harnessed to produce motion. The first part focuses on an *in vitro* system, which allowed observation of actin filaments growing off microtubules. The second part describes our efforts to characterize baculovirus-induced actin tails. Various pathogens, like *Listeria* and *Rickettsia*, as well as *Vaccinia* virus and baculovirus, hijack the actin machinery of cells to propel themselves through the cytoplasm and to move from one cell to another, to propagate their infection. Since baculoviruses are small, around 250 by 50nm in size, the comet tails are correspondingly smaller and filament arrangements more easily resolved by electron microscopy. We used two systems to study the structure of the actin tails: First, an *in vitro* assay, including the isolated virus, Arp2/3 complex, actin and other components. Second, suitable cell types like goldfish fibroblasts and B16 cells were infected with concentrated virus and the tails observed in situ. Fluorescence microscopy enabled us to establish the ability of baculovirus to infect several eukaryotic cell types and analyze new aspects of baculovirus-induced tails. Electron microscopy revealed the 'fishbone'-structure of *in vivo* as well as *in vitro* tails and, finally, electron tomography allowed us to conceive models of how pathogen-induced actin tails are formed.

Table of contents

INTRODUCTION

Actin

Actin is a highly conserved, eukaryotic protein capable of polymerizing into long, helical filaments of about 7nm diameter. It is prominently involved in muscular function, but also in many processes in non-muscle cells, including internalization of membrane vesicles, sensing environmental forces, cellular stability, motility and cell division. (Reviewed in [1]) Actin acts as an ATPase, whereby the ATP-bound form produces long filaments and slowly hydrolyzes ATP. This mechanism, together with the different dissociation constants at the front and rear of a filament – the barbed and pointed end – enable a phenomenon called head-to-tail polymerization or treadmilling [44]. Adjusting the concentration of ATP-G-actin within a certain range enables the cell to exploit treadmilling for actin-based protrusion.

Lamellipodium

The morphological structure at the front of crawling, eukaryotic cells like fibroblasts, keratocytes or melanocytes is termed the 'lamellipodium' [42]. This sheet-like cell organelle confers cell motility together with the rod-like filopodia, by pushing the cell membrane outwards. A dense network of actin filaments has been shown to be the main constituent of the lamellipodium [43], which is between 100 and 200µm thick [44].
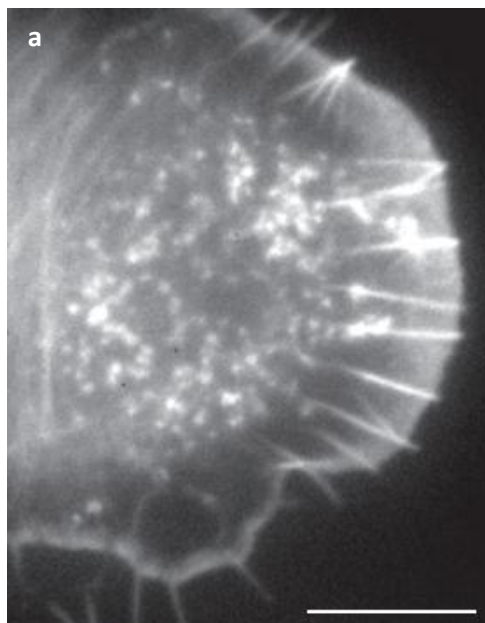
Figure 1 Examples of lamellipodia. **(a)** Video frame of a B16 melanoma cell expressing actin-GFP. The lamellipodium is clearly visible as a dense region at the cell front together with several filopodia and microspikes. **(b)** Electron micrograph of a cross-section of a plastic-embedded keratocyte lamellipodium. The flat shape of a typical lamellipodium, around 100 to 200nm, allows the use of transmission electron microscopy. Images taken from Köstler, 2008 [69] and Urban, 2010 [23]. Scale Bars: **(a)** 10µm; **(b)** 500nm.

The flat lamellipodial shape allows full penetration of the electron beam in a transmission electron microscope, making the lamellipodium a suitable object for electron microscopy. Experiments using fluorescent recovery after photobleaching (FRAP) [14] and fluorescence

loss after photobleaching (FLAP) [15] showed a constant retrograde flow of actin monomers through the filaments of the lamellipodia network – thereby new actin monomers are incorporated at the cell edge pushing the cell forward. Important regulators of this process have been uncovered since then by different approaches:

Nucleators like the **Actin related protein (Arp)2/3 complex**, which was found to be an actin-binding protein [45] that mediates actin polymerization in response to extracellular signals [46]. This heptameric complex [47] emerged as a key player in actin regulation, showed to be responsible for not only lamellipodial protrusion but also movement of the intracellular pathogen *Listeria* [48] and a yeast homolog regulates actin polymerization at yeast actin patches [49]. There are other important actin nucleators, namely **Formin** [50],[51], **Spire** [52] and **Cordon-Bleu** [53], but Arp2/3 is most relevant for this study.

Nucleation-promoting factors (NPFs) activate Arp2/3 at the cell membrane, serving as mediators between signals affecting the cell motility from outside the cell and altered actin polymerization as cellular response. **Wiskott-Aldrich syndrome protein (WASp)** is a prime example for an NPF, being located at the membrane and activating Arp2/3 to nucleate filamentous actin upon stimulation by the Rho GTPase CDC42 [54]. **Scar/WAVE** is closely related to WASp, but present within a large complex, the WAVE regulatory complex [55], and regulated by small GTPases of the Rac family. Both WASp and WAVE feature the VCA domain, which stimulates Arp2/3 to nucleate actin. The VCA domain contains three parts, the V motif, short for Verprolin-homology, or WH2 (Wiskott-Aldrich Homology 2), the C motif (connecting or central hydrophobic region) and the A (acidic) motif. Upon activation, for example by binding of a small GTPase, the VCA domain is released from an inhibitory, intracellular interaction and activates Arp2/3 in complex with actin to nucleate an actin filament [56].

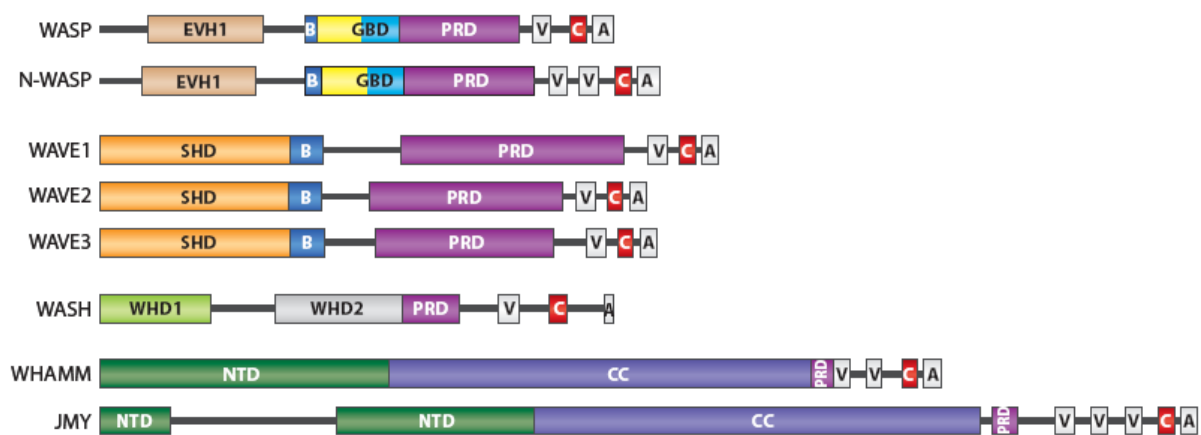**Figure 2** Schematic summary of WASp/WAVE family members. A, acidic region; B, basic region; C, central hydrophobic region; CC, coiled-coil domain; EVH1, Ena/VASP homology domain 1; GBD, GTPase-binding domain; NTD, N-terminal homology domain; PRD, proline-rich domain; SHD, Scar homology domain; V (also WH2), verprolin homology domain; WHD1,WASH homology domain 1; WHD2,WASH homology domain 2. From Padrick, 2010 [56].
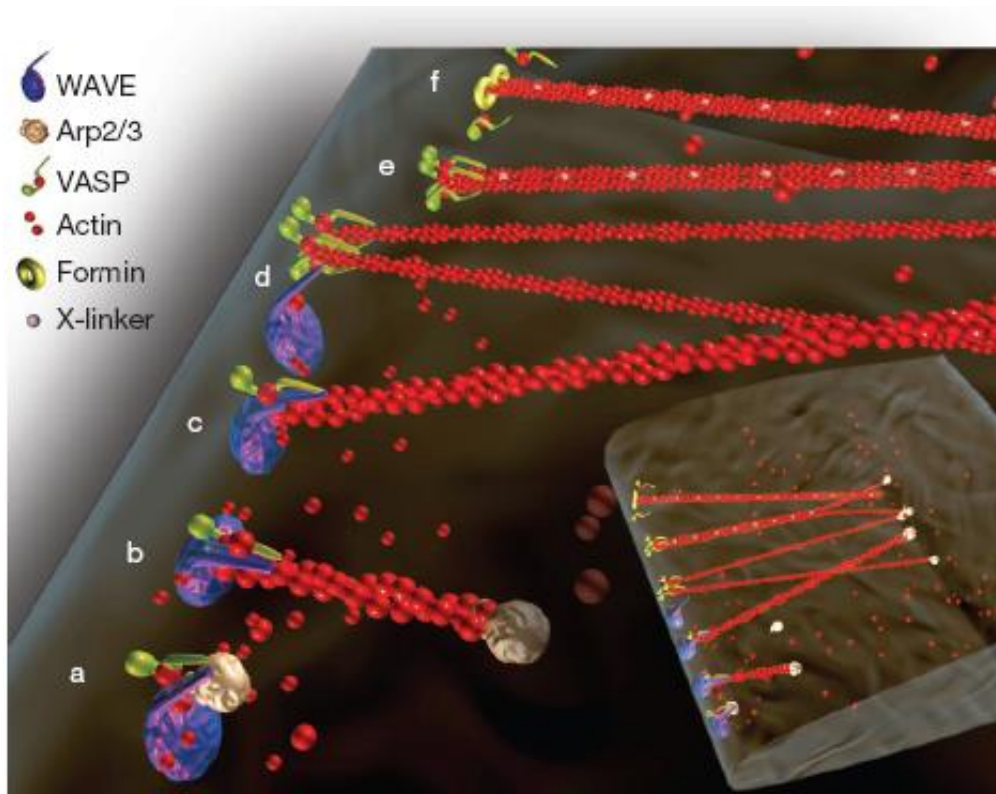
Figure 3 Scheme of actin filament nucleation and elongation at the cell front. **(a)** Filaments are nucleated by activated Arp2/3 and **(b)** elongate tethered to the NPF WAVE with Arp2/3 bound to the pointed end. **(c)** VASP family proteins can then take over the elongation from WAVE and **(d),(e)** closely aligned filaments can be linked to bundles. **(f)** Another form of actin nucleation is entirely dependent on Formins. From Urban, 2010 [23].

Other important actin-regulating proteins include the **Actin depolymerizing Factor (ADF/Cofilin)**. This protein acts towards filament depolymerization by increasing the rate of monomer dissociation off the pointed end by 25-fold [57]. The actin-binding protein **Profilin** contributes to increased filament turnover by exchanging ADP bound to actin to ATP, maintaining a steady pool of ATP-actin-profilin which is available for nucleation and elongation [58],[59]. **Gelsolin** and **Capping Protein (CP)** bind to the barbed end of filaments with nanomolar affinity and block addition of subunits, inhibiting further elongation. This process was termed filament capping [60],[61]. Proteins like **α-actinin** are able to crosslink actin filaments in order to form a network held together by interconnected filaments [62]. A wide array of other proteins including Zyxin and other proteins of adhesion sites, Myosin, Fascin and Filamin are associated with actin regulation. Discussing them would go beyond the scope of this work, therefore this brief introduction focused on the proteins of relevance for the present study.

Biomimetic motility assay

In 1999, the successful *in vitro* reconstitution of actin-dependent movement, regulated by a set of purified proteins was reported [16] setting off a series of studies with different *in vitro*

motility assays using beads of different sizes [17],[39],[25], bacteria [18],[19],[20],[65],[66] and giant unilamellar vesicles (GUVs) [67],[68],[63].
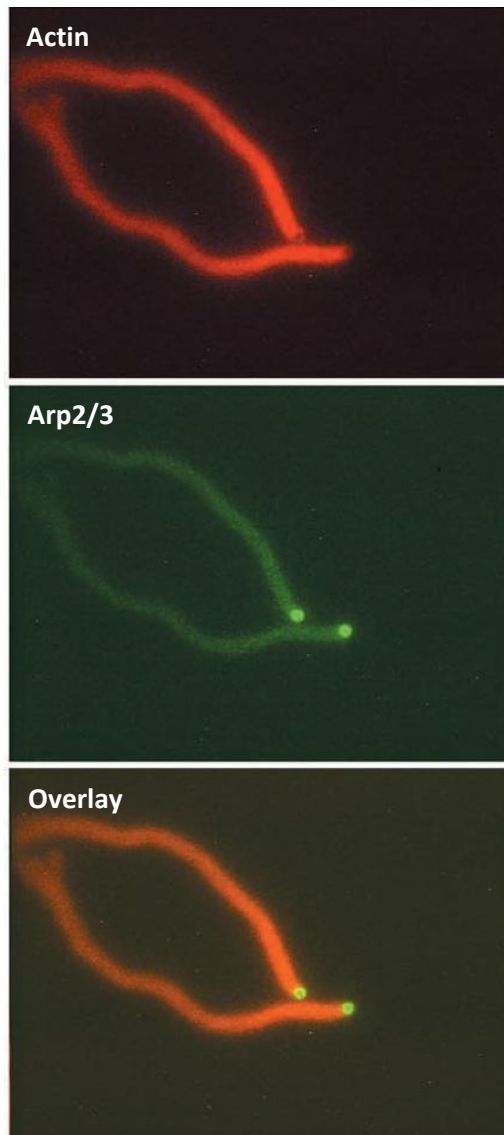

Figure 4 Video frames of 2µm-sized beads propelled by an actin tail. This experiment shows the presence of Arp2/3 (red) along the whole length of the tail, a finding with profound implications on models of tail formation. The shown tail was polymerized at a relatively low gelsolin concentration (50nM) leading to rather loose tails but high enough to prevent the 'fishbone' appearance (see later), observed at concentrations as low as 25nM. Images taken from Wiesner, 2003 [17].

In the seminal study [16] beads coated with N-WASP, the neuronal form of the Wiskott-Aldrich syndrome family of proteins, were induced to move by incubation in a protein cocktail (see figure 4) containing purified Arp2/3, ADF, Profilin, Gelsolin and actin at defined concentrations. Other studies were performed using cellular extracts instead of isolated proteins.

This reductionist approach helped to elucidate the core set of proteins necessary and sufficient for actin-based propulsion and has had tremendous success uncovering various properties of actin tails and actin dynamics themselves. To give a few examples, different laboratories investigated the forces exerted on the load by polymerizing actin filaments [66],[63], the build-up of stress in the actin gel [64], the nucleation ability of a bacterial surface protein [62] and the biochemical properties of the involved proteins [17],[18].

Remarkably, relatively few studies have been undertaken to reveal the structure of the comet tail by a suitable technique like electron microscopy. The only relevant pictures of *in vitro* tails polymerized from beads were published by Svitkina, Borisy and coworkers in 2001 and 2004, shown in figure 5 [25],[39]. In these micrographs actin appears heavily bent and actin branches are abundant. The samples were prepared using the platinum replica technique, whose drawbacks are discussed in the next chapter.

The other notable transmission electron microscopy study on *in vitro* actin comet tails revealed the influence of Fascin on the structure of the actin tail [65]. Figure 6 shows the striking effect of the actin bundling protein Fascin on the shape of the actin tail, which can continue Arp2/3-independent polymerization at sufficient Fascin concentration.
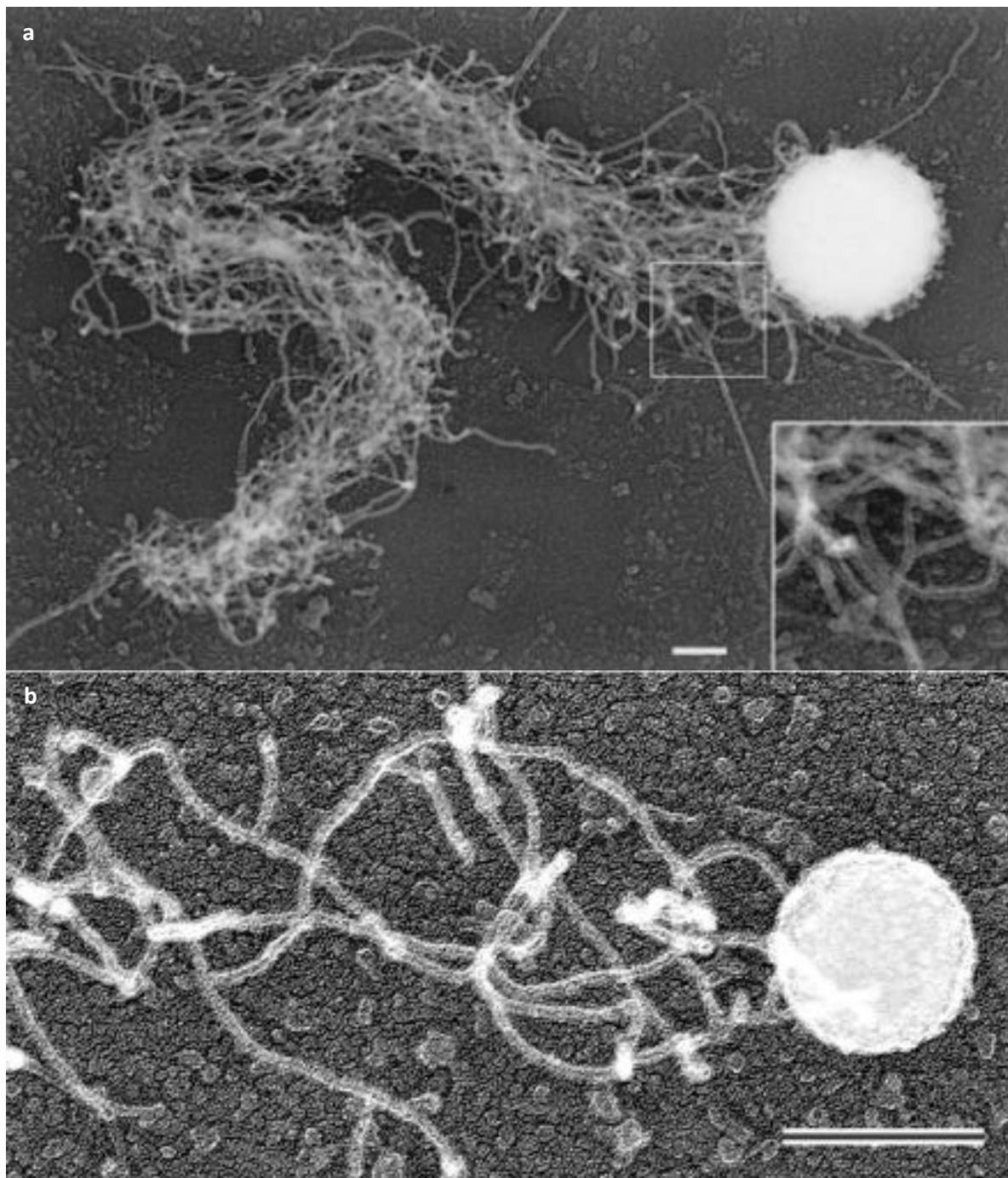
Figure 5 Electron micrograph of platinum-coated actin tails polymerized from WASP-coated beads. **(a)** 500nm and **(b)** 200nm beads were used in this experiment. The actin filaments in these images look heavily bent and curved. This appearance was explained by forces exerted on either end of the filament. However, the electron microscopy data presented in the current study does not feature filaments of this nature, but rather straight ones. This discrepancy is most likely due to differences in the preparation procedures, as discussed below. Another study has shown the introduction of branches by the use of the platinum replica technique [106], further calling the validity of the shown results into question. Images taken from **(a)** Jeng, 2004 [39] and **(b)** Cameron, 2001 [25]. Scale bars: **(a)** 100nm; **(b)** 200nm.

The authors also reported a densely branched network formed by Arp2/3-mediated branching at the rear ends of *Listeria*. However, it seems problematic to judge the inner build-up of a three-dimensional structure from thin sections like the one shown in figure 6.

Figure 6 Thin section of a *Listeria*-induced actin tail. This actin tail appears 'fishbone'-like at an early stage, but upon changing the motility medium to a high Fascin concentration, the bacterium forms a straight tail without emanating filaments. The shown image was interpreted to display two different modes of actin propulsion: First, Arp2/3 dependent nucleation and branching. Second, Fascin-mediated elongation. The appearance of the structure on the left exemplifies the difficulties in determining the presence of branches from this kind of images. Image taken from Brieher, 2004 [65]. Scale bar: 1μm.

Branching model

Although considerable advances have been made in the last decade using *in vitro* as well as *in vivo* approaches to elucidate the exact lamellipodial structure and function, the field is still far from a common agreement on the molecular events that contribute to pushing at the leading edge of moving cells. One of the main points of dispute involves the molecular structure of lamellipodial actin filaments: More than ten years ago, branched actin filaments were observed in the lamellipodium of fish keratocytes [21],[76] in electron micrographs of samples prepared by the platinum replica technique, as shown in figure 7. The dendritic
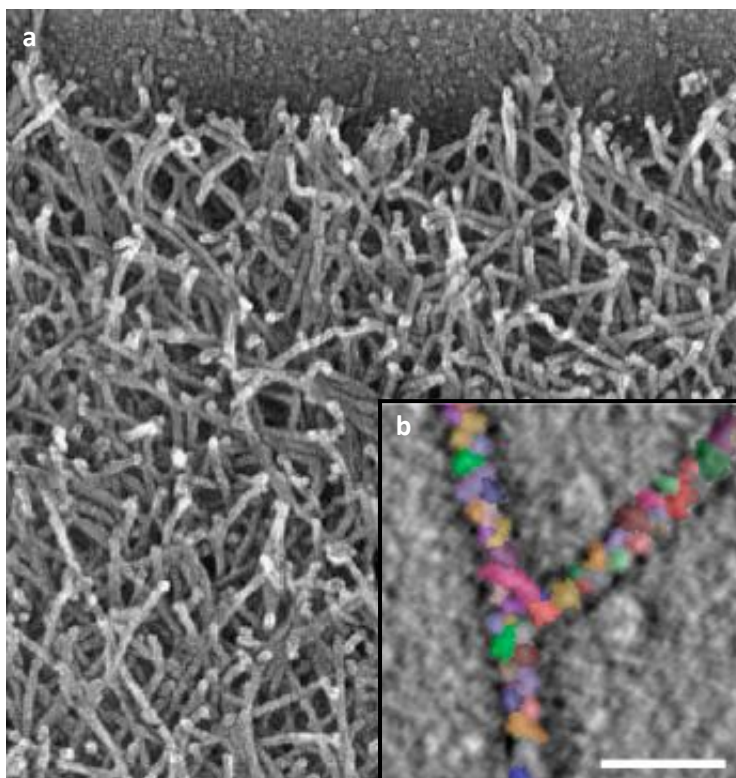
Figure 7 Electron microscopy studies showing Arp2/3 dependent branching. **(a)** Electron micrograph showing a black tetra keratocyte lamellipodium prepared by the platinum replica technique. Many branches can be observed across the whole image, though concerns about the validity of these pictures have not been dispelled. **(b)** Electron micrograph showing a negatively stained, *in vitro*-polymerized actin branch. The shapes of individual actin monomers have been modeled into this image. Images taken from **(a)** Svitkina, 1997 [21] and **(b)** Rouiller, 2008 [75]. Scale bar: **(b)** 20nm.

branching model based on those images and the observation of actin filaments growing as branches from existing filaments [22] as well as biochemical studies [18] gave rise to the dendritic branching model of actin [70]. The *in vitro* actin branch was then investigated in detail using fluorescence TIRF microscopy [71],[72], biochemical approaches [73] and using a combination of electron microscopy and NMR [74],[75] (see figure 7).
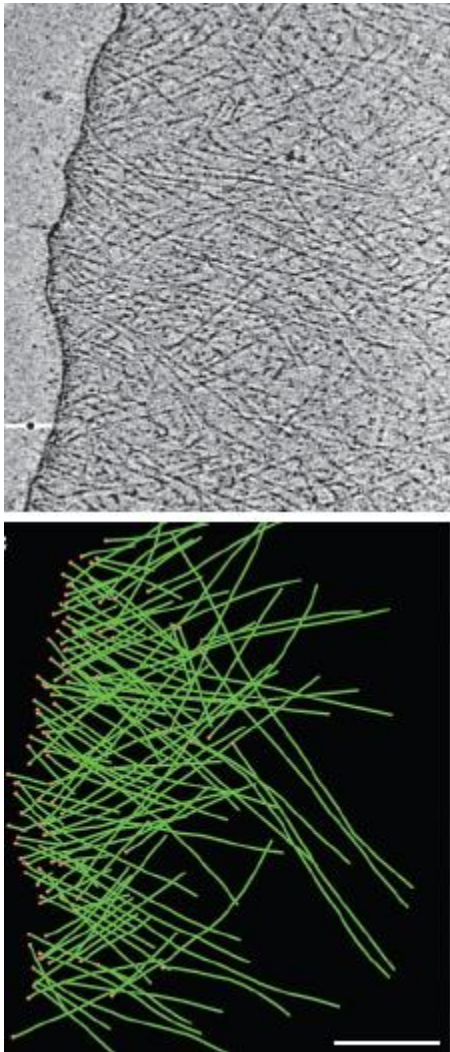
Figure 8 Cryo-electron tomography data and corresponding model of actin network structure. **(a)** Tomogram section of 4.8nm and **(b)** 3D model produced based on the cryo-data. The model did not show a significant amount of branches at the cell front, contradicting earlier findings (see figure 7). Figure taken from Urban, 2010 [23]. Scale bar: **(b)** 200nm.

This model has been challenged, most importantly by recent findings of arrays of unbranched filaments in vitreously frozen cells imaged by 3D cryoelectron tomography [23]. This technique combines the arguably smallest possible interference with the sample – thereby reducing the chance of artifacts – with a 3D image of the actin structure. Using this approach it was shown that filaments are not arranged in branched, dendritic arrays in protruding lamellipodia, as originally thought. Rather, the new 3D data shows that lamellipodia are composed of networks of mainly overlapping filaments, as illustrated in figure 8. Further doubts about the validity of images obtained by the platinum replica technique were raised by the finding that this technique produced distorted and branched actin filaments even in pure F-actin samples [106]. The absence of actin regulating proteins, which could act as potential branching factors, suggests the emergence of these structures by the preparation technique.

Another concern with *in vitro* data supporting the dendritic branching model is the use of soluble, constitutively active forms of the membrane bound protein N-WASP, the activator of Arp2/3. Mostly, the activating VCA-domain without the regulatory parts of the protein was used [22]. Under these circumstances VCA could activate an Arp2/3 bound to an actin filament which then would give rise to a branching filament in an unphysiological manner, creating an artifact. To clarify this problem I set out first to establish an *in vitro* assay using a system whereby N-WASP would be bound to a surface, as it would be in *in vivo* situations where it activates the Arp2/3 complex. A second requirement was that the object used should be small enough to allow structural analysis of associated filament arrays by electron tomography. In this context I first chose microtubules as a substrate, since they are only 25nm in diameter, only three times larger

than actin. The strategy was to use a construct of an active domain of N-WASP (WA-domain) cloned next to the microtubule-binding domain of MAP4 (MBD) to provide a link to the microtubule surface. This setup (shown in figure 9) would more closely resemble the *in vivo*-situation, with the activator at the plasma membrane. The recombinant protein would be expressed in the *Escherichia coli* expression system, incubated with *in vitro* polymerized microtubules and assayed together with the other essential proteins of the motility assay. We planned on imaging the resulting structures by fluorescent labeling in the light microscope as well as in a transmission electron microscope after fixation and negative staining with an aqueous heavy metal solution.
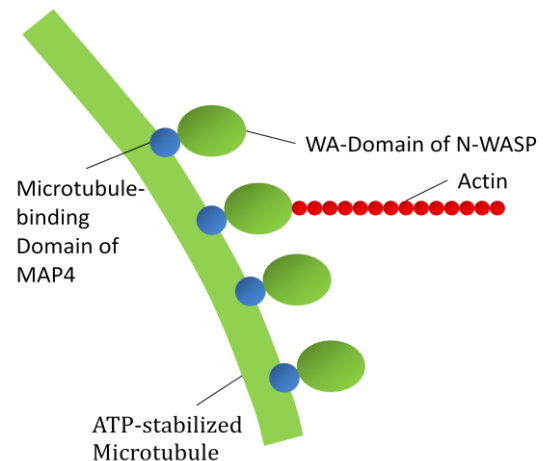

Figure 9 Diagram of the *in vitro* approach described in this work. A transgenic protein containing a microtubule-binding domain and an actin-nucleating domain was used to nucleate actin filaments from microtubules.

Intracellular pathogens hijack the cellular actin machinery

Strikingly, intracellular parasites have evolved to take advantage of the high concentration – sometimes up to 5% of the whole protein content – of actin in many eukaryotic cells: Species like the bacteria *Listeria* [2], *Shigella* [3] and *Rickettsia* [4] among others are capable of polymerizing a tail of actin and use it to move through the cytoplasm of their host. The pathogen *Listeria* was used notably as a substrate in the reconstituted motility assay, establishing the molecular machinery involved in actin-dependent, bacterial propulsion [18]. Although viruses mostly employ their host's microtubules for their movement, the human *Vaccinia* virus, a member of the Poxviridae, has been shown to use the actin cytoskeleton during a certain stage of its life cycle [5]. It was not until very recently, that a mechanism of movement including actin comet tails was proven for a baculovirus species (*Autographica californica multiple nuclear polyhedrosis virus, AcMNPV*) [6].

Baculovirus

Baculoviruses are a family of rod-shaped DNA viruses infecting different species of invertebrates. The *A. californica* species is a member of the genus Nucleopolyhedrosis virus within the family of baculoviruses. *A. californica* is the best studied species of the Baculoviridae and will be simply referred to as baculovirus in the course of this work. This virus is widely used as a tool in insect protein expression systems, which are capable of producing high yields of protein with the additional benefit of the eukaryotic posttranslational processing machinery compared to bacterial expression systems. Other applications are gene delivery into cultured mammalian cells and baculovirus capsid display.

(Reviewed in [7], [8]) Furthermore, researchers aim to capitalize on the ability of baculoviruses to infect many insect species but being safe for humans and other vertebrates: Baculoviruses are a promising example of biological insecticides for agriculture [9]. Another major focus in baculovirus research is the development of viral vectors for gene delivery into mammalian cells. While baculoviruses do not cause diseases in humans they can efficiently infect a variety of mammalian cells in culture and deliver genes into the nucleus. However, they do not replicate in these cells and are therefore a potential tool for gene therapy approaches. For example, in a recent study tumor-inoculated mice survived significantly longer when bone marrow stem cells transduced by baculoviruses with the Herpes simplex thymidine kinase were administered [10].

Baculovirus life cycle

The life cycle of baculoviruses comprises several stages and three distinct forms of virus [11]: The virus is present in the environment in occlusion bodies, which are taken up by insect larvae during feeding. The protein matrix covering many virions is degraded in the alkaline midgut of the host, setting free the occlusion derived virus (ODV) which is taken up by gut epithelial cells via adsorptive endocytosis [12]. Acidification in late endosomes triggers the fusogenicity of the major envelope glycoprotein gp64, which is sufficient to fuse the viral and host membranes and facilitates baculovirus escape from endosomes [40]. Once inside the cytoplasm the virus starts polymerizing actin filaments which are used to propel the virion within the cytoplasm and through the nuclear pores into the nucleus [6].

Then a striking mode of viral pathogenesis takes place: Massive actin translocation into the nucleus is necessary for viral replication [13]. Thereupon the late phase of the life cycle featuring viral gene expression ensues with virions being assembled in the cytoplasm and leaving the cell as enveloped infectious agents to spread the infection systemically, the budded form of baculoviruses (BV). This form enters the cell via adsorptive endocytosis. In the very late phase of the infection new occlusion bodies are produced and the host is lysed by virally encoded proteinases, releasing the occlusion bodies and setting up another round of infection.

Baculovirus genome

The baculovirus genome as well as that of several related nucleopolyhedroviruses features a minor capsid protein termed p78/83 [31] (see figure 10). This protein is closely related to
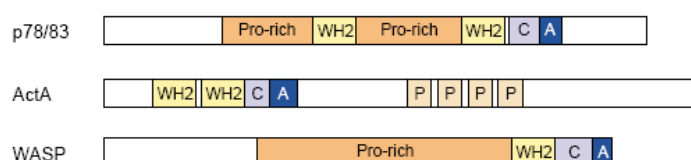
Figure 10 Graphic representation of conserved domains in Baculovirus p78/83, *Listeria* ActA and human WASP. P, Pro-rich, prolin-rich sequences; WH2, WASP-homology 2 (actin binding); C, central basic; A, acidic (Arp2/3 binding); Taken from Machesky, 2001 [31].

human WASP and the *Listeria* protein ActA, suggesting a similar function as activator of Arp2/3. Both the actin-binding WH2 domain as well as the acidic domain (A) is present in the

viral protein. It is unknown where this protein is localized exactly in the assembled virion, which is made up in a helical way by multiple copies of the major capsid protein vp39 together with several others like vp1054, 38K and the DNA-binding protein p6.9 [32]. Based on sequence homolog, it has been speculated that p78/83 induces actin polymerization [31] consistent with biochemical analysis of fractionated baculovirus [11]. The recent findings of Ohkawa and others [6] provide further support for this theory, as they reported impaired actin nucleation and elongation in p78/83 mutants.

Structure of pathogen-induced actin tails

The presented findings classify baculoviruses together with several bacteria and viruses as actin-propelled pathogens. The growing list of these agents includes the gram-positive genera *Listeria* [2] and *Mycobacterium* [33] and the gram-negative *Shigella* [3], *Burkholderia* [77] and *Rickettsia* [4], but also viruses like *Vaccinia* [5] and a several other Poxviridae [78]. Many other pathogens have been shown to polymerize actin, however not all in the form of actin tails. Examples include Enteropathogenic *Escherichia coli* (EPEC) [34], enterohemorrhagic *Escherichia coli* (EHEC) [35],[36] which create actin pedestals and retroviruses like Human Immunodeficiency Virus (HIV) [37],[38].
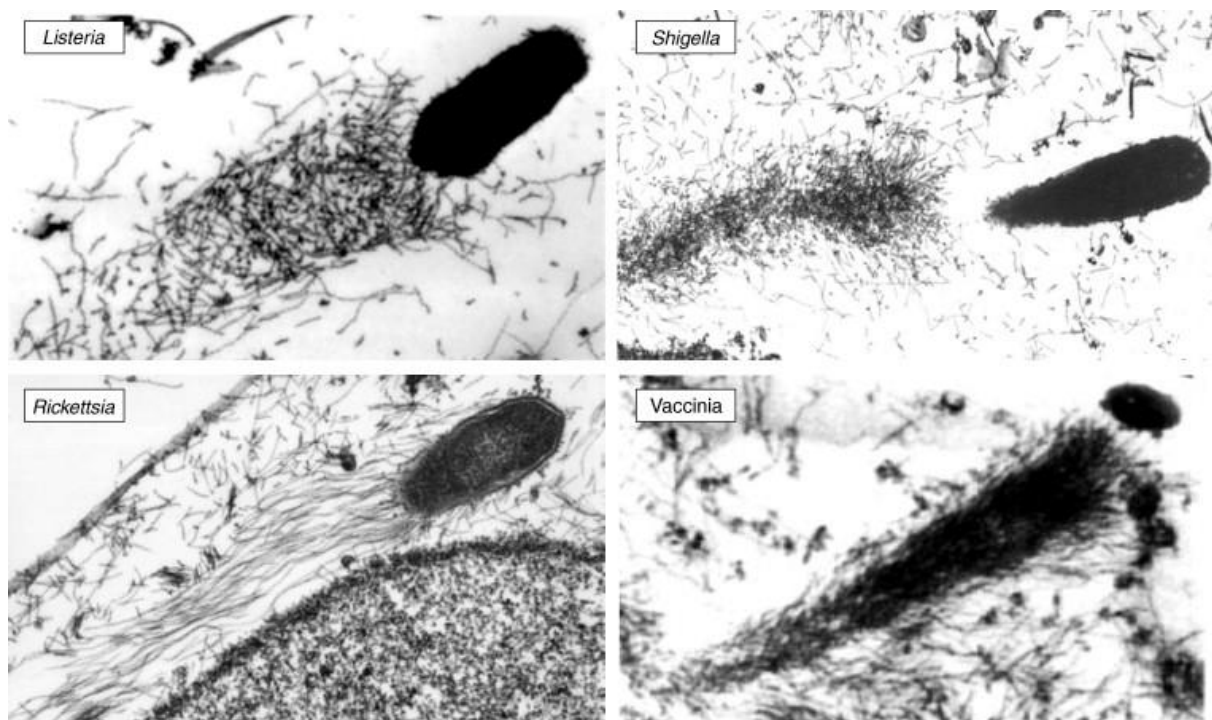
Figure 11 Comparison of the appearance of four actin-nucleating pathogens. *Listeria*, *Shigella* and *Vaccinia* seem to produce tails of similar structure. Strikingly, *Rickettsia*-induced tails are the only ones in this summary to show a very different architecture. The similarities in structure could mean that unraveling the exact actin filament structure of a representative of the first group of pathogens, would also shed some light on the actin-tail organization of all the other members. Image taken from Gouin, 2005 [26].

Many efforts to elucidate the structural organization of these pushing machineries have been undertaken including electron microscopy studies of *Listeria monocytogenes* [24] and N-WASP coated beads of different diameter [25]. The authors of the latter study again reported branched actin structures earlier in the lamellipodium [21], possibly accounting for the observed 'fishbone'-structure observed under the light microscope [17],[19], but harboring the same potential for misleading artifacts as other platinum replica electron microscopy studies of actin. The 'fishbone' is seen at low concentrations of capping protein *in vitro* and therefore longer actin filaments but also in many electron microscopy studies of mentioned actin-propelled pathogens with the notable exception of *Rickettsia conorii* [26],[27]. A 'fishbone'-structure tail features actin filaments protruding away from the tail at an angle from the direction of movement. An example of a *Listeria*-induced 'fishbone' tail is shown in figure 12. The existence of

Figure 12 Video frames taken every 3min of *Listeria* moving in reconstituted motility medium. The low Gelsolin to actin ratio (16nM Gelsolin, 8µM actin) causes actin filaments to grow exceptionally long before being capped. These filaments emanate sideways, resembling a fishbone. Images taken from Pantaloni, 2000 [18].

these emanating filaments has been put forward as an argument for branching, as the filaments pointing sideways were interpreted as branched actin continuing to grow away from the mother filament at an angle of roughly 70° [17]. Regardless of the implications of the 'Fishbone'-structure on branching controversy in the actin field, this widely conserved appearance points to an underlying universal mechanism of how pathogens build up actin comet tails at their rear ends [27]. Although the pathways that lead to the formation of an actin tail can differ amongst the different pathogens, the structure looks remarkably similar in the available electron micrographs (see figure 11). The exception is *Rickettsia*, whereby the tail shows mainly parallel filaments wrapped around each other in a helical fashion [80]. Remarkably, *Vaccinia* virus exhibits a 'fishbone'-structure while the virus is located outside the cell [78]. A viral receptor crosses the plasma membrane and manipulates the host actin cytoskeleton [79].

The only electron micrographs that clearly show actin comet tails polymerized by pathogens *in vivo* up to date are the sections shown in figure 11 and the negatively stained images of the rather big *Listeria*-induced tails, which could only be viewed at a distance from the bacteria [24], as well as images of platinum replica coated samples [33]. Because of the high density and number of actin filaments close to the bacterial surface it was not possible by any of the conventional electron microscopy techniques used to resolve the detailed

arrangement of filaments, namely to determine whether filaments were branched or not [25],[39]. Since baculovirus is considerably smaller than *Listeria*, it presented itself as a more suitable object for analysis of actin comet tail architecture. A schematic size comparison of the different objects which have been used in the motility assay is shown in figure 13. The effective size of the comet tail polymerized by baculoviruses is further decreased as the filaments are only polymerized from the rear end of the virus and not along over the whole surface, as with plastic beads coated with N-WASP.
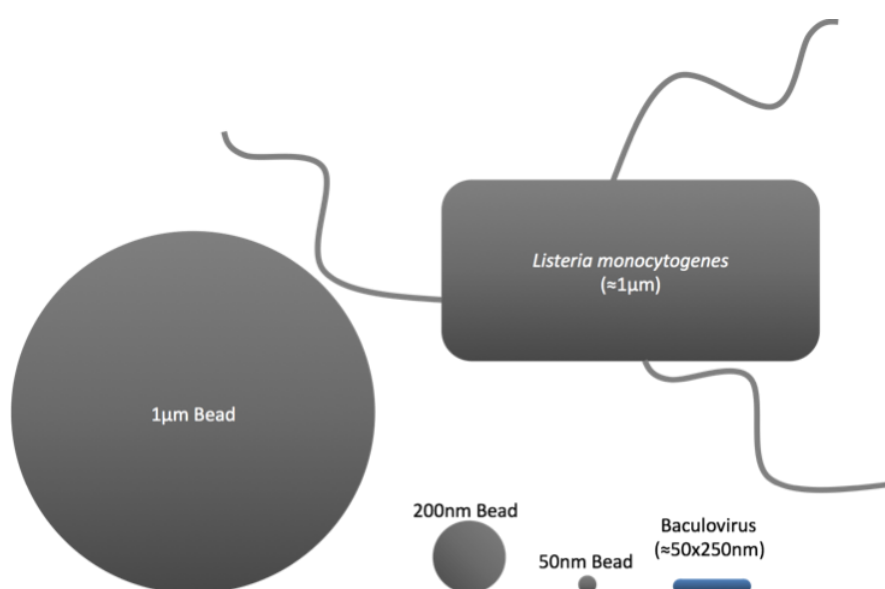

Figure 13 Size comparison of different actin-nucleating objects. *Listeria*, beads of different diameter and baculovirus can all be added to the motility assay to nucleate actin *in vitro*. Among these known objects, baculoviruses belong to the smallest. The produced actin tails are correspondingly small-sized, facilitating their analysis by electron microscopy techniques.

Several groups have tried to model the molecular basis of actin tails. At the moment there are two competing models explaining actin polymerization at the rear of an actin-nucleating object: The elastic ratchet model [107],[108] and the clamped-filament model [109]. Implications of the presented results on the existing models are discussed in the appropriate chapter.

Aims

To clarify the molecular architecture of an actin comet tail, which shows the typical 'fishbone'-structure – albeit at a smaller scale – we set out to examine baculovirus polymerized tails by transmission electron microscopy. The small size of the viruses and their correspondingly smaller tails would allow full penetration by the electron beam and therefore enable us to resolve the samples without the need to resort to sectioning. This novel approach could not only help to shed some light on the underlying structure for all known 'fishbone'-like comet tails, but also on the very principles of actin-based locomotion itself. Taking advantage of electron microscopy on baculoviruses we aimed to develop a tool that would allow us to study the events during actin filament nucleation and elongation at a very small scale – at single filament and even monomer level – while at the same time working under conditions at or very close to the actual *in vivo* situation. The overlying aim

was to contribute to the general knowledge about actin dynamics by providing clues about actin regulation in the baculovirus model system.

To this end we adopted two approaches:

First, we used the *in vitro* motility assay established by Loisel et al. [16] together with purified and de-enveloped baculoviruses. *In vitro* actin tails and clouds, which could be modified by adding different concentrations of capping protein, were observed.

Second, we infected different cell types, most notably goldfish fibroblasts, taking advantage of their flat shape suitable for electron microscopy. Baculoviruses proved efficient at infecting many different cell types, thereby polymerizing actin tails equivalent to those observed *in vitro*. Baculovirus-induced actin tails were characterized using fluorescence microscopy as well as electron microscopy. Finally, we used electron tomography to acquire tomograms and produce a 3D model of an actin comet tail.

METHODS

Virus preparation

Baculovirus supernatant after three rounds of infection was supplied by Venugopal Bhaskara from the Institute of Molecular Pathology (IMP), Vienna, Austria. Usually 1.8ml were precleared at 2,500g for 5min, then centrifuged at 18,000g for 1h and resuspended in 50µl of baculovirus buffer (10mM HEPES, 0.5M KCl, pH 7.4) to avoid clustering of the viruses. Virus yield and purity were assessed by electron microscopy and SDS-PAGE analyzed by ImageJ. For infection of cells, this preparation was added to 2ml culture medium of different cell types in a 30mm Petri dish: The virus preparation was added directly to the medium and incubated at 27°C for 1h. For *in vitro* assays, de-enveloped viruses were required and prepared by adding 2% Triton X-100 (Fluka) to the virus suspension and incubating the mixture on a shaker for 30min at 37°C. The suspension was then centrifuged at 500rpm to remove large debris and the supernatant centrifuged at 20,000g for 1h to sediment the viruses. The resulting pellet was resuspended in 50µl baculovirus buffer supplemented with 1% BSA and mixed together with the motility assay.

Plasmids

To yield a His-MBD-WA carrying plasmid, pEGFP-MBD-WA, created by Stefan Köstler (Rheinische Friedrich-Wilhelms-Universität, Bonn), was cut out using a double digest with the restriction endonucleases SacI and SalI (Fermentas) and ligated by T4 DNA Ligase (Fermentas) with the pET28a(+) vector which was cut the same way. In short, the pEGFP-MBD-WA was cut in between pEGFP and MBD by SacI (GAGCTCCCA) and at the end of the MBD-WA by SalI (GCAGTCGAC). The digests were incubated at 37°C for 1h in Tango buffer

(Fermentas) to generate sticky ends. The cut-out MBD-WA fragment and the cut pET28a(+) vector were then incubated with T4 DNA Ligase in Tango buffer for 1h at 22°C. After transformation into competent DH5α *E.coli* (see next chapter) and culturing the transformed cells the recombinant pET28a(+) plasmid was extracted using a Mini prep kit (Quiagen). The identity of the DNA was confirmed by DNA sequencing with two primers complementary to the T7 promotor (TAATACGACTCACTATAGGG) and T7 terminator in PET-vectors (GCTAGTTATTGCTCAGCGG) and the plasmid was used for protein expression in *E.coli*.

Protein expression and purification

The His-MBD-WA containing plasmid was transformed into competent DH5α *E.coli* by adding around 150ng of DNA to 100µl of competent cells and incubating the mixture on ice for 30min. After 30s heat shock at 42°C in the water bath 250µl prewarmed SOC medium were added and the cells were incubated on a shaker for 1h at 37°C. After this recovery time they were plated out on LB agar containing Kanamycin. The next day a colony was picked to inoculate 5ml LB with Kanamycin and incubated for several hours on a shaker at 37°C. The cells were then pelleted by 5min centrifugation at 5,000g and the DNA extracted by Mini prep (Quiagen). The identity of the plasmid was confirmed by agarose gelelectrophoresis, UV/Vis spectrometry and sequencing. The *E.coli* strain BL21(DE)-CodonPlus-RP was used for protein expression: First, the plasmid was transformed into competent cells as described above and a transformed colony was chosen to set off a 5ml day culture. 1ml of this culture was used to set off 100ml LB with Kanamycin and Chloramphenicol, which was incubated on a shaker at 37°C over night. The next day 1-2l of LB with antibiotics were incubated with 20ml over night-culture each and incubated for about 3h until they reached an OD_{600} between 0.8 and 1.2. At this point the culture was cooled down to 23°C, induced with 0.75mM IPTG (Fermentas) and incubated over night at 23°C and 130rpm. The cells were then harvested by centrifugation at 5,000g for 15min and the pellet from 1l culture was washed once and resuspended in 40ml ice cold resuspension buffer (50mM NaPi, 500mM NaCl, 10mM Imidazole, ph 8.0) with 5mM β-mercaptoethanol, 1mg/ml Lysozyme and 1% protease inhibitor cocktail (Sigma). After nutating for 1h in this solution the cells were flash frozen in liquid nitrogen and thawed at room temperature with magnetic stirring. Sonication in an ultrasonic homogenizer (Omni Ruptor 250, Omni International) was employed for three times 2min with 30sec pause in between cycles to disrupt the cells. The homogenized solution was centrifuged at 20,000g for 1h at 4°C and the supernatant was transferred to a chromatography column (Bio-Rad) with 2ml Ni Sepharose 6 Fast Flow slurry (Sigma Aldrich) per 1l expression culture. The column was washed three times with a column volume of resuspension buffer and twice each with resuspension buffer with 30mM and 50mM of Imidazole. The bound protein was eluted with 4ml resuspension buffer with 250mM Imidazole and dialyzed over night into storage buffer (50mM NaPi, 300mM NaCl, 1mM DTT, 10% Glycerol, pH 8.0) with a Slide-A-Lyzer 10,000 MWCA device (Pierce). The purified protein was then analyzed by SDS-PAGE and mass spectrometry, flash frozen in liquid

nitrogen and stored at -80°C. Mass spectrometry analysis was performed at the IMBA mass spectrometry facility.

Microtubules

Tubulin purified from pig brain was kindly supplied by the lab of Stefan Westermann (IMP). Due to stability problems with GTP-polymerized microtubules, they were polymerized in the presence of ATP. Therefore, Tubulin and Rhodamine-Tubulin (Tebu-Bio) in a ratio of 10:1 were precleared in a Sorvall S100AT3 rotor at 300,000g for 5min. 15µM Tubulin and 1.5µM Rhodamine-Tubulin were then incubated in PEM (80mM PIPES, 1mM EGTA, 1mM $MgCl_2$, 1mM DTT) with 2.5mM ATP and 12% Glycerol for 1min at 37°C. Then 1/10 of the volume of 1.5µM Taxol (Sigma) was added to the solution and incubated for 8min at 37°C, followed by 1/10 of the volume of 15µM Taxol for 8min and finally 1/10 of the volume of 150µM Taxol was added for 15min at 37°C. The polymerized microtubules were pelleted over a cushion of 100µl 40% Glycerol in PEM by centrifugation at 140,000g for 20min. The pellet was then resuspended in PEM containing 2.5mM ATP and 50µM Taxol to give a final tubulin concentration of about 20µM.

The His-MBD-WA was thawed, diluted 1:20 in PEM with 2.5mM ATP and 50µM Taxol and concentrated to 2µM in a Vivaspin 500 30,000 MWCO concentrator (Sartorius) operated at 10,000g and 4°C. The concentrated solution was centrifuged for 20min at 300,000g and the supernatant used together with the microtubules.

The ATP-polymerized microtubules were then mixed 1:1 with the His-MBD-WA, incubated 25min at 37°C and centrifuged at 140,000g for 20min. Optionally, the microtubules with the bound protein were sheared at this step by pipetting several times through a 26-gauge needle.

In vitro motility assay

The *in vitro* assay was basically performed as described [16]: ADF (3.7µM), Profilin (2.5µM), Gelsolin (25-200nM), Arp2/3 (75nM), G-actin (7.6µM) and the purified, de-enveloped baculovirus were mixed in X-buffer (10mM HEPES, 100mM KCl, 1mM $MgCl_2$, 0.1mM $CaCl_2$, pH 7.8) supplemented with 1% BSA, 2mM ATP, 4mM $MgCl_2$ and 6.7mM DTT. The proteins were supplied by Christophe LeClainche and Marie-France Carlier from the Laboratoire d'Enzymologie et Biochimie Structurales, Gif-sur-Yvette, France.

For studies with microtubules, the His-MBD-WA coated microtubules were flowed under a custom-made flow chamber, which was heated up to 37°C. After about 30min the chamber was washed with X-buffer containing 50µM Taxol, followed by flowing in the complete motility mix supplemented with 50µM Taxol. The sample was then observed on an inverted Zeiss Axioscope (Carl Zeiss) equipped with epifluorescence optics using phase contrast or 565nm and 488nm wavelength filters. Time-lapse images were recorded on a Roper

Micromax, 512×512 rear-illuminated, cooled CCD camera controlled by Metamorph software at intervals of 10s unless stated otherwise.

To produce *in vitro* baculovirus-induced actin tails, 1/60 volume of the total volume of 36x concentrated de-enveloped baculovirus preparation were added and incubated for 20-45min. Then the assay was fixed with 0.5% Glutaraldehyde, blotted carefully with filterpaper and negatively stained.

Cell culture, transfection and infection

B16 mouse melanoma cells were cultured in Dulbecco's Modified Eagle's Medium (DMEM) (Sigma-Aldrich) with 10% fetal calf serum (Thermo Fisher Scientific) 1% Penicillin/Streptomycin and 1% L-Glutamine. B16 cells were transfected as subconfluent monolayer cultures on 30mm Petri dishes using 2µg of DNA, 100µl Optimem (Invitrogen) and 6µl Fugene (Roche). This transfection mix was incubated for 20min, the growth medium was changed and the mix added to the cells over night. The next day, the medium was changed again and the transiently transfected cells were put on coverslips coated with 25mg/ml Laminin (Sigma) to be imaged on a fluorescence microscope. NIH 3T3 mouse fibroblasts were maintained in DMEM with 10% fetal bovine serum (Thermo Fisher Scientific), 1% Sodium pyruvate, 1% Penicillin/Streptomycin and 1% L-Glutamine. 3T3 fibroblasts were transfected like B16 cells but coverslips coated with 0.01% Poly-L-Lysine (Sigma) were used for imaging. Drosophila S2 cells were kept in Schneider´s Drosophila Medium with 1% Penicillin/Streptomycin and 1% L-Glutamine.

Goldfish fin fibroblasts (line CAR, No. CCL71) were maintained in Basal Eagle's Medium (Sigma-Aldrich) supplemented with 1% nonessential amino acids, 2.5% Hepes (Invitrogen), 1% Penicillin/Streptomycin, 1% L-Glutamine and 12% fetal bovine serum (Thermo Fisher Scientific) at 27°C. For transient transfection, subconfluent monolayer cultures on 30mm Petri dishes were used. The transfection mixture was prepared as follows: 2µg of DNA and 12µl of Superfect lipofection agent (QIAGEN) were mixed in 200µl Optimem (Invitrogen). After 15min incubation at room temperature, a further 5% serum-containing medium with transfection mixture was added to the cells for 5h. The cells were then washed and returned to normal medium. Transfected cells were replated after 24h on 15mm coverslips coated with human fibronectin (Roche) at a concentration of 50µg/ml.

Plasmids used for transfection were mCherry-actin, pEGFP-actin, pEGFP-p16, pEGFP-tubulin, pEGFP-VASP and pEGFP-WASP.

50µl baculovirus preparation were added to 2ml of a subconfluent CAR cell culture growing on a fibronectin-coated coverslip and incubated at 27°C. For live cell imaging the coverslips were mounted in an open chamber on a heating platform (Harvard Instruments) on an inverted Zeiss Axioscope (Carl Zeiss) as described above. Timelapses were acquired at 2s

intervals. First intracellular virus-induced tails were usually observed at about 20min post infection.

Electron microscopy

Fish fibroblasts were grown on Formvar-coated 200 mesh hexagonal nickel grids (Agar Scientific) or 135 mesh NHF15-A gold Finder grids (Maxtaform) in standard medium and allowed to spread over night. After 50μl of baculovirus preparation were added and incubated for 1h, the samples were washed with cytoskeleton buffer (10mM MES or PIPES, 150mM NaCl, 5mM EGTA, 5mM glucose, 5mM $MgCl_2$, pH 6.8), fixed and extracted with 0.5% Triton X-100 and 0.25% Glutaraldehyde in cytoskeleton buffer for 1min and kept in 2% Glutaraldehyde with 1μg/ml Phalloidin in cytoskeleton buffer at 4°C.

For routine inspection of samples nickel grids were stained with 60μl 2% Sodium Silicotungstate (SST) with 1μg/ml Phalloidin, blotted carefully and imaged on a 100kV transmission electron microscope (Morgagni, FEI).

For electron tomography gold Finder grids were used and either 8% SST or 4-6% SST supplemented with 3.4% $MgAc_2$, 1-3% Glucose or 0.5% polyvinyl alcohol (PVA) staining with 1μg/ml Phalloidin and around 1:10 BSA-gold colloid preparation from a gold stock. Tilt series were acquired on a FEI Tecnai F30 Helium (Polara) microscope, operated at 300 kV and cooled to approximately 80 K. Automated acquisition of tilt series was driven by SerialEM 2.8.x. Normally, the tilt range was -60 to +60 using the Saxton tilt scheme based on 1° increments from 0° tilt, at a defocus value of -5μm and -7μm. For every sample two tilt series around orthogonal axes were recorded on a Gatan UltraScan 4000 CCD camera at magnifications typically from x23,000 to x59,000.

In vitro polymerized actin tails were incubated on carbon-coated 400 mesh hexagonal copper/palladium grids (Agar Scientific) or carbon-coated 135 mesh NHF15-A gold Finder grids (Maxtaform) fixed with 0.5% Glutaraldehyde and stained and imaged like the intracellular samples.

Re-projections from the tilt series were generated using IMOD software from the Boulder Laboratory for 3D Electron Microscopy of Cells [28], using the gold particles as fiducials for alignments. Using IMOD, filaments were manually tracked and models generated. A typical tomogram comprised a Z-stack of 60-120 sections of 0.4-1.1nm each. To compare different additives in terms of Z-preservation, baculovirus-induced comet tails in the cytoplasm of CAR fibroblasts were analyzed in constant intervals from the virus and the average thickness was recorded.

RESULTS

Microtubules

ATP-polymerized microtubules are stable in ATP-containing buffer

To stabilize microtubules for at least a few hours in X-buffer, which contains 2.5mM ATP, proved to be a challenging task. Attempts with Taxol-stabilized, GTP-polymerized microtubules failed, as well as using GMPCPP-polymerized microtubule seeds and glutaraldehyde-fixed microtubules. Polymerizing tubulin in the presence of ATP and glycerol yielded morphologically normal microtubules, which are stable in ATP and high salt containing buffer for
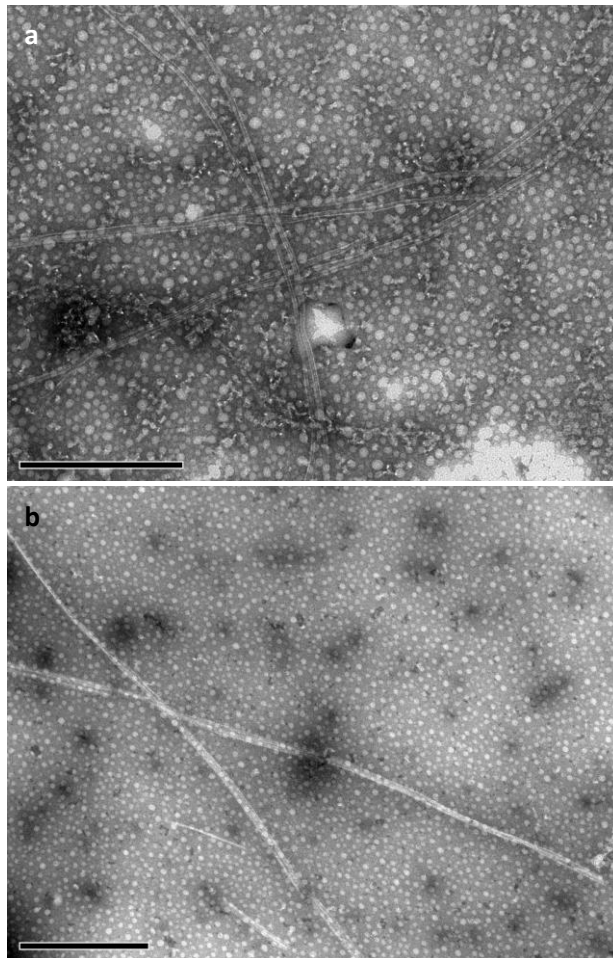
Figure 14 Comparison of GTP- and ATP polymerized microtubules. **(a)** GTP-polymerized microtubules and **(b)** ATP-polymerized microtubules did not show the morphological difference visualized by electron microscopy, as reported in earlier work [29]. **(c)** Decay of GTP-polymerized, 50mM Taxol-stabilized microtubules in a solution containting 2mM ATP. In contrast, microtubules polymerized with ATP were stable for many hours in this buffer. Both samples were imaged on Poly-L-Lysine-coated grids. Magnification: **(a)**,**(b)** 44,000x; **(c)** 100x. Scale bars: **(a)**,**(b)** 500nm; **(c)** 10µm.
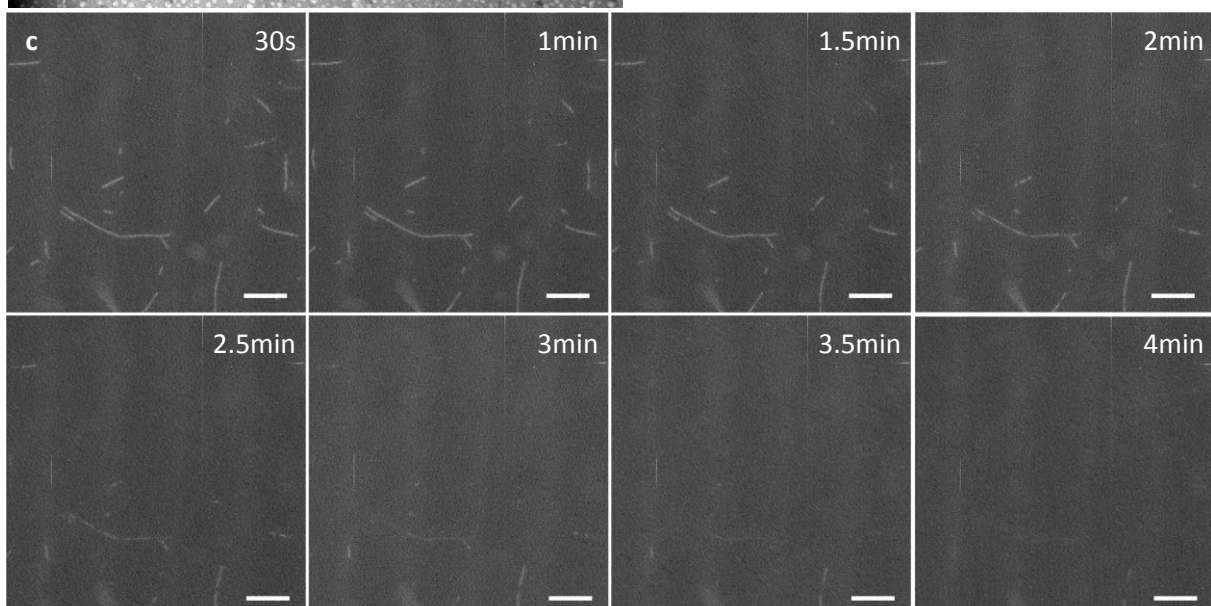
days. Figure 14 the left shows an electron micrograph of ATP-polymerized microtubules. The globular tubulin structures with radially emanating short protofilaments reported for ATP-polymerized microtubules [29] were not observed.

MBD-WA bundles microtubules

The bundling function of the microtubule-binding domain of MAP4 has been described earlier [30]. As shown in figure 15, bundling of microtubules was also observed with MBD-WA, whereby shearing of microtubules by pipetting through a needle apparently could not disrupt bundles into single microtubules but just shortened the average length of the bundles by breaking them into shorter pieces.
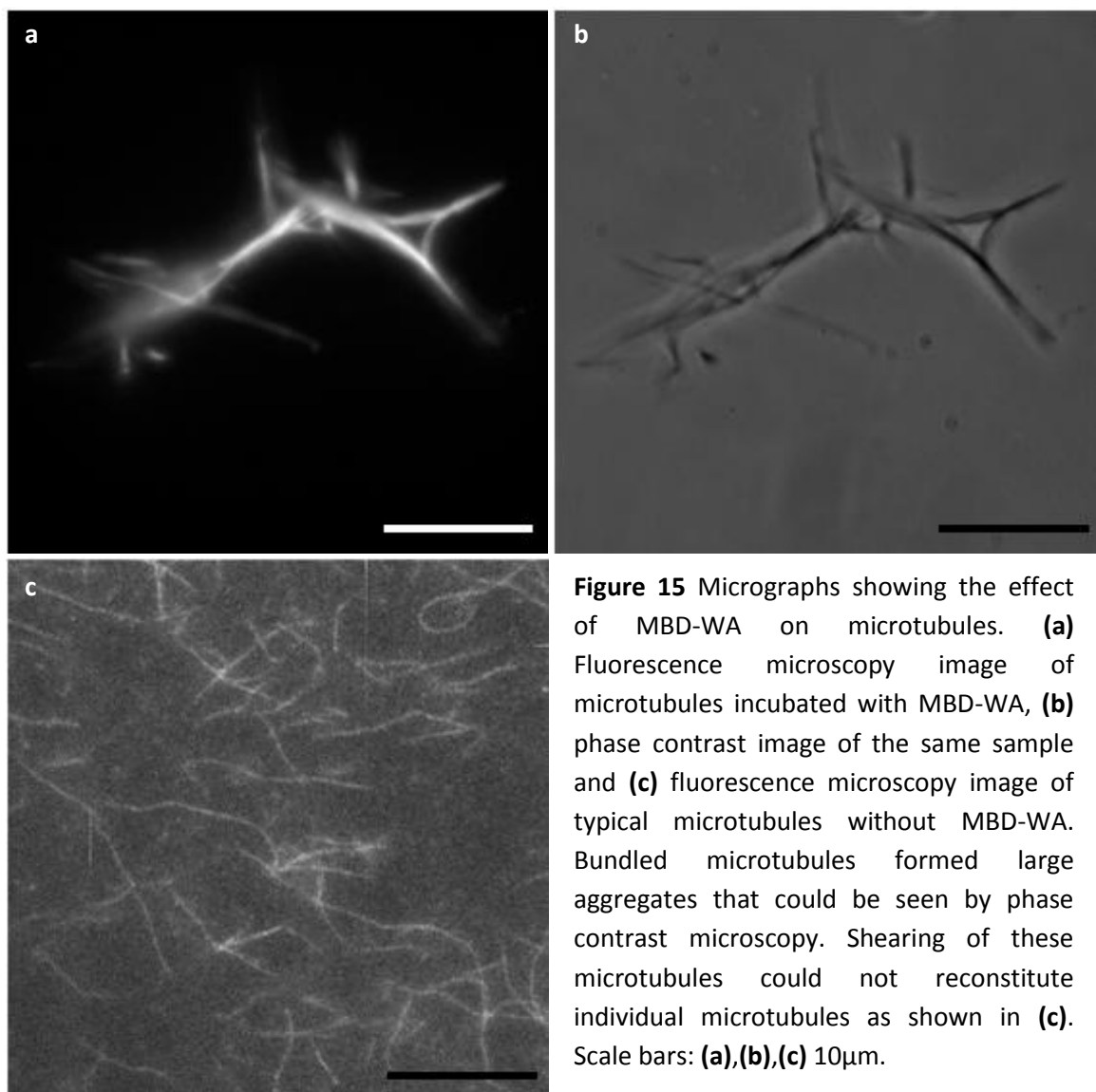

Figure 15 Micrographs showing the effect of MBD-WA on microtubules. **(a)** Fluorescence microscopy image of microtubules incubated with MBD-WA, **(b)** phase contrast image of the same sample and **(c)** fluorescence microscopy image of typical microtubules without MBD-WA. Bundled microtubules formed large aggregates that could be seen by phase contrast microscopy. Shearing of these microtubules could not reconstitute individual microtubules as shown in **(c)**. Scale bars: **(a)**,**(b)**,**(c)** 10µm.

MBD-WA nucleates actin filaments from microtubules

Actin was nucleated from MBD-WA coated microtubules and mostly covered the whole microtubule bundles probably by aligning alongside the tubulin. Figures 17b and 17c show electron micrographs of a microtubule bundle covered with actin. Sheared MBD-WA coated microtubules also nucleated actin filaments that grew away from the activator as shown in figure 16.
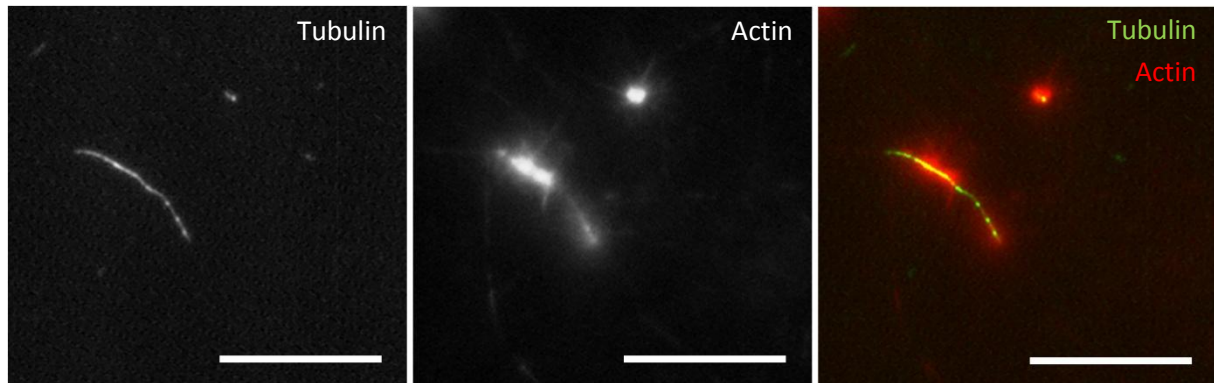

Figure 16 Actin nucleated from microtubules. These images acquired by fluorescence microscopy show actin filaments emanating from microtubules coated with MBD-WA. The coated microtublues were broken into smaller pieces by pipetting through a 26-gauge needle and incubated together with the components of the *in vitro* motility assay. Scale bars: 10µm.

Taken together, we managed to express a recombinant protein consisting of the MBD of mouse MAP4 and the WA domain of human N-WASP. This protein then bound *in vitro* polymerized microtubules with its MBD domain and, via activation of Arp2/3 with its WA domain, nucleated the growth of actin filaments from the microtubule surface.
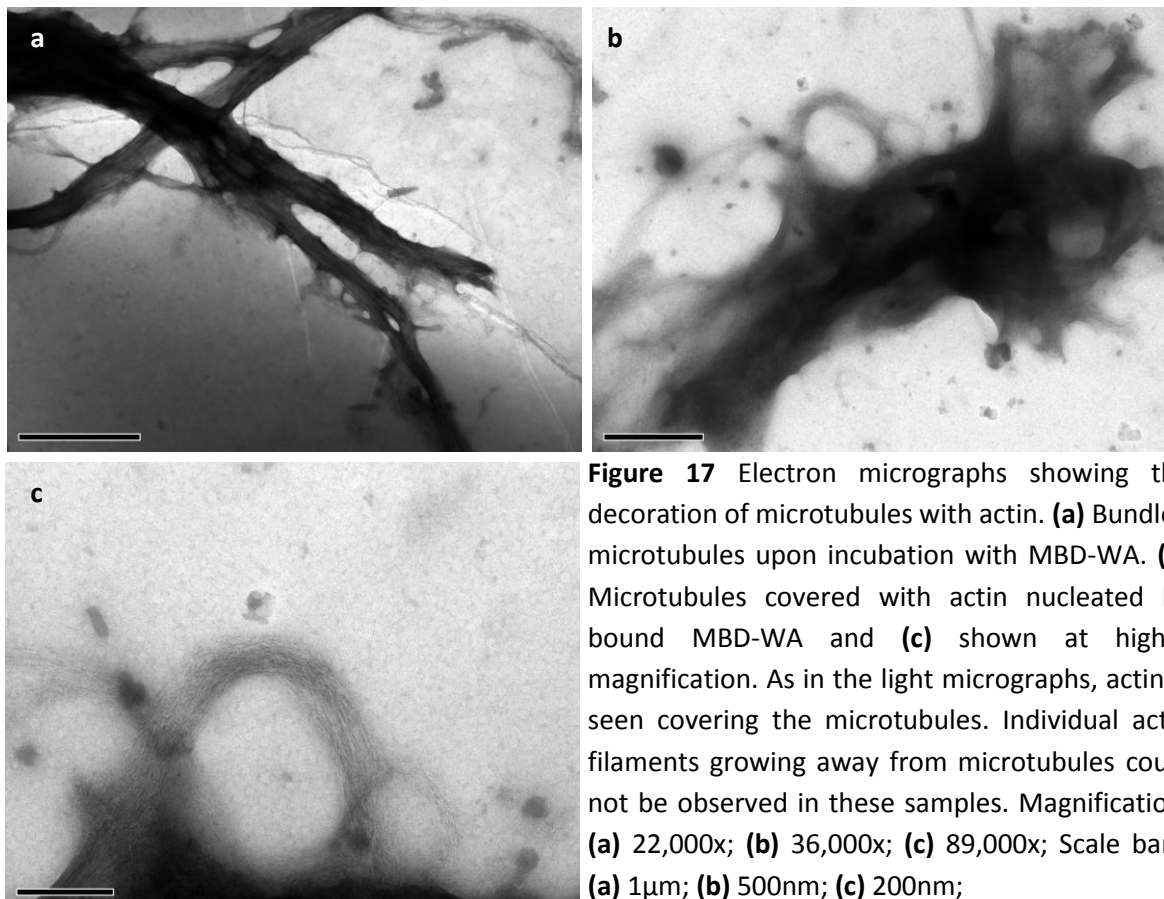
Figure 17 Electron micrographs showing the decoration of microtubules with actin. **(a)** Bundled microtubules upon incubation with MBD-WA. **(b)** Microtubules covered with actin nucleated by bound MBD-WA and **(c)** shown at higher magnification. As in the light micrographs, actin is seen covering the microtubules. Individual actin filaments growing away from microtubules could not be observed in these samples. Magnification: **(a)** 22,000x; **(b)** 36,000x; **(c)** 89,000x; Scale bars: **(a)** 1µm; **(b)** 500nm; **(c)** 200nm;

Baculovirus

Baculoviruses can be purified quickly and efficiently by centrifugation

Figure 18 shows a summary of the simple purification method routinely used for baculovirus purification from baculovirus/Sf9 protein expression supernatants. Preclearing and centrifugation at 20,000g proved to be enough to yield clean material for our studies.
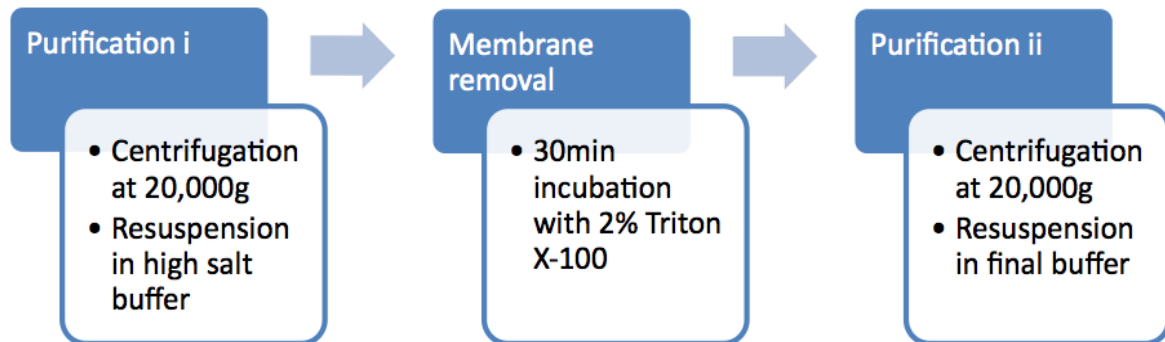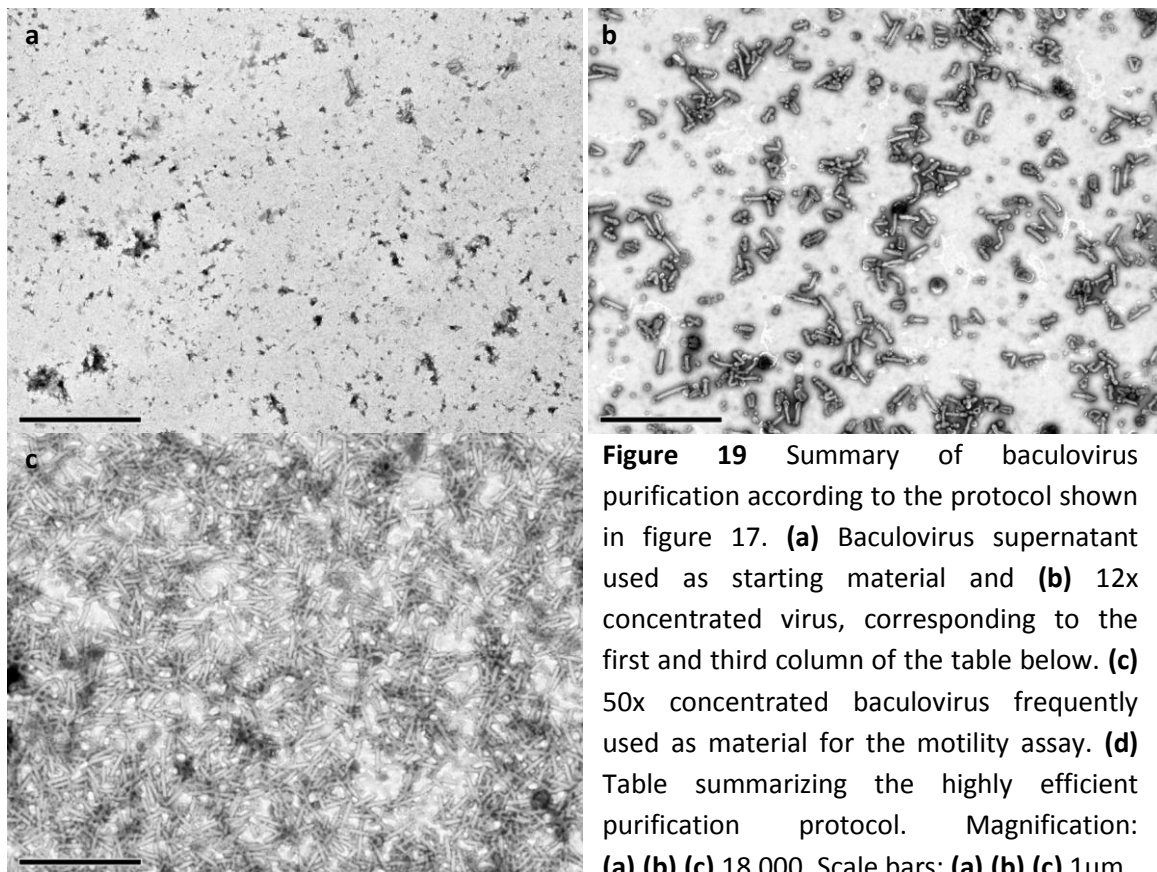

Figure 18 Diagram showing the baculovirus purification protocol used for this work.

The purification was assessed by SDS-PAGE and electron microscopy. As shown in figure 19, this simple, one-step purification protocol was sufficient to concentrate up to 200fold and purify baculoviruses from supernatants.

Figure 19 Summary of baculovirus purification according to the protocol shown in figure 17. **(a)** Baculovirus supernatant used as starting material and **(b)** 12x concentrated virus, corresponding to the first and third column of the table below. **(c)** 50x concentrated baculovirus frequently used as material for the motility assay. **(d)** Table summarizing the highly efficient purification protocol. Magnification: **(a)**,**(b)**,**(c)** 18,000. Scale bars: **(a)**,**(b)**,**(c)** 1μm.

d

Legend: Baculoviruses per grid square (blue), Total protein amount (red)

X-axis categories: 5,000xg Supernatant (a), 20,000xg Supernatant, 20,000xg Pellet 12x (b), 20,000xg Pellet 1x

Left Y-axis: Virions per grid square (0–1800); Right Y-axis: Percent of max (0–100)
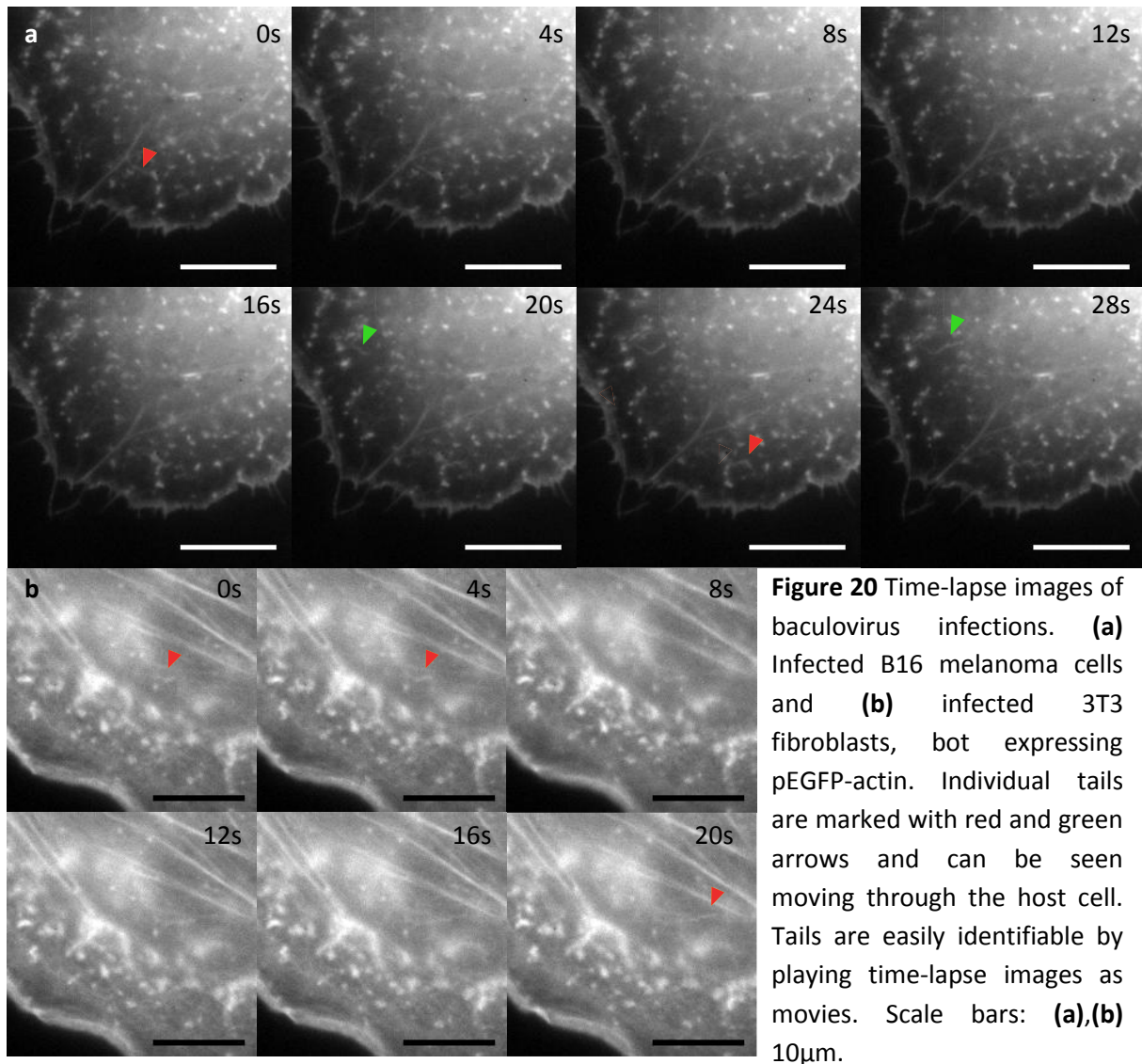
Baculoviruses infect several eukaryotic cell lines

To study changes in cellular actin upon baculovirus infection, I infected four different cell types with actin-GFP background. The infection protocol was simplified to adding 100μl of the twelve-fold concentrated pellet (see 'Methods' section) directly to the growth medium of the imaged cells. All the studied cell lines – Goldfish fin fibroblasts (CAR), NIH 3T3 mouse fibroblasts, B16 mouse melanoma cells and drosophila S2 cells – were infected readily by adding the concentrated virus solution. After an average time of 30min I observed the first baculovirus-induced actin comets. These actin structures were moving around the cell at a speed ranging from 8 to 22μm/min for about 2h30min. Tails in B16 and 3T3 cells appeared shorter than in the CAR cell line. Figures 20 and 21 show different cell types infected with baculovirus and imaged with a fluorescence microscope. After about 2h30min the movement slowed down gradually until a complete stop. As many as four viruses were sometimes seen to share a common tail for about a minute and then disperse into distinct viruses that move with tails on their own. The 'corkscrew' motion described by Ohkawa et al. [6], employed by the cells to penetrate the nuclear pores, was frequently observed in all cell types.

The electron micrographs in the lower part of figure 21 show the effect of extraction conditions on the actin cytoskeleton: Lowering the pH in the Glutaraldehyde-Triton X-100 solution extracts most of the actin cytoskeleton, but preserves the baculovirus-induced actin tails. A 'Fishbone'-like actin array was already visible, however, the tail structure was elucidated in more detail by electron tomography and is presented in the corresponding chapter below.

Figure 20 Time-lapse images of baculovirus infections. **(a)** Infected B16 melanoma cells and **(b)** infected 3T3 fibroblasts, bot expressing pEGFP-actin. Individual tails are marked with red and green arrows and can be seen moving through the host cell. Tails are easily identifiable by playing time-lapse images as movies. Scale bars: **(a)**,**(b)** 10μm.

Baculoviruses move preferentially along microtubules

As demonstrated in the video frames in figure 22, intracellular baculoviruses were frequently observed moving along microtubules within the host cell. While moving along microtubules baculoviruses did not show any consistent movement towards the plus or minus end (i.e. nucleus or periphery). Instead they were moving around the cell randomly and, upon encountering a microtubule, continued their movement along the microtubule in a manner that necessitated the smallest change in direction. Baculoviruses were also observed to move freely around the cell, then – upon making contact with a microtubule – move alongside the microtubule and dissociate again to once more migrate independently. Electron micrographs like the one shown in figure 22 show the 'microtubule-guided' movement of baculoviruses at higher magnification, whereby physical contact between the anterior part of the virion and the microtubule could be observed.
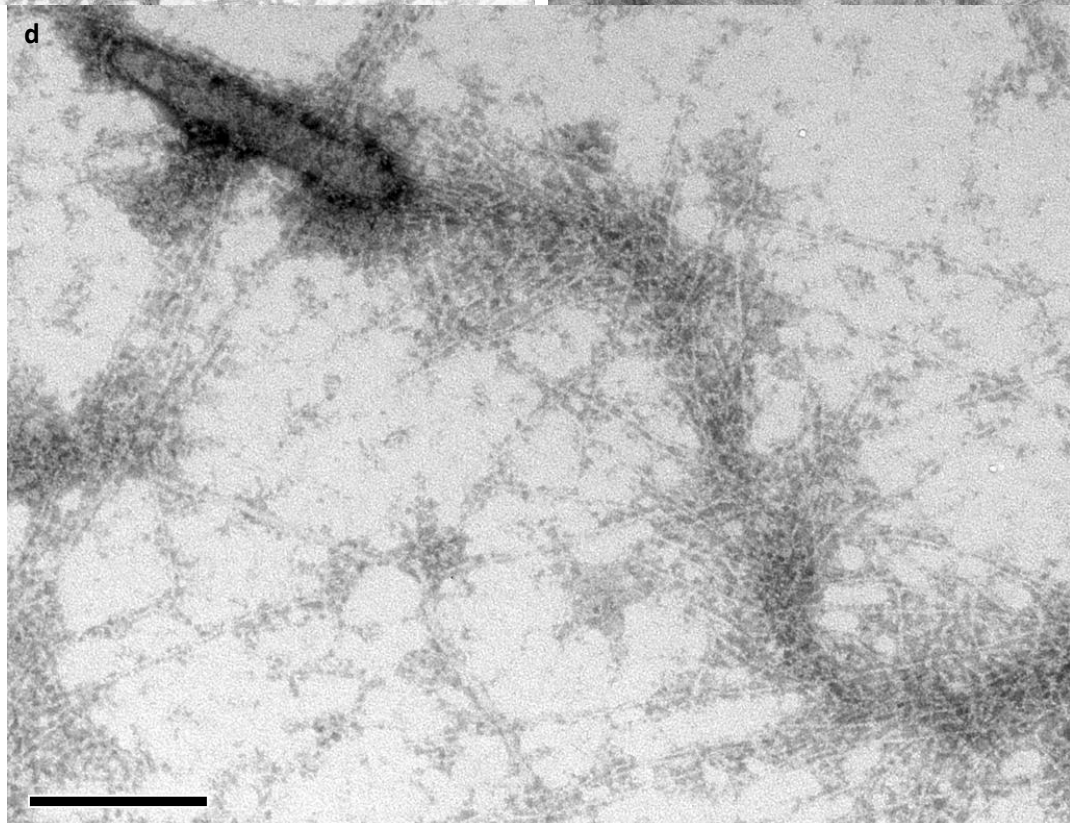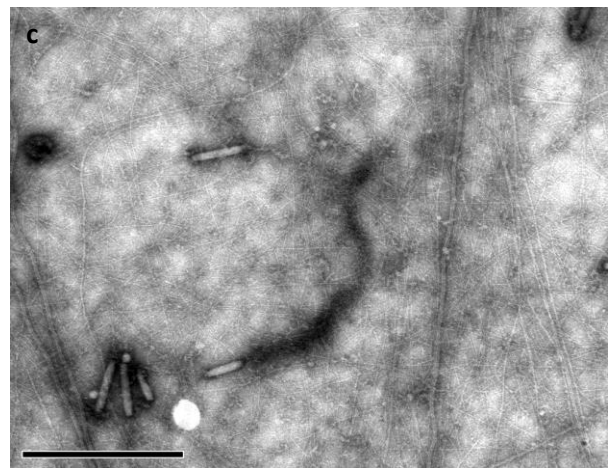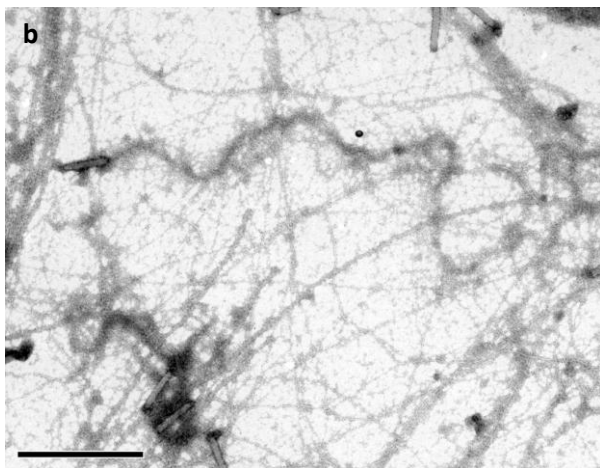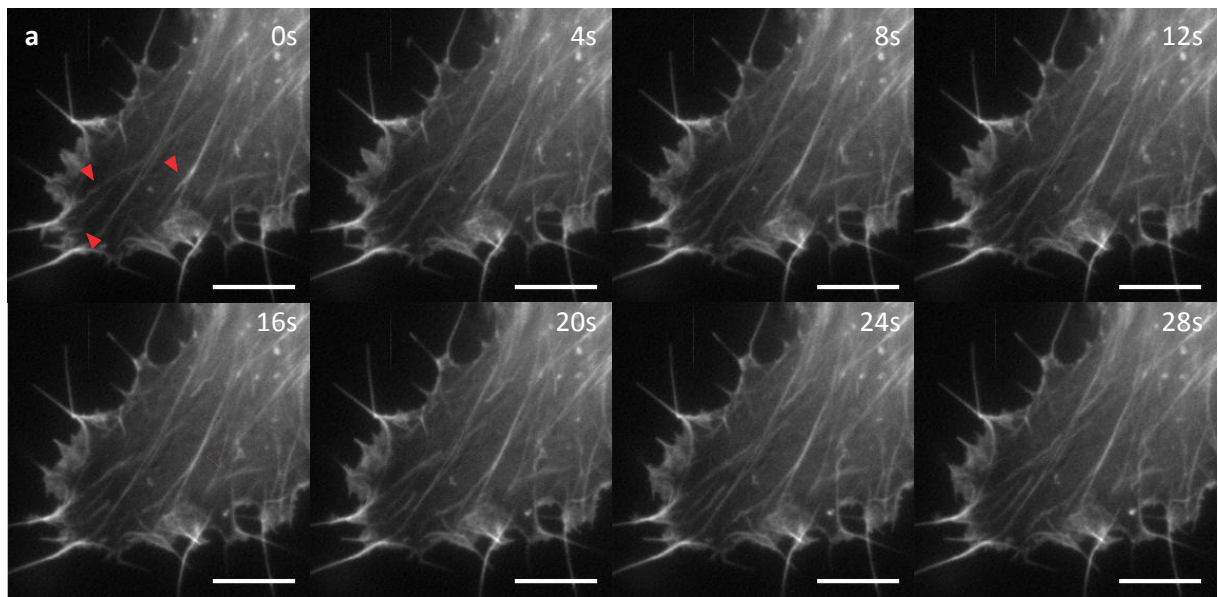
Figure 21 Baculovirus infection of CAR fish fibroblasts. **(a)** Time-lapse acquisition of an infected cell with three individual baculovirus-induced tails marked with red arrows. **(b)** Infected fibroblasts extracted at a pH of 6.8 and **(c)** 6.1. The extraction at higher pH proved stronger and removed a larger fraction of the cellular actin, but remarkably the actin tail was preserved. Weaker extraction conditions and more residual background actin caused difficulties with tracing of individual filaments as will be discussed in the next chapter. **(d)** Detailed analysis of the tail shown in **(c)** reveils fishbone-like arrangement of the actin filaments. Magnification: **(a)** 100x; **(b)** 22,000x; **(c)** 28,000x; **(d)** 89,000x. Scale bars: **(a)** 10µm; **(b)**,**(c)** 1µm; **(d)** 200nm.
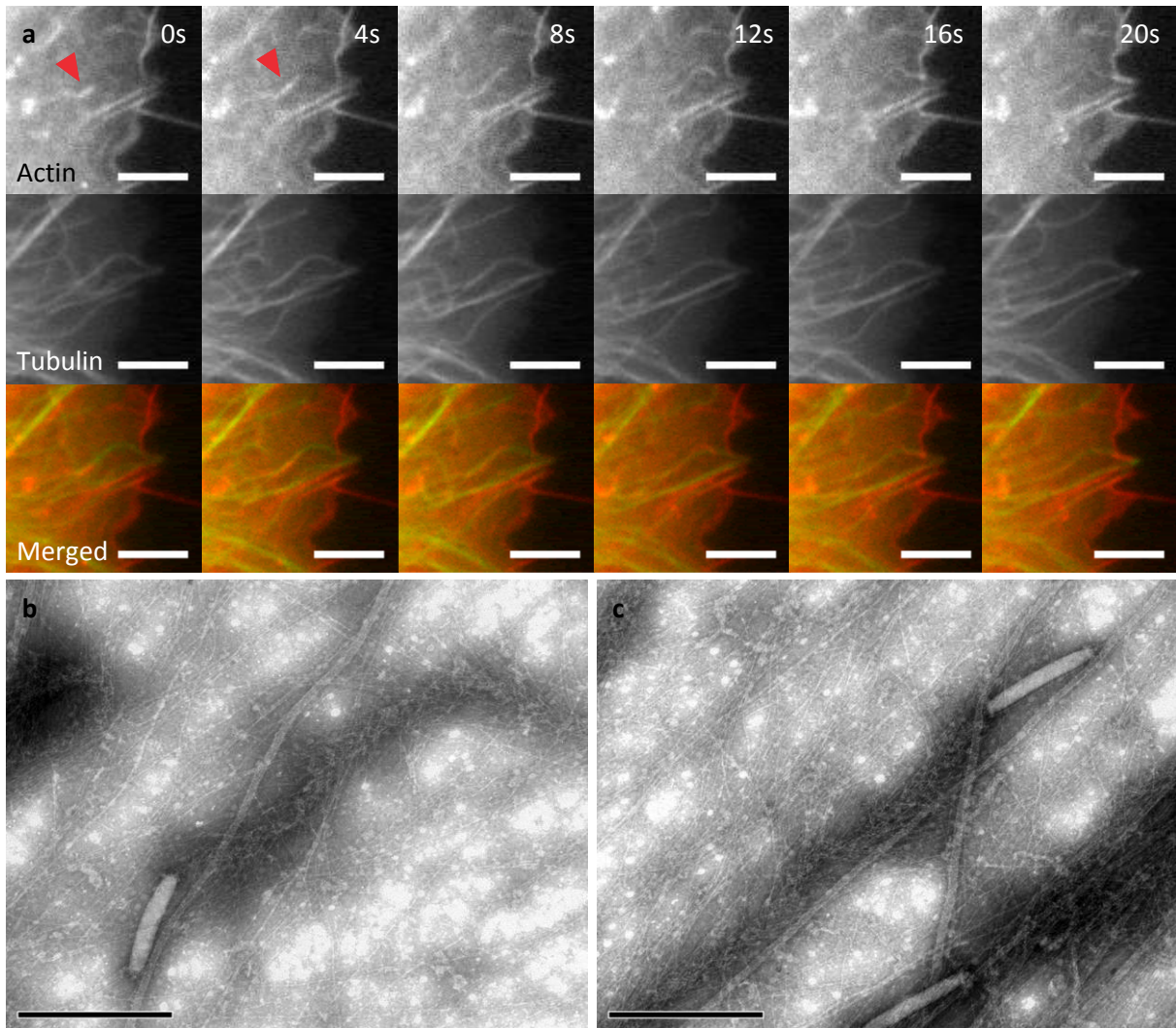

Figure 22 Movement of baculoviruses alongside microtubules in CAR fish fibroblast lamellipodia and lamellae. **(a)** Video frames of an infected CAR fish fibroblast expressing fluorescently labeled actin and tubulin. Red arrows mark a viral actin tail polymerizing along a cellular microtubule. This particular baculovirus was moving towards the cell edge – most probably the microtubule plus-end. **(b)**,**(c)** Electron micrographs showing individual baculoviruses in contact with microtubules. Physical interaction was usually observed between the anterior region of the virus and the microtubule. **(d)** Several baculoviruses connected to their actin tails, which all are seen aligned alongside microtubules. Harsh extraction conditions were used for preparation of the electron microscopy samples, consequently few remaining cellular actin is visible. Magnifications: **(a)** 100x; **(b)**,**(c)** 56,000x; **(d)** 4,400x. Scale bars: **(a)** 10µm; **(b)**,**(c)** 500nm; **(d)** 2µm.
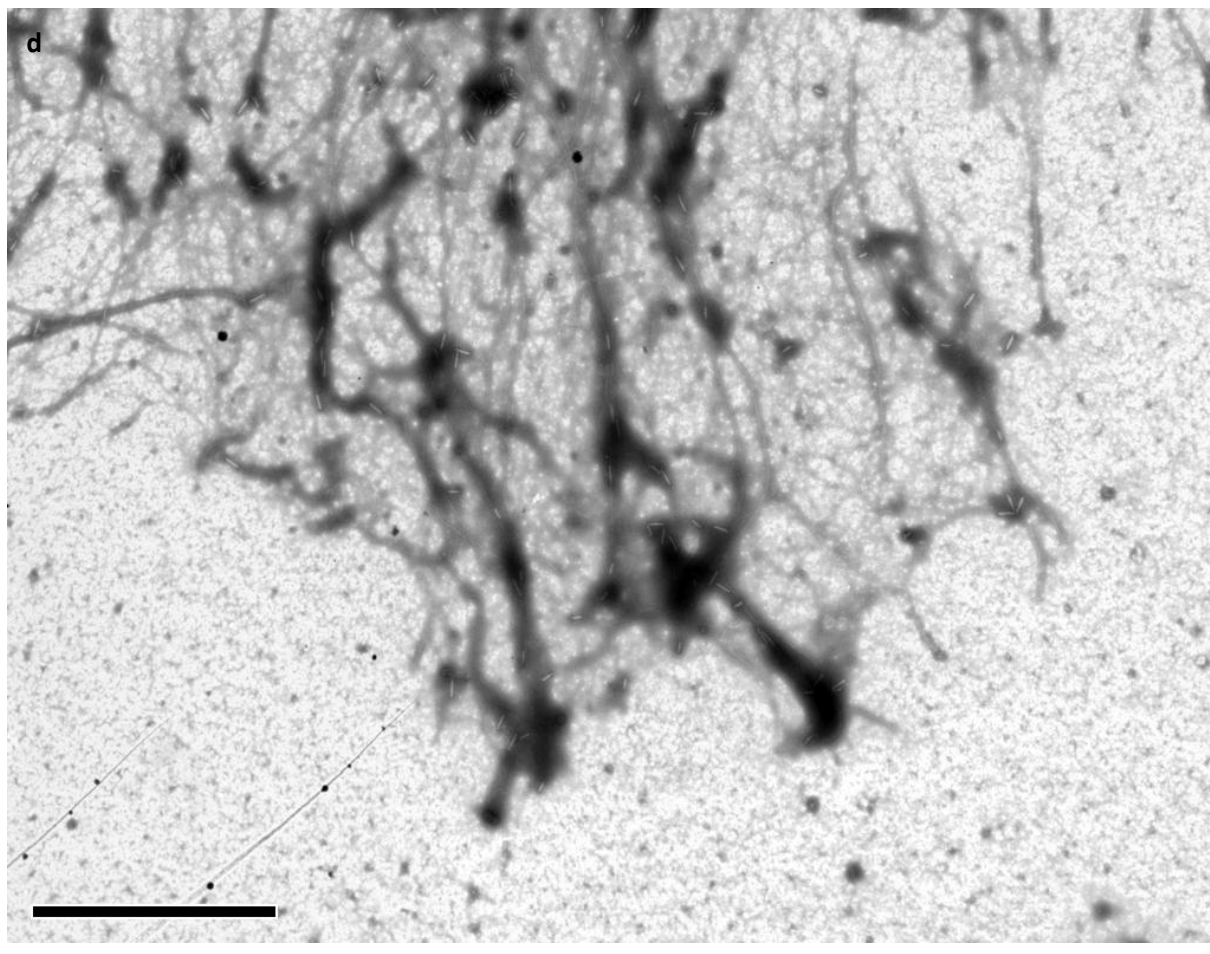
The Arp2/3 complex is incorporated into the actin tail

Infection of GFP-actin and mCherry-p16Arp labeled CAR fibroblasts showed colocalization of the signals from the two channels as shown in figure 23. Actin labeling showed known structures like stress fibers and a lamellipodium whereas mCherry fluorescence signal was seen at the cell edge as expected, indicating a successful transfection of both plasmids. The actin and p16 signal were always observed to co-localize along the full length of the tail. WASP and VASP on the other hand were not incorporated into the tail (data not shown).

De-enveloped baculoviruses nucleate actin *in vitro*

When incubated with a set of actin-regulating proteins (Arp2/3, Gelsolin, ADF, Profilin) and a sufficiently high actin concentration (7.5μM), purified baculoviruses did not colocalize with actin filaments. Figure 24(a) shows budded baculoviruses with nearby actin filaments, both randomly scattered on the carbon-coated grid.

Only following treatment with 2% Triton X-100 de-enveloped baculoviruses started nucleating actin at one end after about 10min of incubation at room temperature. Figure 25(a) shows a typical, beginning actin tail. Surprisingly, the majority of virus-associated actin flilaments was usually oriented towards the virus and could be seen flanking the virion on
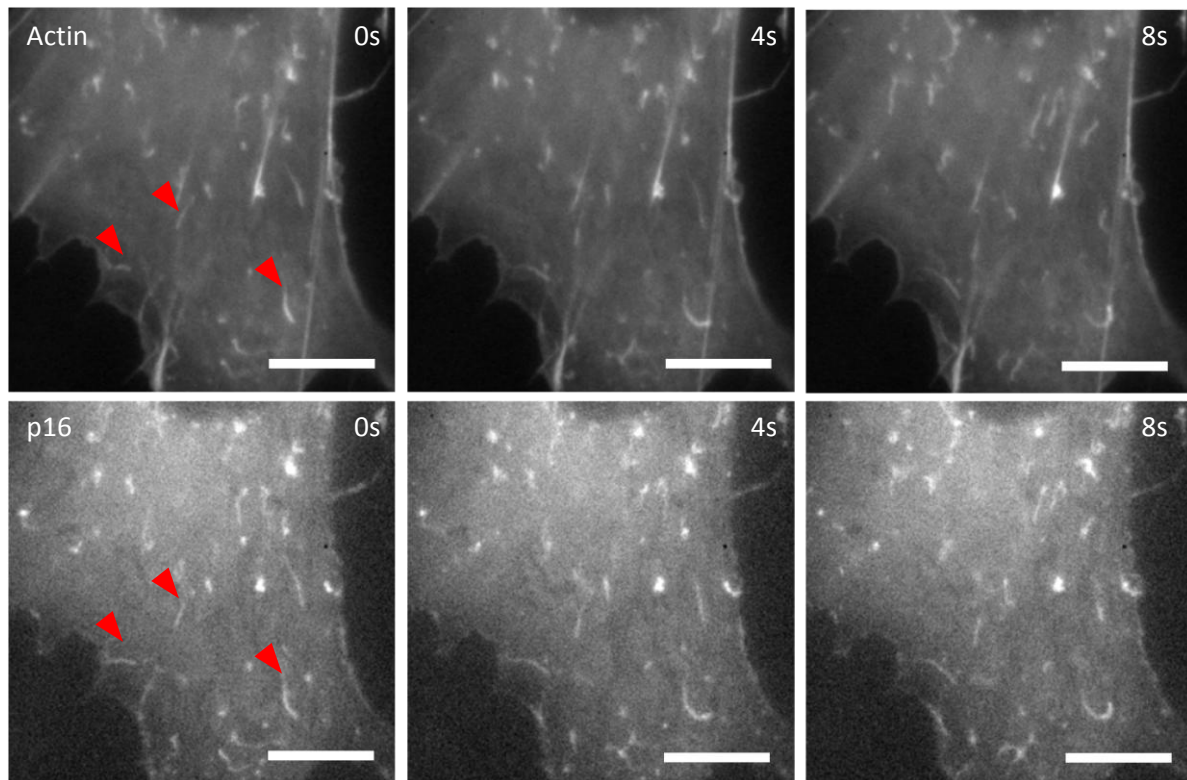
Figure 23 Incorporation of the Arp2/3 complex in the actin tail. Video frames of a CAR fish fibroblast expressing fluorescently labeled actin and p16 showing colocalization of actin and Arp2/3 in baculovirus-induced comet tails. Three prominent tails in are marked in both channels with red arrows. Magnification: 100x. Scale bar: 10µm.

both sides. Obvious branches were not observed in these 2D electron micrographs. After 10min until about 45min the number of baculoviruses associated with actin increased until at optimal conditions most of the visible viruses had nucleated actin filaments. Many actin associations consisted of a large cloud of actin with no apparent organization, oftentimes enclosing and covering the entire virus or several viruses with actin filaments. Most of the baculovirus-induced tails were halted at an early stage as shown in figure 25(c), but very few longer actin tails could also be observed *in vitro* like the ones in figure 25(d).

The overall appearance of the actin structure observed *in vitro* was always similar to what was seen *in vivo* (see figures 21 and 22) in that the individual filaments pointed away at an angle from the longitudinal axis of the tail and flanked the virus on both sides. The fraction of actin-nucleating viruses was generally higher in less purified samples with more background protein stemming from the viral supernatant, so a compromise between yield of tails and cleanliness of the images had to be established. An example of a preparation with considerable amount of background and a high yield of actin-nucleating viruses is shown in figure 24(e).
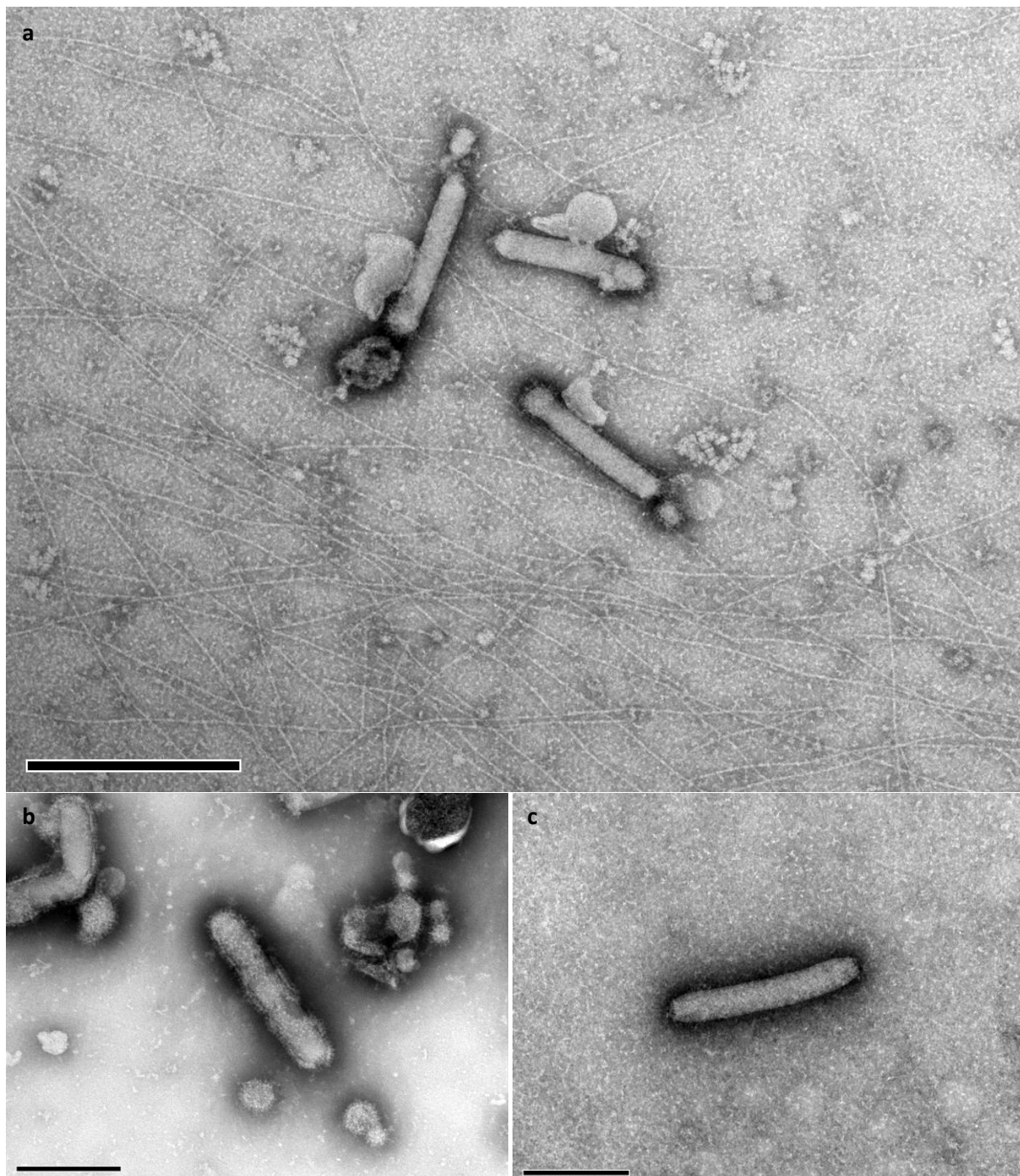
Figure 24 Budded baculovirus and de-enveloped baculovirus. **(a)** Budded baculoviruses are surrounded by a lipid membrane and were not observed with an actin tail. The actin filaments seen in this electron micrograph stem from the motility assay, a feature frequently observed even without a nucleating object present. They were not formed by the enveloped baculoviruses. **(b)** A high magnification image of the budded form of baculovirus shows the lipid membrane, which was always seen somewhat damaged (probably a result of the purification procedure). As these viruses still proved to effectively infect eukaryotic cells, slight damage of the membrane does not seem to impair functionality. **(c)** After treatment with Triton X-100 de-enveloped baculoviruses could be observed. The absence of a lipid membrane is clearly visible. These viruses were used for *in vitro* experiments. Magnifications: **(a)** 44,000x; **(b),(c)** 110,000x. Scale bars: **(a)** 500nm; **(b),(c)** 200nm.
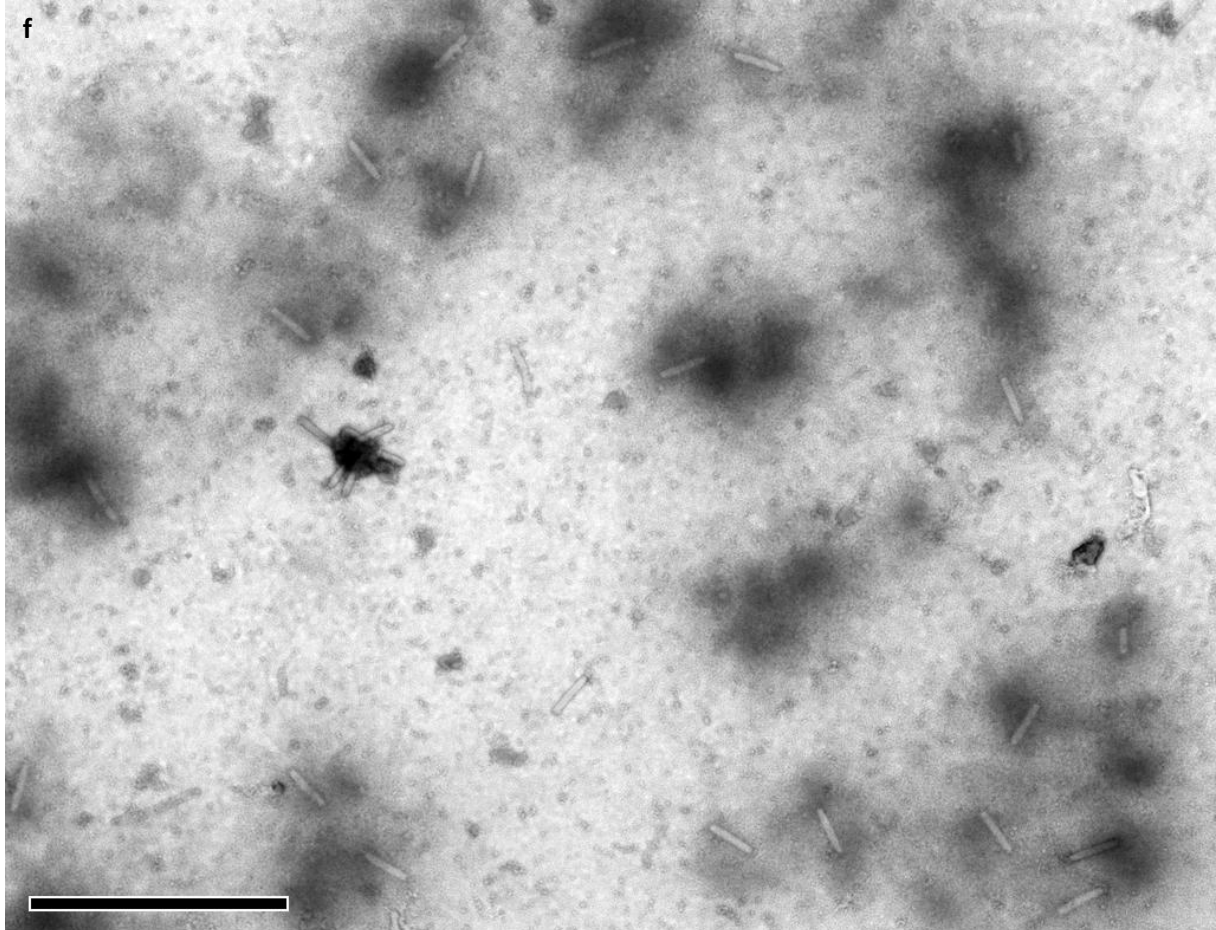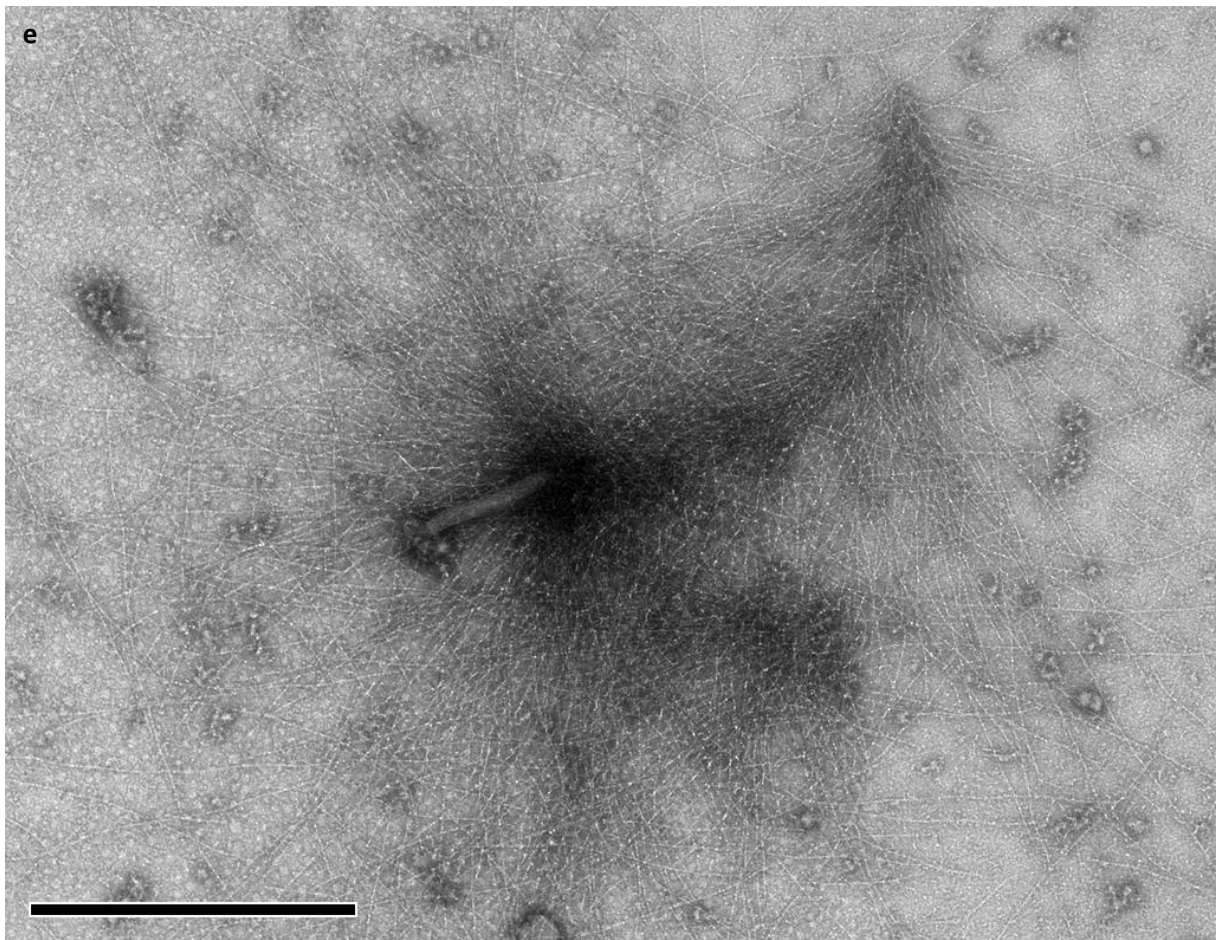
a

b

c

d

e

f
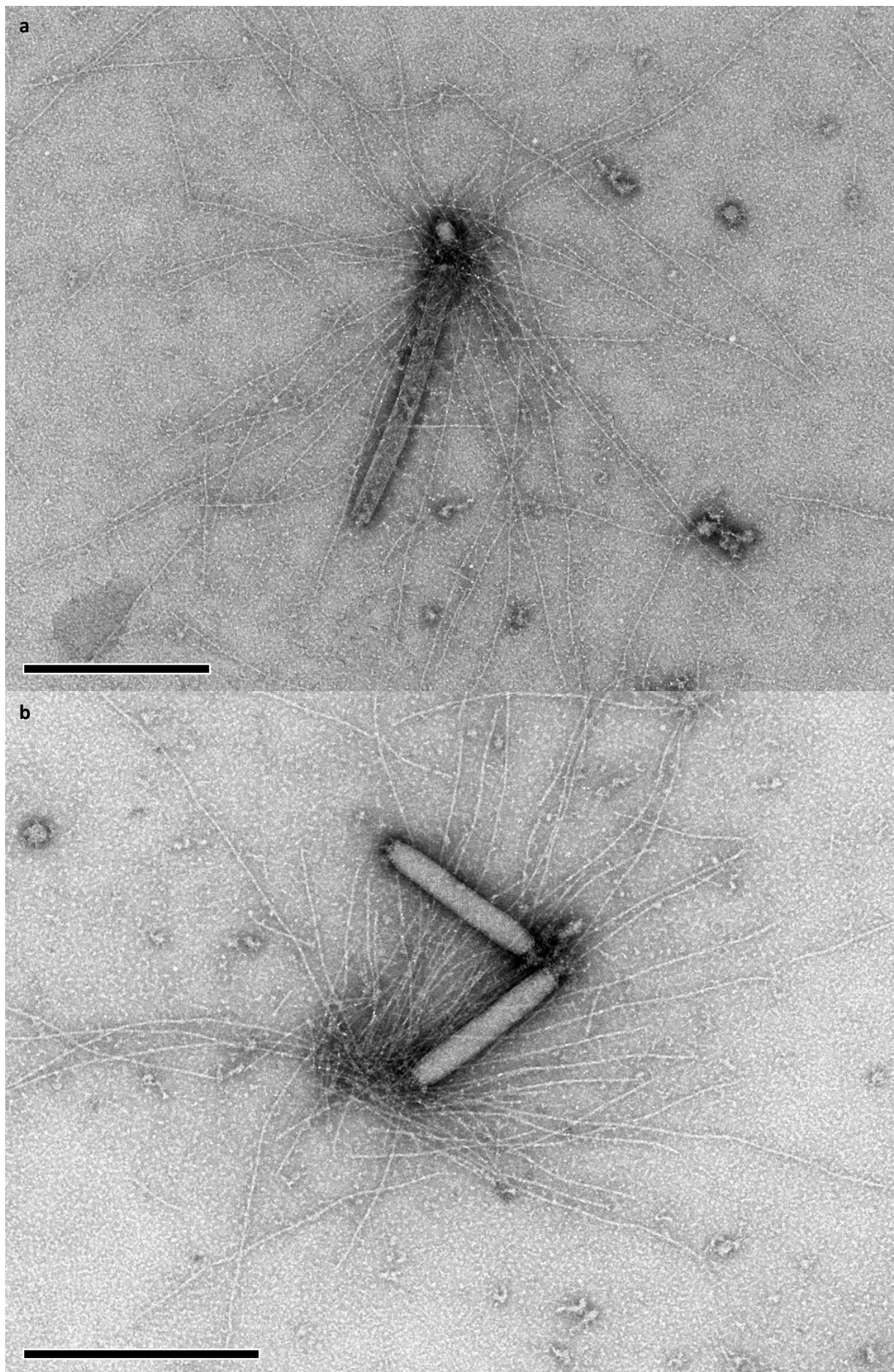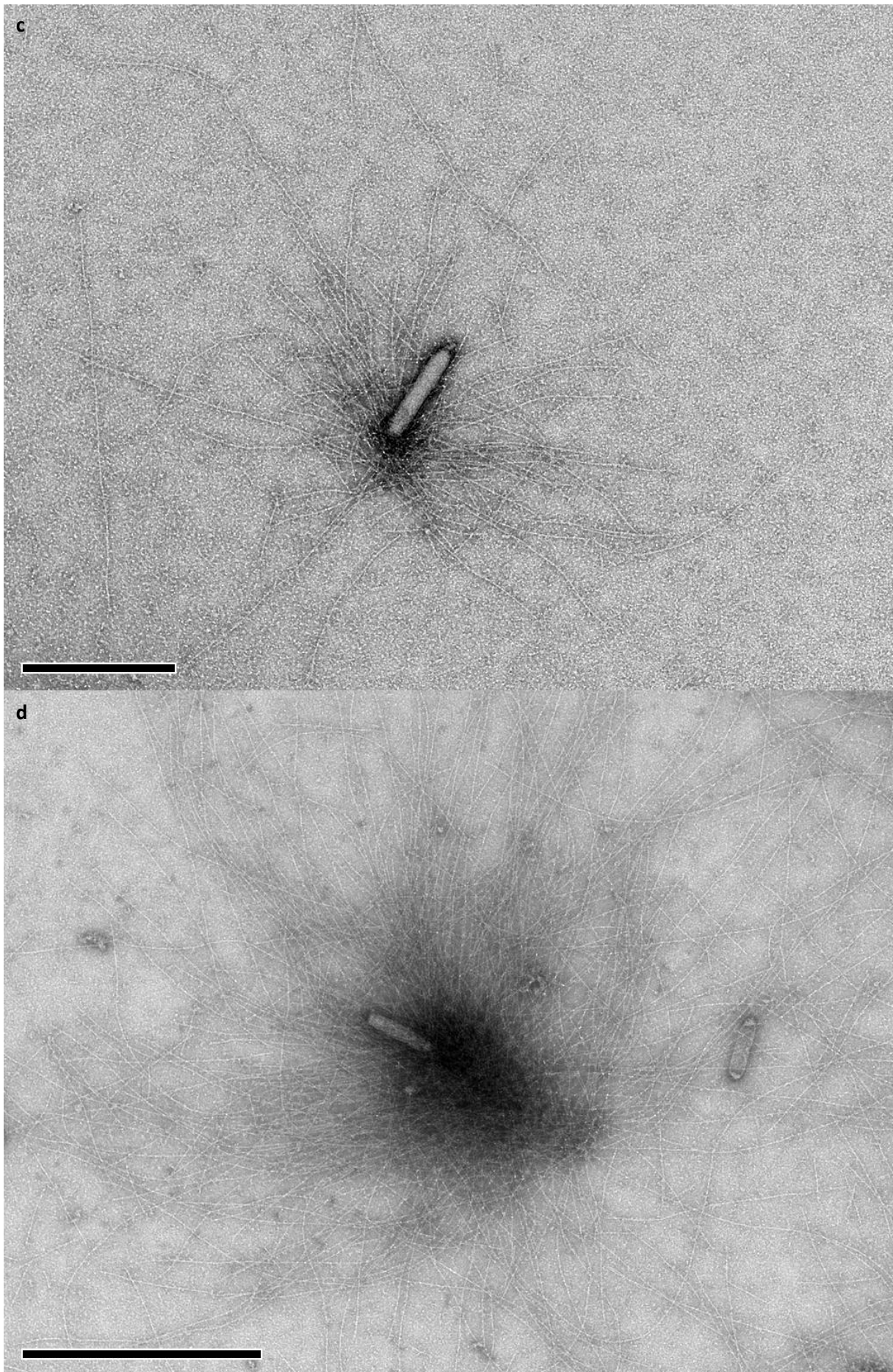
Figure 25 *In vitro* baculovirus-induced actin tails. **(a),(b),(c)** Typical examples of a beginning *in vitro* actin tail. Actin is seen polymerizing from one end of the virus and aligns in a typical pattern on both sides of the virus. **(d)** Further actin polymerization often leads to formation of actin clouds, sometimes even larger than in this image. **(e)** Longer actin tails have rarely been observed *in vitro*, in contrast to *in vivo* samples. Possible explanations are discussed in the next chapter. **(f)** The yield of viruses with an associated actin tail or cloud was increased to nearly 90% by including medium supernatant to the motility mixture. Magnifications: **(a)** 44,000x; **(b)** 56,000x; **(c)** 36,000x; **(d),(e)**28,000x; **(f)** 11,000x. Scale bars: **(a),(b),(c)** 500nm; **(d),(e)** 1µm; **(f)** 2µm.

Gelsolin concentration determines filament length in *in vitro* tails

By altering the concentration of the actin filament capping protein Gelsolin in a range between 20nM and 250nM it was possible to vary the length of individual filaments in the actin tail. Decreasing the Gelsolin concentration yielded longer filaments and vice versa. The length of the entire actin tail was generally higher at increased Gelsolin. Figures 26(a) till 26(d) show the drastic effect of the barbed end capping protein on the length of actin filaments in *in vitro* samples.

Different Arp2/3 and Profilin concentrations did not show significantly different baculovirus-induced actin tails, whereas decreasing ADF as much as two-fold led to a total lack of actin-associated baculoviruses.
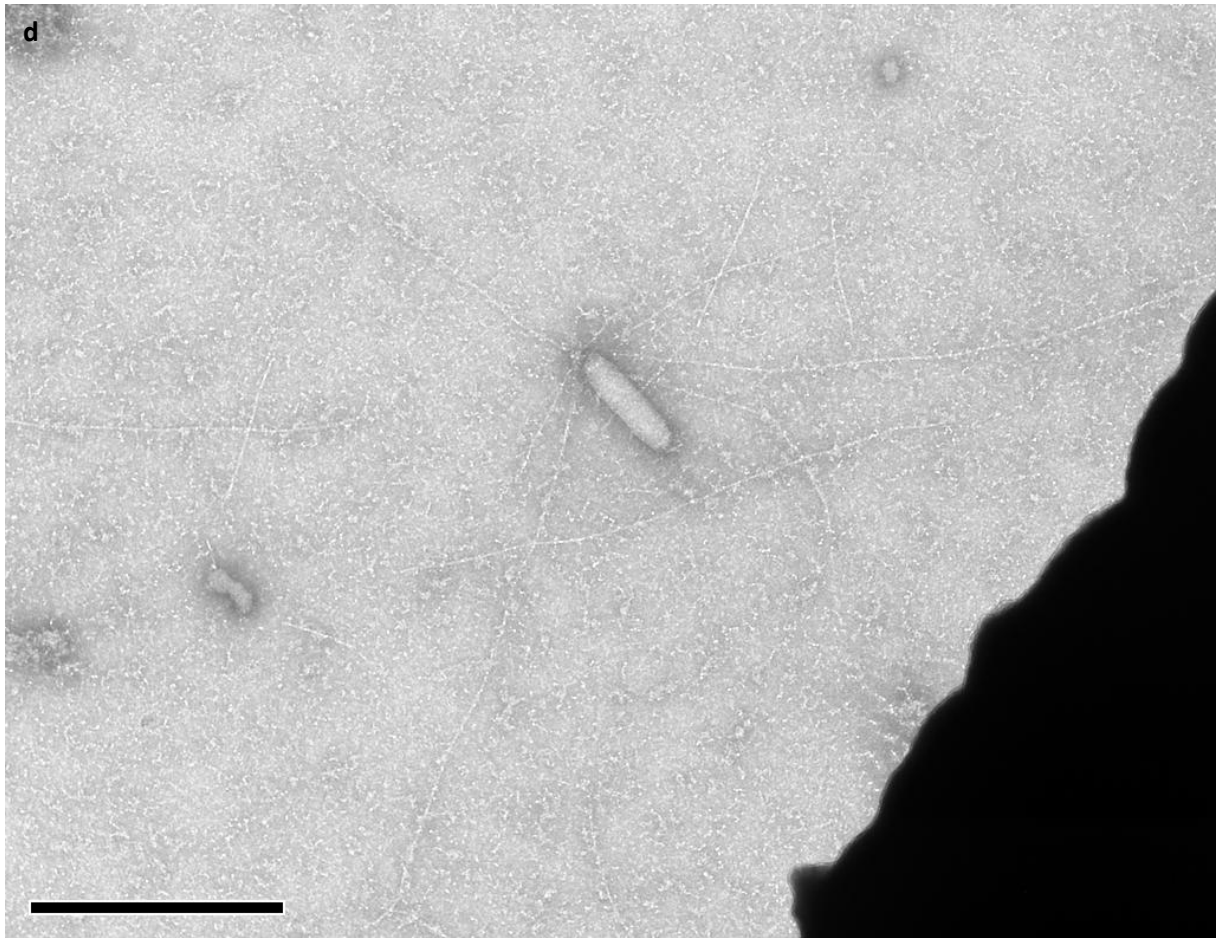
b

c
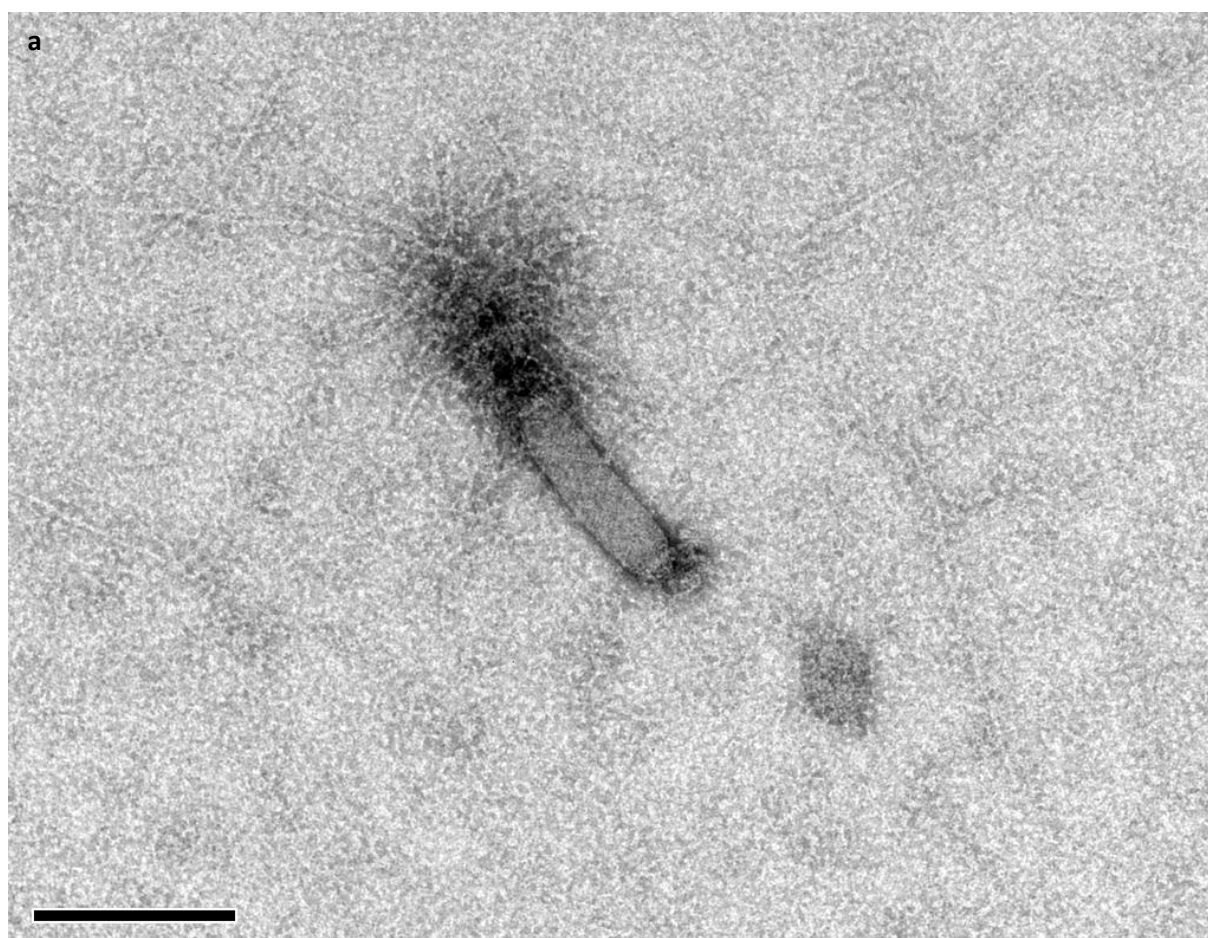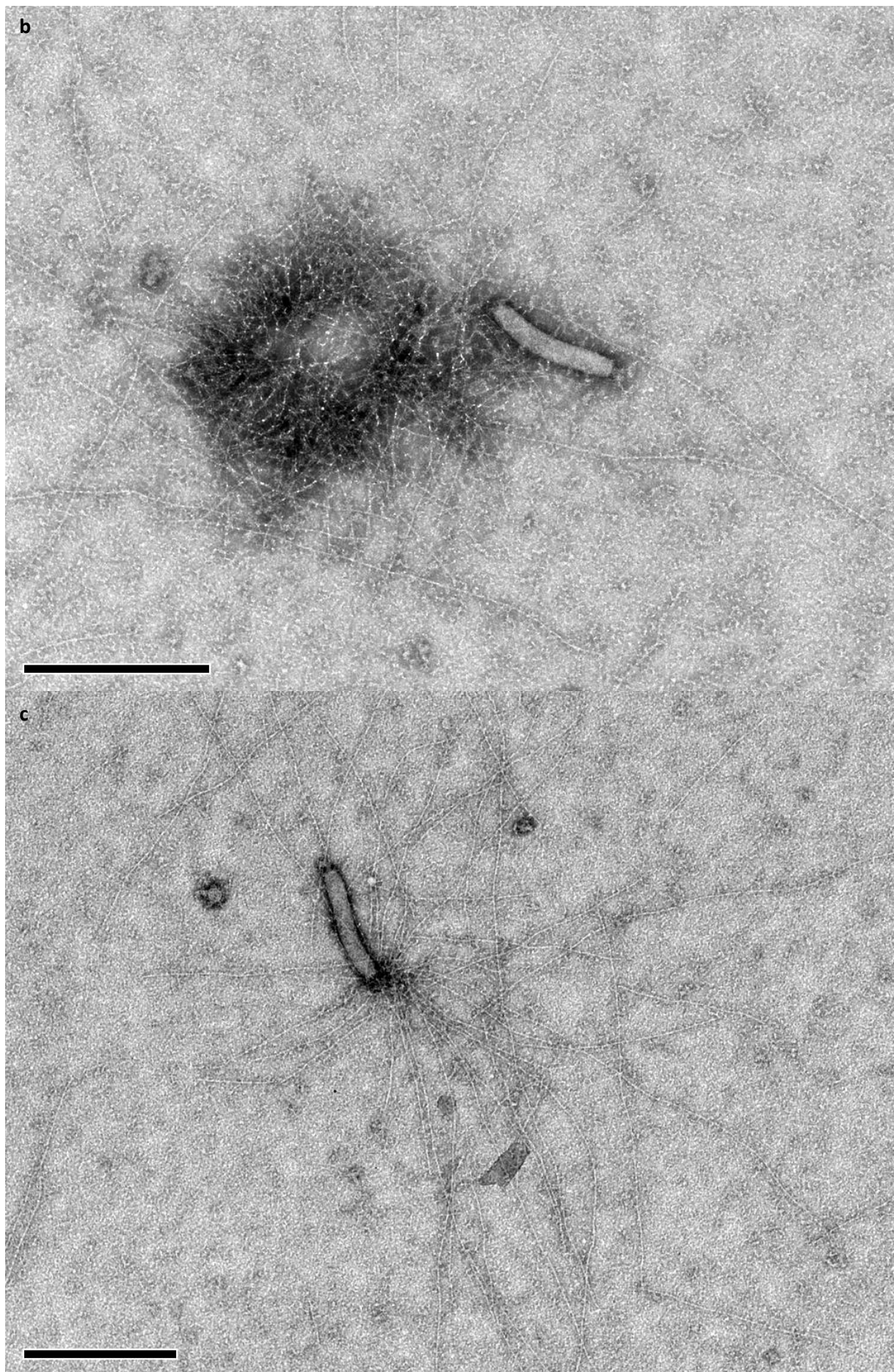
Figure 26 Effect of Gelsolin on the length of *in vitro* polymerized actin filaments. **(a)**,**(b)** At 200nM Gelsolin actin filaments are capped after about 30 to 50nm yielding a very dense tail. At this concentration of capping protein the fishbone-like structure of the tail would not be visible in a light microscope as reported by Wiesner et al. [17]. **(c)**,**(d)** A concentration of 25nM Gelsolin yielded baculoviruses with just a few, very long filaments. Taken together, average filament length was reciprocal to capping protein concentration. Magnifications: **(a)** 89,000x; **(b)** 44,000x; **(c)** 36,000x; **(d)** 44,000x. Scale bars: **(a)** 200nm; **(b)**,**(c)**,**(d)** 500nm.

Electron tomography reveals the 'fishbone'-structure of actin comet tails

As one can see in figure 27, baculovirus-induced actin-tails showed clear-cut fishbone-structure. The filaments emanating from the tail at a distinct fashion were observed by using the conventional electron microscope before, a finding, which was affirmed by the tomography data. More difficult to establish was the exact, three-dimensional position of each individual filament, even more so, as the *in vitro* samples were very collapsed (see figure 27), decreasing the resolution at the Z-direction. *In vivo* comet tails showed less collapse, especially when embedded in deep negative stain retained by adjacent cellular structures like microtubules and actin bundles. Contrariwise cellular actin made tracing virally nucleated filaments an even more difficult task, making harsh extraction conditions necessary, as demonstrated in figure 21.
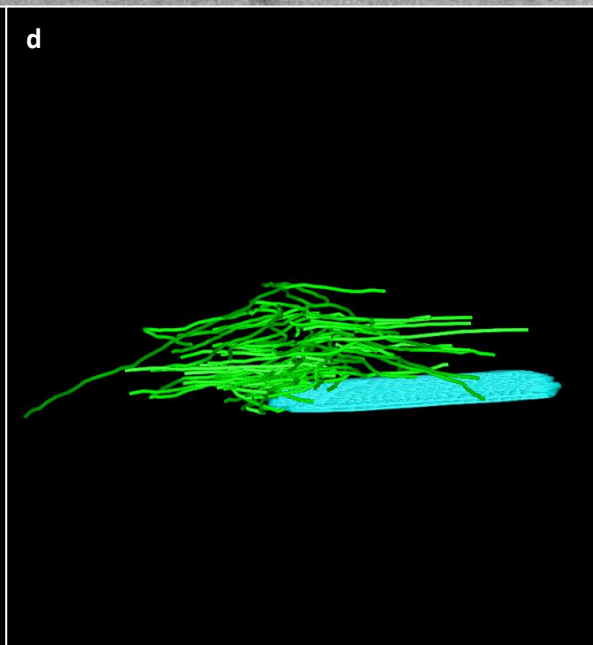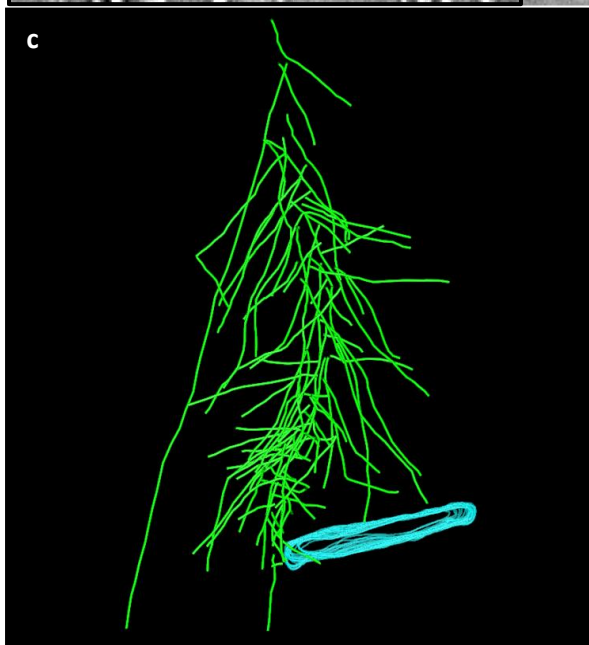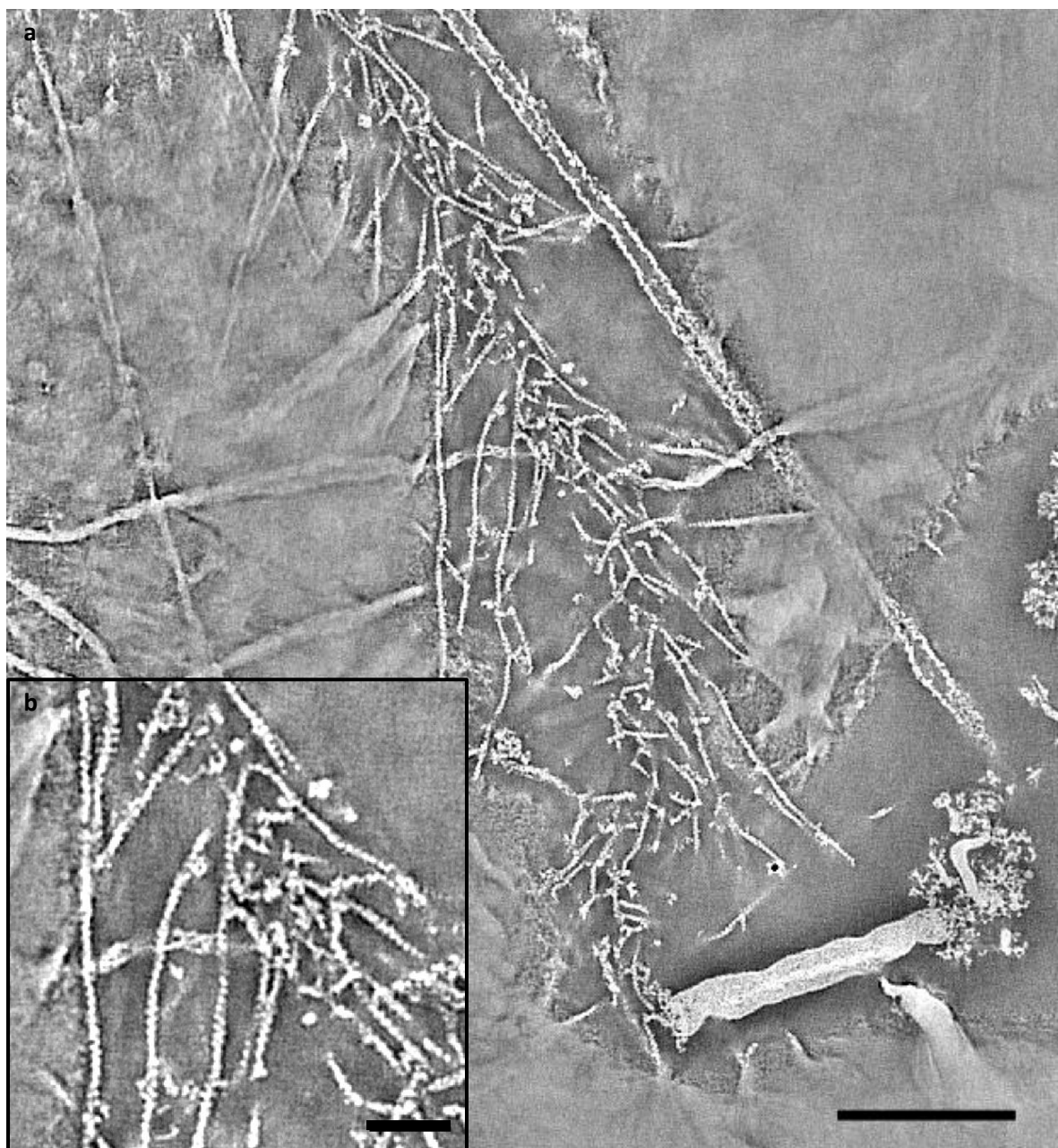
Figure 27 Electron tomography analysis of an *in vivo* actin tail stained with 8% SST. **(a)** Middle section of a baculovirus with a polymerized actin tail and **(b)** detail of the center of the tail with discernable actin substructure. The sample was stained with 8% SST including 1µg/ml Phalloidin. **(c)** Top view of a model based on the tomographic data. Traced filaments of the baculovirus-induced actin tail are shown in green and the virus in blue. **(d)** The front view of the tail serves to demonstrate our difficulties in tracing individual filaments as the tail is collapsed to about 50nm in the Z-dimension. This shrinkage could for example cause overlaps to appear like branches. Scale bars: **(a)** 200nm; **(b)** 50nm.

8% SST yielded the best resolution, estimated around 3nm, but the sample also suffered the most collapse: The tail extended just 30-32nm in the Z-direction (see figure 27), which proved to be an average value for samples stained solely with SST (see figure 28). The ambivalent appearance of a tail stained with 8%SST is illustrated in detail in figure 29: While the sample shows satisfactory actin substructure, the whole height amounts to just 32nm and tracing of the filaments is impaired. Additives to the SST influenced the resulting tomogram, shown in the table below (figure 28): A mixture of 6% SST and 3% $MgAc_2$ ameliorated the situation: The produced tomogram had an average thickness of around 45nm. Although the resolution in the Z-direction was correspondingly better, the tracing of individual filaments was impaired by the thickening effect of the additive. As seen in figure 30, $MgAc_2$ led to thicker appearance of actin filaments and masked the filament substructure, which could be clearly observed with pure SST. Addition of 1% or 2% Glucose did not result in notably decreased collapse but addition of 0.5% poly-vinylalcohol (PVA) helped increase the height to about 50nm on average, without interfering with visualization of the filament substructure.
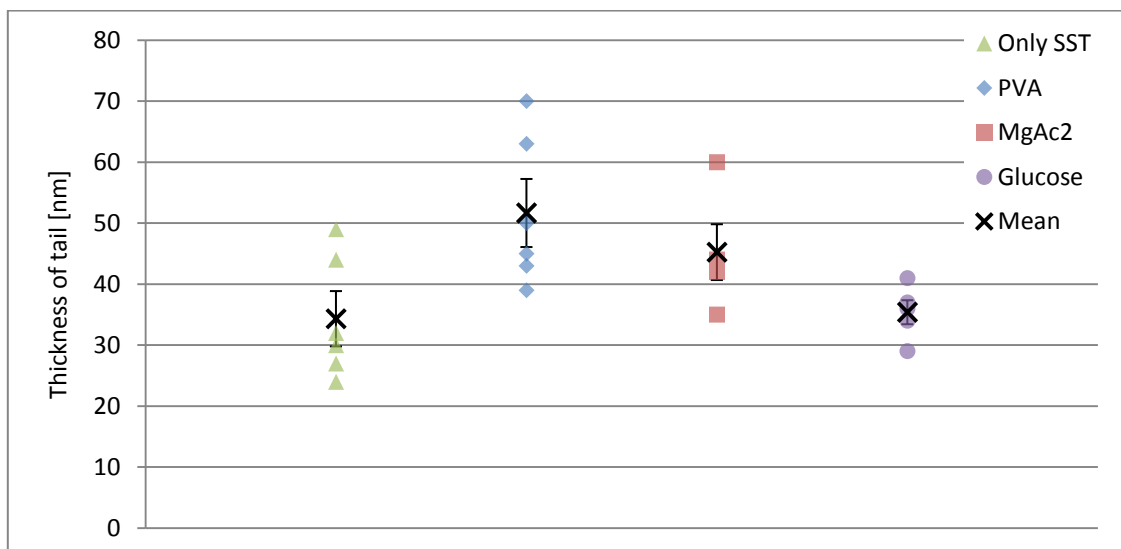
Figure 28 Effects of different additives on tail thickness. To improve resolution in the Z-dimension different substances were added to pure SST. From these three additives PVA proved to be the most advantageous, combining a significant increase in thickness and preservation of substructure. The outliers seen for pure SST, PVA and $MgAc_2$ were invariably observed at samples with exceptional retention of stain by larger adjacent structures demonstrating the equal or even more important influence of the cellular environment on sample preservation.
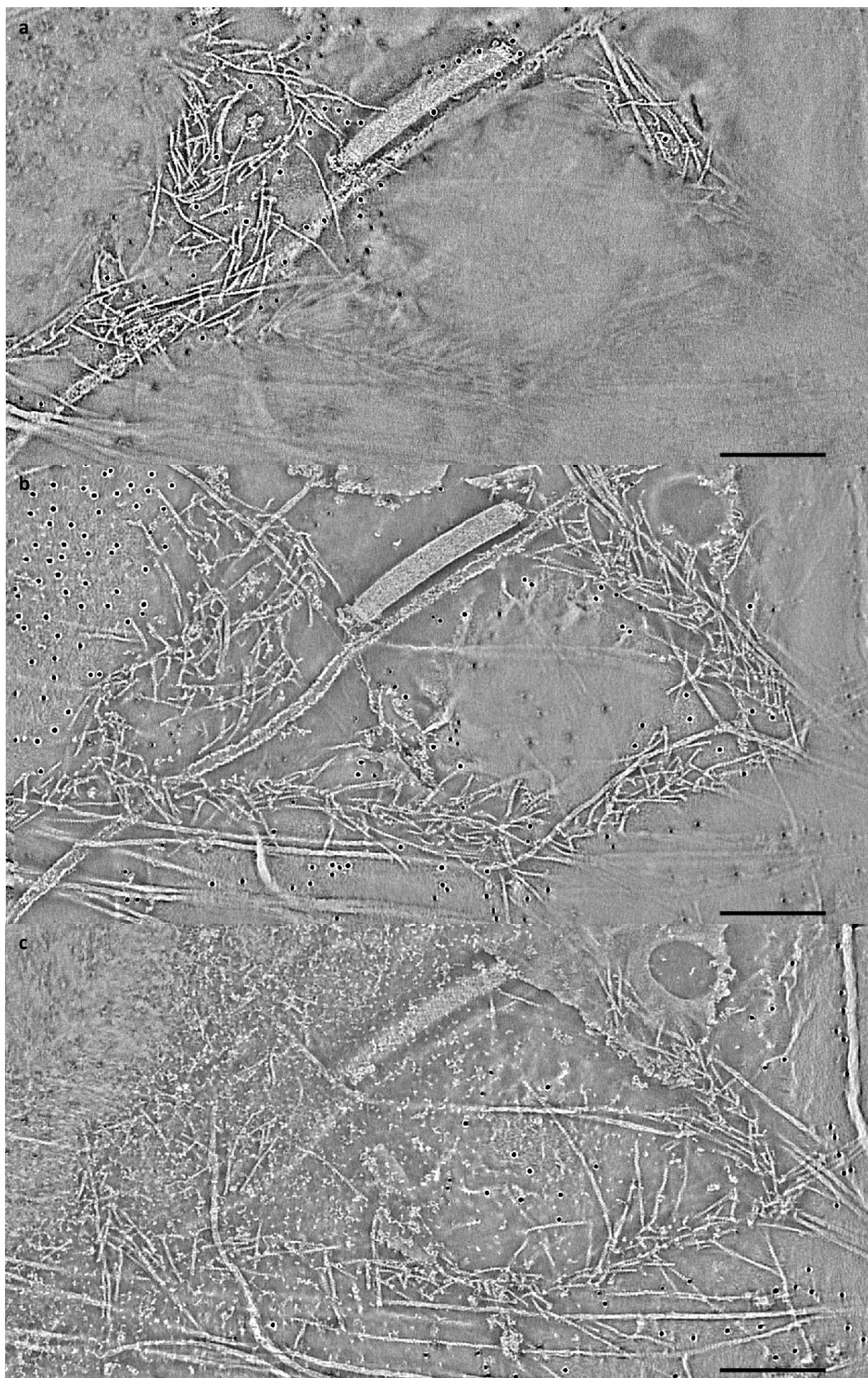
Figure 29 Thickness of a typical sample stained with 8% SST. **(a)** Top, **(b)** middle and **(c)** bottom section of the actin tail. The chosen sections are 6.5nm apart and do not represent the very last sections used for thickness measurement but rather positions in the upper and lower fifth of the tomogram. The whole tail amounts to about 32nm in the Z-direction. Scale bars **(a)**,**(b)**,**(c)** 200nm.
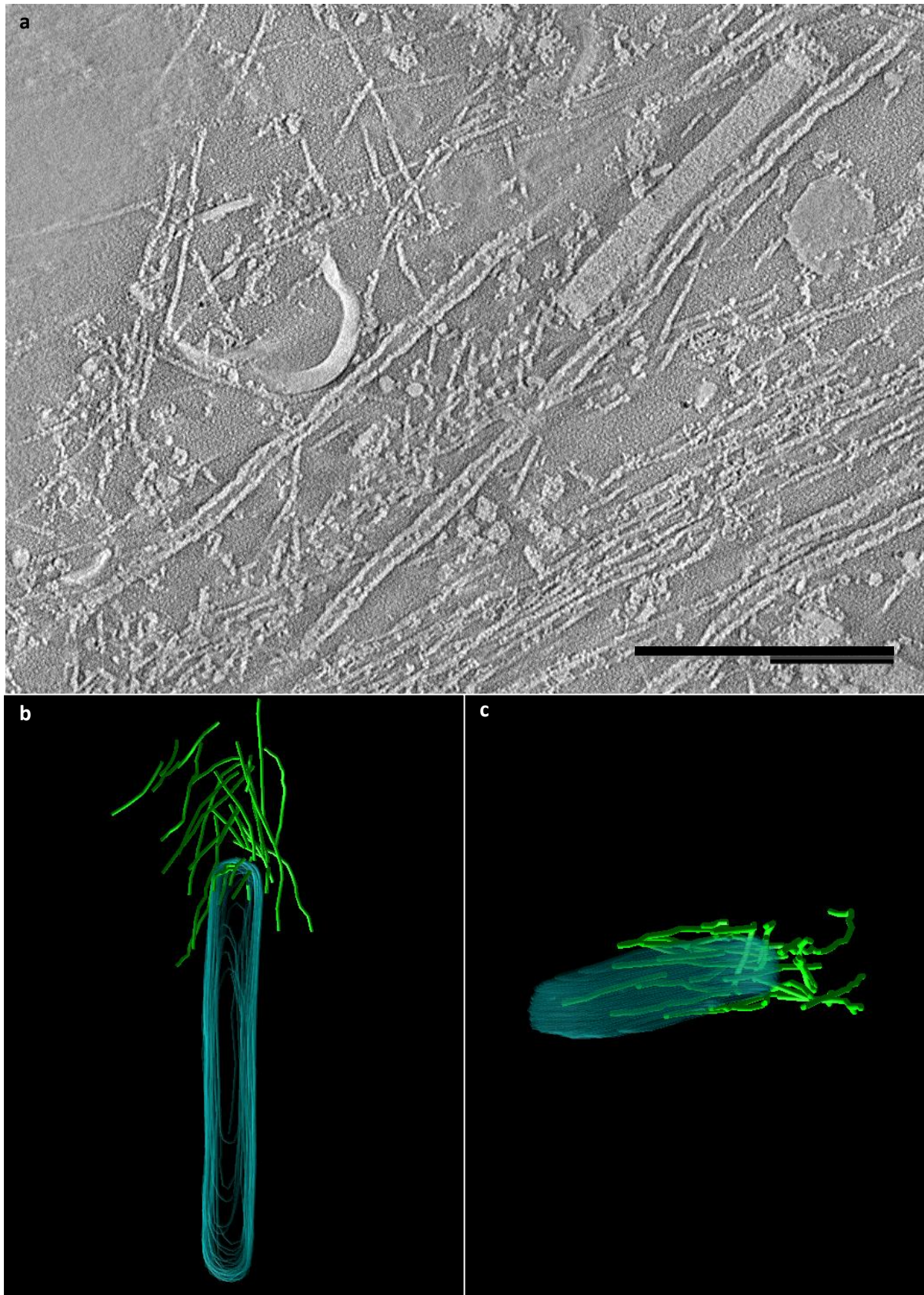
Figure 30 Baculovirus-induced actin tail stained with 5% SST supplemented with 3.2% $MgAc_2$. **(a)** Tomogram middle section corresponding to a slice of 6nm. The unusual, thickened appearance of actin filaments made tracking difficult. Two microtubules can be seen flanking the actin comet tail on both sides. The deep pool of negative stain formed thereby conferred an exceptional thickness of 63nm. **(b)** Top and **(c)** front view of the baculovirus with connected actin tail, showing better Z-preservation than the sample with only SST (figure 27). However, tracing was hampered by the thickened filaments. Scale bar: **(a)** 200nm.

An example of a baculovirus-induced actin-tail stained with 6% SST and 0.5% PVA is shown in figure 31. Samples located in between two larger structures, which formed a deeper pool of negative stain, were even up to 70nm in height. Generally, the local microenvironment of the virus-induced tail appeared to have a profound influence on tomogram quality and thickness. A summary of the diverse effects of different additives is shown in figure 28.

Despite prolonged efforts it proved very difficult to trace actin filaments in the middle of a comet tail unambiguously.
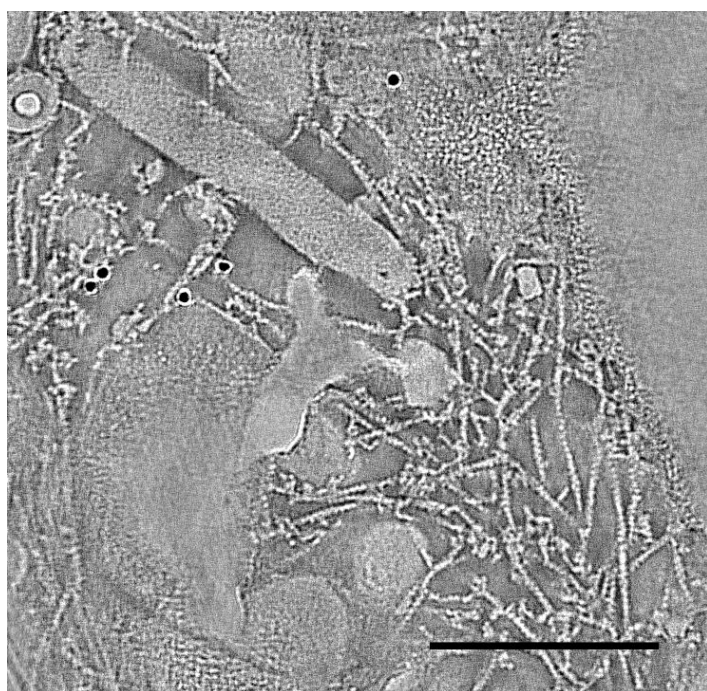
Figure 31 Baculovirus-induced actin tail stained with 5% SST supplemented with 0,5% PVA. This mixture preserved actin filament substructure, which is seen in the middle section corresponding to 4nm on the right. Furthermore PVA provided better preservation of sample thickness. A model based on a tomogram acquired of an SST- and PVA-stained sample is presented in the discussion chapter. Scale bar: 200nm.

DISCUSSION

Microtubules

ATP-polymerized microtubules are stable at high ATP concentrations

The agreed-upon dogma in biochemistry is that microtubules use the energy derived from GTP hydrolysis for polymerization, whereas actin filaments use ATP. Indeed, ATP causes rapid microtubule depolymerization *in vitro* as shown in figure 14. Attempts to stabilize microtubules polymerized by GTP with Taxol or even Glutaraldehyde failed, as did tries with GMPCPP-seeds, which also depolymerized at high ATP concentrations. Incubating Tubulin with ATP was shown to polymerize microtubules slower than with GTP and bind to microtubules with more than 100-fold lower affinity [80], but ATP lowered the critical concentration of Tubulin for microtubule polymerization [81]. I did not monitor kinetic parameters in my experiments, so from the obtained data one can only describe the morphology of ATP-polymerized microtubules.

As described in the results, I never observed any difference between GTP- and ATP-polymerized microtubules neither in fluorescence nor in electron micrographs, different from earlier results (see figure 32). One explanation for this apparent inconsistency could be residual GTP in the Tubulin or fluorescently labeled Tubulin used for polymerization. As mentioned before and already shown in another study [82], ATP and GTP can act synergistically to polymerize microtubules at below critical concentrations for each individual nucleotide. The 2.5mM ATP in the polymerization mix could have been complemented by a small, but significant amount of residual GTP, so the microtubules were polymerized at the presence of both nucleotides. If this was indeed the case, then these 'mixed' microtubules with both ATP and GTP would also be resistant to high levels of ATP without showing the morphological abnormalities described in earlier studies.

Another explanation could be the use of glutaraldehyde for fixing ATP-polymerized microtubules in the mentioned, earlier study [29]. This fixative could have preserved the globular state of ATP-polymerized microtubules shown in figure 32, which could be only transient and therefore disappear in the unfixed samples presented in figure 14.

Taken together, I managed to yield ATP-resistant microtubules with normal appearance by polymerization at high ATP. This small adaptation could prove useful for different applications: Most importantly for *in vitro* assays of ATP-consuming processes, but also in the field of nanotechnology for construction of systems with ATP-driven motors in the presence of F-actin.
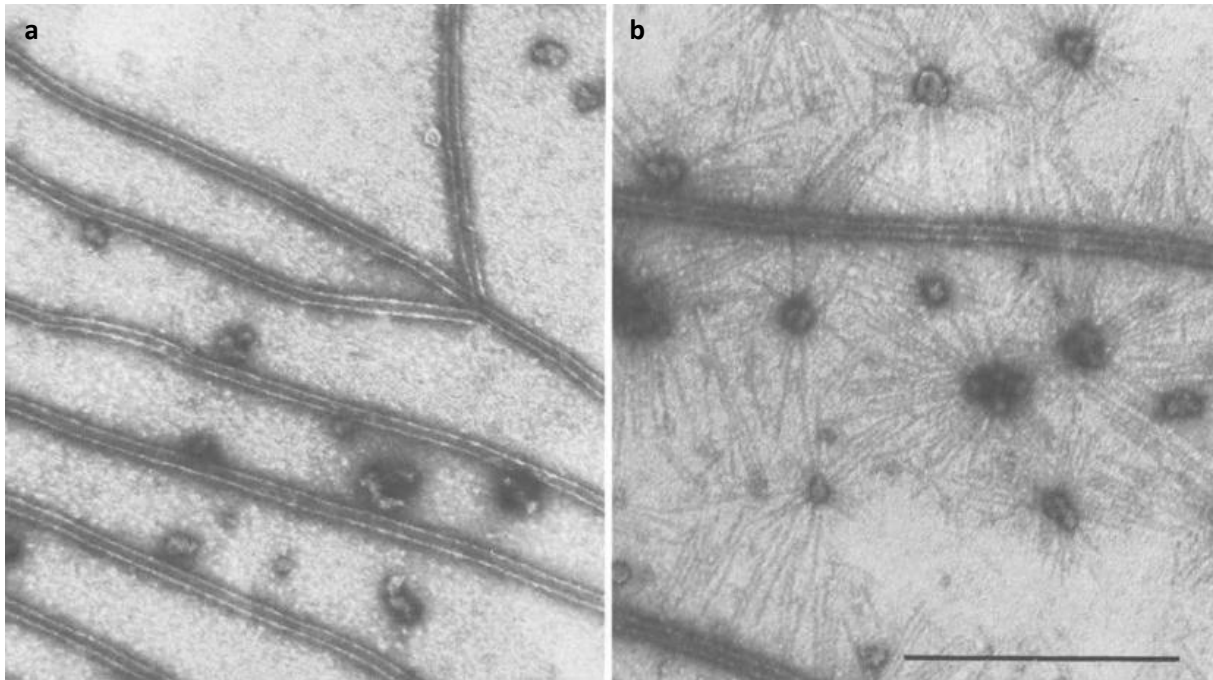
Figure 32 Comparison of GTP- and ATP-polymerized microtubules in an earlier study. **(a)** Microtubules polymerized at 50μM GTP and **(b)** 50μM ATP. In this study by Islam et al. in 1984, the ATP-polymerized microtubules were morphologically abnormal: They formed globular structures with single protofilaments radiating out on every side [29]. These abnormalities were not found in our samples (see figure 14). Scale bar: 500nm.

MBD-WA bundles microtubules and nucleates actin
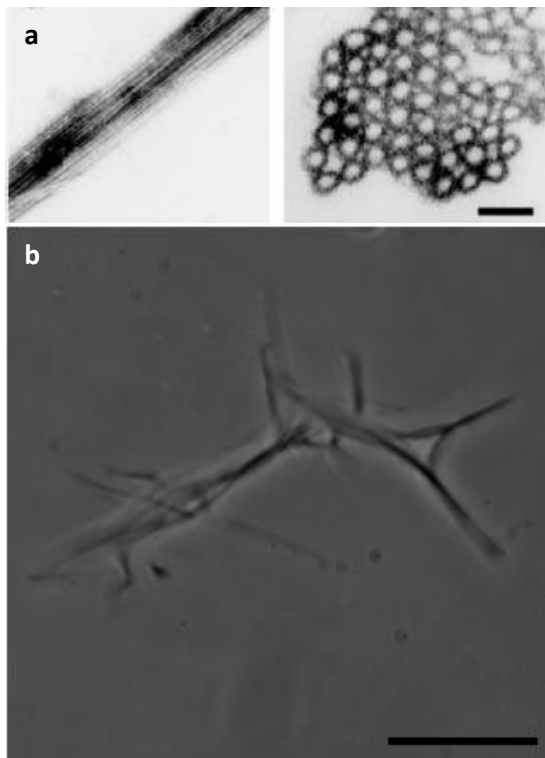
The region of MAP4 used for this study only contains the microtubule-binding domain (MBD) of the MAP4 R4β isoform. The cDNA sequence was cloned between a His-tag and a mouse WA-domain, schematically shown in figure 34. As described earlier, the N-terminal acidic

Figure 33 Effect of the microtubule binding domain of MAP4 on microtubules. **(a)** Thin section electron microscopy of microtubules bound to the microtubule binding domain of MAP4 [30] Image taken from Iida, 2002 [30]. **(b)** Phase contrast microscopy of microtubules decorated with MBD-WA, showing a bundling effect as well. To produce single microtubules bound to a nucleator, the cloning of a larger fragment of MAP4 – including the projection domain – would be necessary. Magnification: **(b)** 100x. Scale bars: **(a)** 50nm; **(b)** 10μm.

projection domain is necessary to avoid MAP4-induced bundling of microtubules [84]. In light of these findings the bundling, I observed following incubation with the truncated form of MAP4, could be expected. If this experiment were to be repeated, one should consider the option to add part of the N-terminal projection domain to the expressed construct. This way the bundling of microtubules could be minimized, possibly allowing a better resolution of individual filaments emanating from microtubules using electron microscopy.
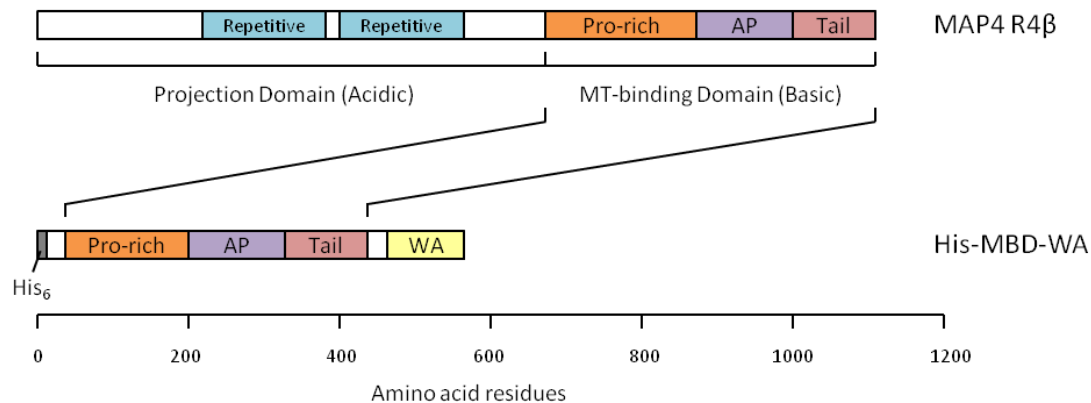
Figure 34 Diagram of the recombinated protein used for binding microtubules and nucleating actin. The projection domain was omitted from the peptide, most probably causing the observed bundling of decorated microtubules.

MBD-WA nucleates filaments from microtubules

This work shows the feasibility of nucleating actin filaments from microtubules by a fusion protein comprising a microtubule-binding and an actin-nucleating domain. A tool to assess actin-nucleating activity *in vivo* is being developed by Margit Oelkers and Klemens Rottner at the Rheinische Friedrich-Wilhelms University of Bonn. Using similar constructs with different nucleators attached to a microtubule binding domain, the nucleating activity can be measured directly with a fluorescence microscope.

Interestingly, the actin filaments were shown to decorate the microtubules rather than emanate away from them as in the fluorescence pictures shown in this work. A possible explanation for this discrepancy could be the concentration difference of actin-regulating proteins like Gelsolin and ADF, which can be manipulated arbitrarily *in vitro* but are set at physiological levels *in vivo*. As was shown with baculoviruses (see 'Results' section), gelsolin shortens the average length of actin filaments by capping free barbed ends.

To thoroughly investigate the differences and the structure of actin filaments attached to microtubules, electron tomography will be necessary. Not only would these studies be valuable to contribute to our understanding of the situation at the cell front, where also an immobilized protein activates Arp2/3 to nucleate filaments, but actin emanating from microtubules is a common phenomenon *in vivo* still awaiting structural analysis [104],[105].

Baculovirus

Quick and efficient baculovirus purification

Various methods for baculovirus purification from viral supernatants including growth medium, serum and catabolic side products have been published. At first, baculoviruses were isolated by plaque purification [87]. Several chromatographic methods were used for baculovirus purification: One approach involved generation of a baculovirus strain expressing a chimeric gp64 fused to a His_6-tag which was then used to purify baculoviruses by immobilized metal affinity chromatography (IMAC) to about 87% purity [88]. This method requires additional cloning and chromatography steps and does not work with de-enveloped baculoviruses as the method applied in this study. Baculovirus purification by Concanavalin A chromatograpy was reported as an elegant approach taking advantage of the affinity of Cancanavlin A to Lectins like gp64. This allowed the authors to omit the cloning step and resulted in elution of baculovirus of 99% purity and 21% recovery [89]. Another group used size exclusion chromatography (SEC) and achieved about 25% recovery [90]. Finally, ion-exchange chromatography was used to capture baculoviruses on a cation-exchange membrane unit and eluted with high NaCl concentrations, a procedure capable of recovering 78% of the baculoviruses [91]. All these methods are more laborious than the one presented in the present study, while yielding similar purities as judged by denaturing gelelectrophoresis. To my knowledge the only published method of similar simplicity employs ultracentrifugation to pellet baculoviruses from supernatants at 45,000g [92]. The authors report recovery of 99% of the infectivity in the resuspended pellet. This method is similar to the one used here, with the difference of demanding considerably higher centrifugation speed, more time and sophisticated equipment.

I could show that baculoviruses can be purified to high purities using a simple benchtop centrifuge at 18,000g. This speed was used as standard protocol, yielding nearly 99% recovery in the pellet (see figure 19). Other results, which were not shown in this work, suggested that baculoviruses can be pelleted at speeds as low as 15,000g. In light of these findings, I believe that baculoviruses could be obtained at very high purities by centrifugation at around 10,000g and a subsequent round at 15,000g. This procedure should yield highly concentrated and purified baculovirus and to my best knowledge would still be quicker and easier as all other published methods of baculovirus purification.

Proteins incorporated into actin comet tails

In 1999 the core proteins necessary for propulsion of *Listeria monocytogenes* were established by Pantaloni, Carlier and coworkers [16]. Since then many additional proteins have been discovered to be part of pathogen-induced actin tails *in vivo*. A comprehensive study from 2008 revealed the entire actin comet-tail 'proteome' by isolating *Listeria*-induced comet tails and analyzing their protein content [85]. Unsurprisingly, comet tails contain up to 95% actin and considerable amounts of Arp2/3, α-Actinin, Coronin, Cofilin and *Listeria* ActA also recruits Ena-VASP to the tail. Activators of nucleation like VASP are probably not

absolutely required in *Listeria* [86] and were not localized in the baculovirus-induced tails. According to this result the WH2 domain of p78/83 is sufficient to nucleate actin in order to form a comet tail.

In 2010 a study on baculovirus proteomics was published analyzing baculoviruses purified by ultracentrifugation from Sf9 cell supernatants [32]. Among the host proteins identified by mass spectrometry are actin and ADF. Furthermore the authors reported the presence of 14-3-3 and the small GTPase Rho, both also observed in *Listeria*-induced tails.

To summarize, the available data suggests the existence of a core set of proteins necessary for actin-based propulsion of pathogens remarkably conserved among different species. The basic proteins seem to be the ones present in the motility assay with the exception of Profilin. A possible candidate, which could be missing from the motility mixture for baculoviruses, is discussed below.

In addition to examining the presence of Arp2/3, WASP and VASP in baculovirus-induced comet tails, I tried to localize the nucleator Arp2/3 by using a biotinylated from of Arp2/3 as well as immuno-labelling. Unfortunately, both efforts failed. This could be due to several reasons: The high presence of soluble Arp2/3 in the sample could have titrated out the antibodies; the affinity of the used antibodies could have been too low for purified Arp2/3; the Arp2/3 complex could have been washed away during one of the washing steps without fixation or the epitopes could have been destroyed by glutaraldehyde fixation.

Baculoviruses infect several eukaryotic cell lines

In line with previous findings of baculoviruses infecting human hepatocytes [93], neural cells [94] and fibroblasts [95] concentrated baculovirus suspensions were capable of infecting each of the used cell lines. The observed viral tails were similar in length, only the tails polymerized in infected 3T3 cells appeared shorter. The propulsion speed was very diverse (8 to 22μm/min) also among measurements in the same cell. This difference could be due to the various microenvironments a pathogen encounters on its way through the host cell. The dense actin meshwork of the lamellipodium as well as microtubules and networks of intermediate filaments are possible physical hindrances slowing down a baculovirus that is pushed forward by polymerizing actin. Electron micrographs of intracellular baculoviruses like the one shown in figure 21 support this hypothesis further: The parts of an actin tail that had been polymerized in front of an obstacle like a microtubule contain more filaments per length unit than areas polymerized in parts of the cell lacking such objects. This locally increased actin density within an actin tail was observed in *Listeria* after a deletion in ActA [96], in WA-coated beads of sufficient size [97] and GUVs incubated at low Gelsolin and high Arp2/3 [19]. All of these studies reported slower movement during the polymerization of a densely packed tail, suggesting a similar effect could occur in baculovirus-induced tails. According to this hypothesis the observed locally slower movement in live-cell images would

correspond to the dense parts of the actin tail in electron micrographs, linking and explaining both observations.

Other parameters like mean length and persistence time of the baculovirus-induced tails differed as well among the studied cell lines as described in the 'Results' section. However, for a thorough investigation this matter would need more extensive experiments with appropriate controls, something I did not have the time to do, as the focus on this work was placed on elucidating the structure of actin tails.

Baculoviruses move preferentially along microtubules

This movement constitutes a different viral approach than the previously described modes of hijacking intracellular trafficking mechanisms [41]. Instead of moving with motorproteins like Dynein, baculoviruses stay associated with an actin tail but slide alongside intracellular microtubules. Unlike vaccinia virus which relies on kinesin during intracellular transport along microtubules [5], baculoviruses clearly cannot distinguish between plus- and minus-ends of the microtubule they are following. In our samples, outward movement was observed as frequently as movement towards the centriole. Indeed, the angle, at which the virus met the microtubule, seemed to be the only factor influencing the direction of movement.

Microtubules are found in other comet tails as minor constituents as well [85]. In baculoviruses they certainly play a role during specific stages of infection. One reason for the virus to move alongside the microtubule cytoskeleton could be the proximity of the centriole to the nucleus – the primary target of actin-polymerizing baculoviruses. As the movement seems to not be influenced by microtubule polarity, another, more basic rational could be a question of sheer speed: In the crowded environment of the cell, microtubules could provide relatively straight 'highways' for baculoviruses to travel through their host. Velocities of baculoviruses attached to a microtubule were in the range of the ones migrating freely, but the tracks of the former viruses appeared much straighter than the latter. Even though the speed would be the same, the viruses would manage to travel between the cell periphery and the nucleus faster, if they followed a straighter path.

As shown in figure 35, baculoviruses usually contact the microtubule with their anterior region. From tomograms like these it appears that the virion contains a microtubule-binding receptor that allows sliding alongside microtubules. No particular microtubule-binding capsid proteins are described, so a simple one-step affinity chromatography with immobilized microtubules could help to clarifiy this issue.
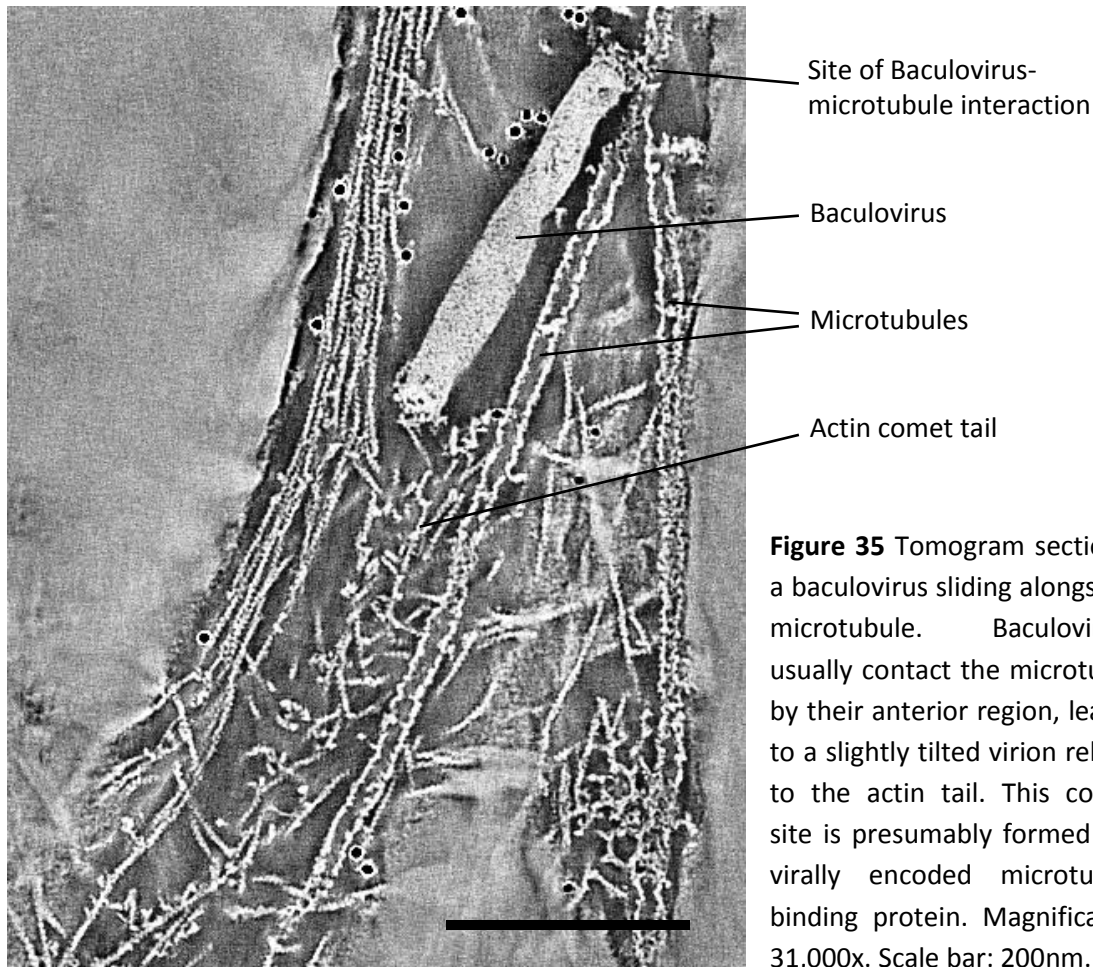
Site of Baculovirus-microtubule interaction

Baculovirus

Microtubules

Actin comet tail

Figure 35 Tomogram section of a baculovirus sliding alongside a microtubule. Baculoviruses usually contact the microtubule by their anterior region, leading to a slightly tilted virion relative to the actin tail. This contact site is presumably formed by a virally encoded microtubule-binding protein. Magnification: 31,000x. Scale bar: 200nm.

In vitro polymerized actin tails

Actin polymerization at the rear ends of purified baculoviruses incubated with the actin motility assay was only seen when Triton X-100-treated viruses were used. This result is consistent with the existing data postulating a baculovirus life cycle, where the viruses shed their lipid membrane together with the major envelope protein gp64 upon entering the host. It is only after the underlying capsid proteins have been exposed, that baculoviruses are capable of polymerizing G-actin into actin filaments.

An interesting form of actin polymerization was observed at the ends of purified, de-enveloped viruses: Actin filaments could be seen emanating from one end of the virus, but counter-intuitively pointing away from the direction of movement. Due to the filaments pointing sideways the tails did not have a streamlined shape, assuming the baculovirus was positioned at the front of the tail, being pushed from behind. Possible models accounting for this observation are discussed below.
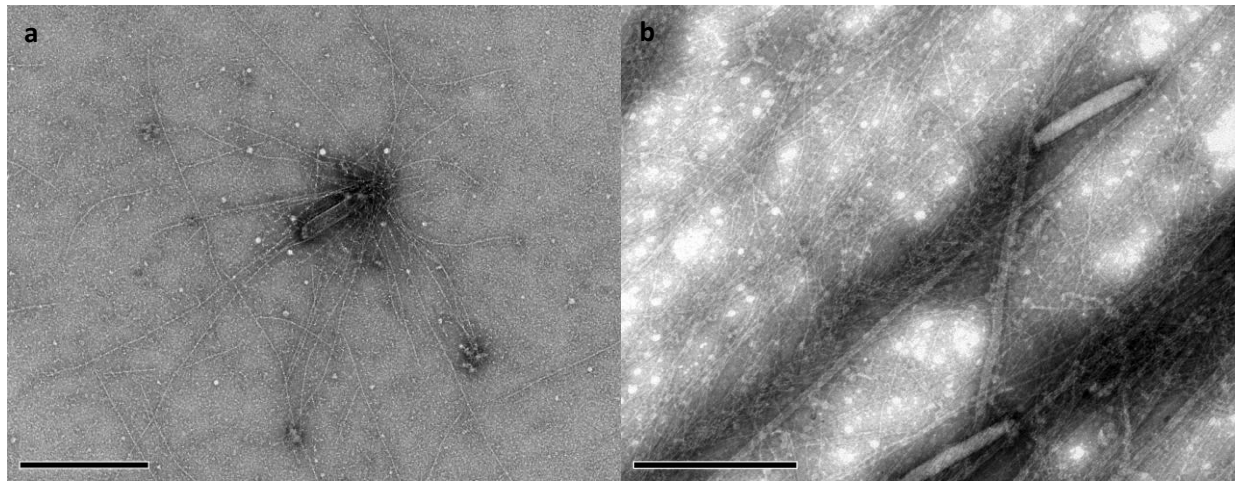
Figure 35 Comparison of *in vitro* and *in vivo* polymerized actin tails. **(a)** Baculovirus-induced actin tail *in vitro* and **(b)** *in vivo*. The most evident difference is the greater length of *in vivo* actin tails, whereas the fishbone-like structure occurs both *in vitro* and *in vivo*. Possible explanations for this observation are discussed in the text. Magnifications: **(a)** 44,000x; **(b)** 56,000x. Scale bars: **(a)**,**(b)** 500nm.

Strikingly, the *in vitro*-tails appeared similar to the *in vivo* polymerized tails, with the exception of being shorter and denser. Perhaps the baculoviruses adhered to the carbon surface, so the actin filament polymerization did not build up enough force to push the virions forward. However, grids coated with BSA, Poly-Lysine and Formvar were examined, all showing viruses producing the same short, dense tails. Another possible explanation is the lack of traction between the polymerizing actin filaments and the substrate. In living cells baculoviruses have access to vast amounts of actin filaments and other cellular structures, where the emerging actin tail could be anchored. These anchors are missing in the motility assay. While beads, GUVs and nanowires coated with nucleator are pushed forward efficiently by polymerizing actin, this could be due to a different mechanism of actin tail formation. Comet tails polymerized from these objects seem to emerge by actin shell build-up and subsequent shell-breaking [99]. Judging by their structure, baculovirus-induced actin tails seem to rely on a different mechanism. A third possibility could be the need for essential proteins present in the cellular environment but absent in the *in vitro* system. α-actinin is a crosslinking protein [62] present in pathogen-induced tails [85]. By crosslinking newly polymerizing actin filaments to older filaments of the actin tail α-actinin could provide traction necessary for pushing a load forward by exploiting actin polymerization. The very few longer tails that were observed *in vitro* could have occurred at spots of high local α-actinin concentration stemming from the semi-purified baculovirus stock. This hypothesis will be tested by a two-step experiment: First, co-transfecting CAR fibroblasts with fluorescently labeled actin and α-actinin and monitor the presence of α-actinin in the baculovirus-induced actin tails. Second, if the assumption is valid, including purified α-actinin to the motility assay should give a morphological difference of *in vitro* tails.

The fraction of actin-polymerizing baculoviruses varied heavily between different preparations. There are many parameters that could affect tail formation including humidity, temperature and incubation time of the grid, protein activity, baculovirus stock, concentration and treatment. At optimal conditions the amount of residual protein

contamination from baculovirus supernatants seemed to play a crucial role during tail formation. As I developed better baculovirus purification methods, samples with less background could be produced, but the fraction of tail-producing viruses dropped significantly as well. Only by adding increasing amounts of supernatant of the final centrifugation according to the purification protocol described above to the motility mixture, virally-induced actin tails could be observed again. This measure allowed adding defined amounts of background protein from baculovirus stock, enabling me to find conditions of acceptable yield and high purity of the sample. The necessity to include a fraction of undefined medium to the motility assay could not be explained by need for molecular crowding, as BSA at high molarity as well as crowding agents like methylcellulose did not improve the situation. One possible candidate that could be absolutely needed in the motility mixture, while not being part of the set of defined proteins is α-actinin. As mentioned before, several indications point to this protein being involved in the formation of baculovirus-induced actin tails, a hypothesis, that will be tested in future experiments.

One crucial aspect when trying to develop models of actin-based movement is actin filament polarity. The traditional way of identifying barbed and pointed end has been decoration of actin filaments with S1 myosin heads [100],[101], though recently an elegant in silico method for polarity determination has been established [98]. Using data from an electron microscope Maeda and colleagues were able to align actin filaments according to azimuth
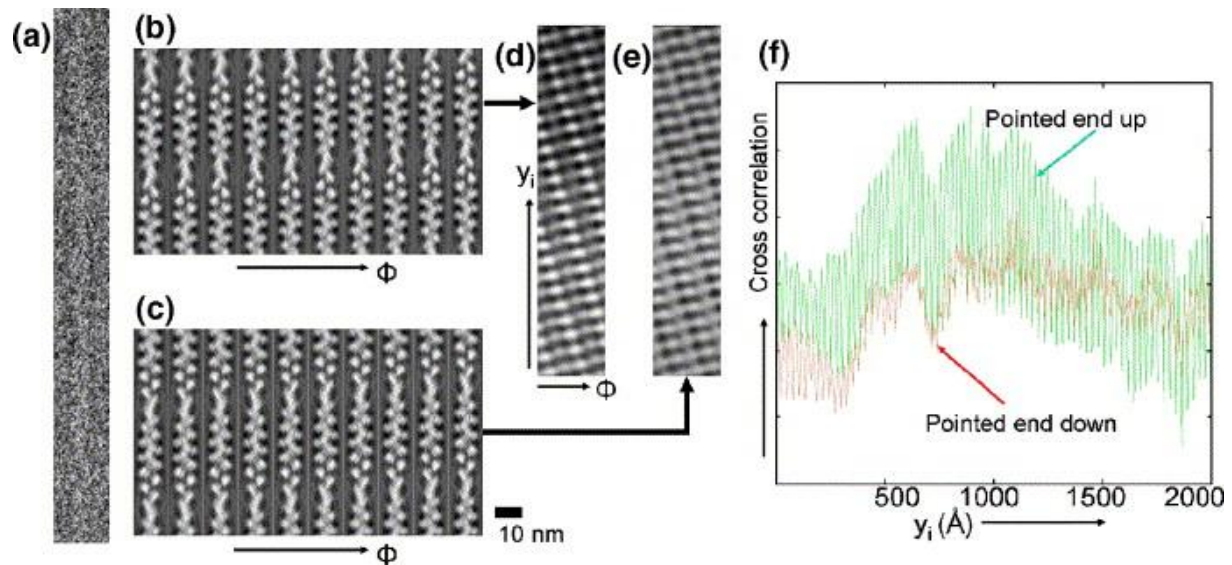
Figure 36 Diagram of polarity determination procedure according to Narita, Maeda, 2006. **(a)** Cryo-data of an actin filament. Tomographic data of actin filaments can be used as input image for polarity determination of filaments in an *in vivo* context. **(b),(c)** Projections prepared from a reference model (not shown) of an actin filament pointing up and down and the corresponding **(d),(e)** correlations maps calculated from the input image with one of the projections. **(f)** A graph showing the level of cross correlation match for **(b)** in green and **(c)** in red shows higher correlation for the filament pointing up, indicating the input filament has its barbed end on top. The same principle will be used to determine the polarity of filaments building up a baculovirus induced actin comet tail. Figure taken from Narita, Maeda, 2006 [89].

angle and significantly reduce the noise by averaging the aligned filaments. By comparing

the correlation map of an averaged sample filament with reference filaments of known polarity, it was possible to determine the polarity of the sample filament (see figure 36). Previous tries suggest the quality of tomograms produced by our microscope of negatively stained samples is sufficient for polarity determination. Localizing the filament barbed ends at the periphery of the fishbone-tail would lend further support to the models discussed below. Furthermore computational analysis of actin filament ends, while difficult, can help to identify end-binding proteins like capping protein. Using this technique to investigate the putative barbed ends of *in vitro*-tails should provide proof of filaments capped by Gelsolin. Analyzing the filament end in the middle of the tail – the pointed end according to our models – could give interesting insights to mechanisms of tail formation. We would expect the Arp2/3 complex to be bound to the pointed end, possibly branching filaments off of existing filaments or rather simply embedded in the dense middle region of the tail without forming branches. Computational analysis of tomograms could help to extract more information from our data, to investigate matters like polarity and protein binding as discussed before.

Tomograms of tails polymerized *in vitro* could hardly be used to analyze the filament organization, as the samples were collapsed in the Z-direction preventing tracing of individual filaments. To avoid collapse due to staining and blotting, we started using cryo-
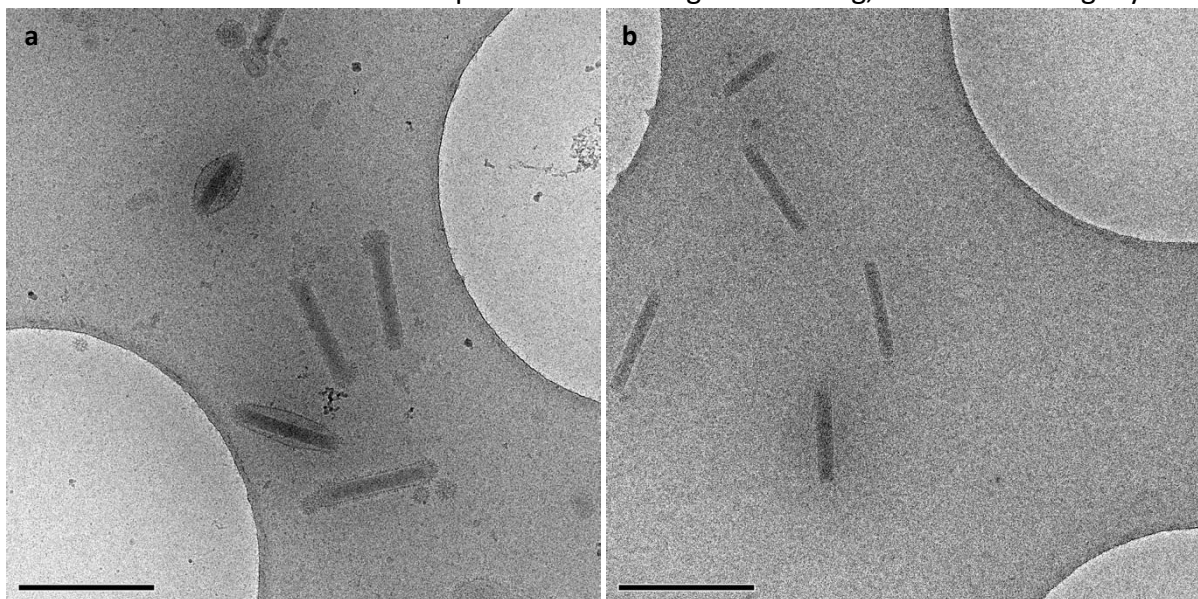
Figure 37 Plunge frozen baculovirus viewed under cryo-conditions. **(a)** Enveloped baculoviruses and **(b)** de-enveloped baculoviruses were rapidly frozen using a Leica EM Grid Plunger. The envelope is visible around the shape of the budded viruses on the left. The affinity of the viruses to the carbon surface and the resulting low frequency of viruses in the grid holes is an issue that needs to be addressed in future experiment. Ultimately, we aim to produce tomograms of plunge-frozen baculovirus induced actin tails and trace the filaments, taking advantage of the superior sample preservation by the plunge freezing method compared to negative staining. Magnification: **(a),(b)** 23,000x. Scale bars: **(a),(b)** 500nm.

Figure 38 Tomographic sections of a negatively stained *in vitro* sample showing the helical nature of baculovirus. **(a)** The top and **(b)** bottom of this virus feature characteristic h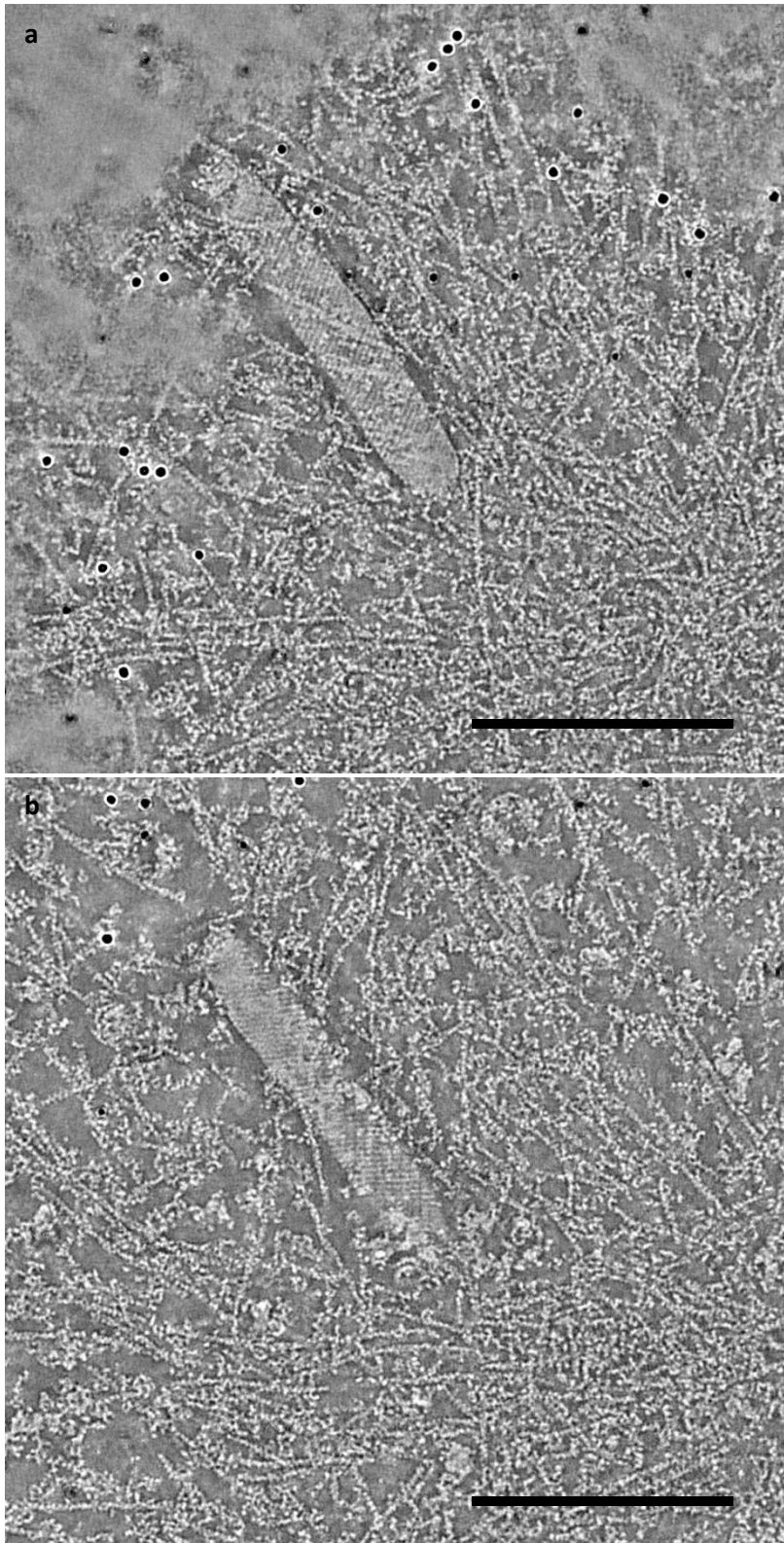orizontal stripes, which are indicative of a right-pitched helix. These stripes were only seen at de-enveloped viruses with the membrane extracted, which would have covered up the viral capsid. Magnification: 31,000x. Scale bars: **(a),(b)** 200nm.

electron tomography to investigate baculovirus-induced actin tails frozen in vitreous ice. Parameters like incubation and blotting time await experiments to determine suitable conditions. As shown in figure 37 first tries are promising, as we were able to see frozen baculoviruses under low-dose conditions on glow-discharged Quantifoil grids.

The high resolution achieved by acquiring double-tilt series enabled visualization of viral substructure. Figure 38 shows two tomographic sections containing the top and bottom of a virus with an *in vitro* polymerized actin tail. While the tail shows the typical collapse and could not be used to trace actin filaments, the virus itself exhibits diagonal stripes from top right to bottom left on the top of the virus and reciprocal on the bottom. These stripes correspond to a 2D-projection of a right-pitched helix seen from the site of the actin tail. As the actin tail was found on the same side of the virus in 25 of the 28 analyzed tomograms, baculoviruses arguably induce actin polymerization

from the bottom of a right-pitched helix predominantly comprised of the major capsid protein vp39. The actin tail was only seen to emerge from one end, without exception, indicating the confinement of the nucleation promoting factor to one end only. However, the arrangement of the presumed viral nucleation promoting factor p78/83 does not seem to be perfectly restricted to this end, as three cases of a left-pitched helix were observed.

Generally, I believe baculoviruses would present appropriate objects for electron microscopic studies due to their helical nature. A similar approach as was used for work on other viruses like the tobacco mosaic virus [110], could help to elucidate the detailed structure of this remarkable virus including the site of the nucleation promoting factor.

In vivo polymerized actin tails

Imaging baculoviruses moving through their eukaryotic host cells by electron tomography provided interesting insights into the molecular construction of actin comet tails. Tracing the filaments was performed at the best samples, albeit the collapse in the Z-direction hampered my efforts to trace the filaments near the middle of the tail. An example is shown in figure 39. In this actin comet tail several filament ends could be seen colocalizing with the side of another filament, marked with red arrows. While better resolution and more data are definitely needed to ascertain the existence and significance of branches, these preliminary data could already be used to add to the existing models of actin tails.

If these observed filaments are indeed formed by branching at a significant rate, the logical ensuing step needs to be to establish, whether the mechanism of forming requires end-branching [17],[18] or side-branching [102],[103].

Filaments branched by **end-branching** from the barbed end of a growing 'mother filament' are expected to possess the same length unless one of them is capped at an early state, as they were nucleated simultaneously [18]. In the schematic drawing of different, hypothetical actin tail formation mechanics shown in figure 41 the two daughter filaments are drawn equally long. As one can see in the *in vivo* sample and the three-dimensional model based on it (figure 39) this is hardly the case in this representative comet tail.

Hence this special case of actin-based propulsion could be based on **side-branching**. A major refutation to filaments branching off the side of existing 'mother filaments' is the geometrical situation at the cell front, where massive actin nucleation occurs. (For a model of the lamellipodial geometry see figure 4.) It is close to impossible to reconcile the postulated existence of many short branches on the side of longer filaments for at least two reasons: First, membrane-bound nucleators like the WAVE complex cannot activate Arp2/3 located several dozens or even hundreds of nanometers removed from the cell front by direct interaction and the existence of an activated, diffusing state of Arp2/3 has not been reported. Second, short branches on the side of the 'mother filaments' would never reach the membrane but nevertheless need ATP for elongation and thus be eliminated by

evolution as a waste of energy. The rear of a baculovirus presents itself very differently than a lamellipodium. Its small shape of around 50nm diameter cannot accommodate more than a few 7nm-thick actin filaments at once and indeed looking at the available data one can see only two to four filaments at a time in contact with the virus surface. Filaments could therefore be displaced by newly nucleated filaments emanating from the putative site of p78/83 and outgrow the baculovirus on either side, as could be seen *in vitro* as well as *in vivo*. These filaments clearly would not contribute to pushing, but could have a stabilizing function keeping the pathogen on track as it makes its way through the crowded cytosol. The growth of these filaments is presumably stopped by barbed end capping by proteins like Gelsolin. Filaments elongating sideways along the baculovirus present a special actin geometry enabling interesting new mechanistic explanations for the observed structure. A filament continuing sideways of the virus could render its side accessible to the nucleator, facilitating the colocalization of the 'mother filament', nucleator, Arp2/3 and actin monomers. This model is also depicted in figure 41 along with the two competing models. Taken together, both of the weighty objections to side branching in lamellipodia – the geometry problem and the biological sense of nucleating filaments, which never reach the membrane – do not apply to this special case of actin polymerization. The side-model could therefore explain the observed tail structure, albeit from in my preliminary data just few filaments could be identified as possible branches, so clearly more data from negatively stained as well as *in vitro* cryo-samples are needed. Thus the third possibility would be a model devoid of any form of branching; of course one could also imagine a 'mixed form', where filaments are created both by branching from older filaments and without branching by direct nucleation at the back of the virus.

The **branching-independent** model postulates nucleation of filaments at the baculovirus rear without the need for a 'mother filament'. As indicated in figure 41, newly nucleated filaments would displace older filaments from the nucleator, again leading to polymerization of filaments on the side of the virus. To generate traction the tails of this model could include α-actinin in order to crosslink the actin network. Mechanistically, these crosslinks would be equivalent to branches in the other two models. Due to the relatively low abundance of branches, which could have just emerged by chance, this model is equally compatible with the tomographic data.

The existing models of pathogen-induced actin tails are termed elastic ratchet model [107],[108] and the clamped-filament model or end-tracking motor model [109]. Their major differences consist in the way new actin monomers are incorporated at the bacterial or viral surface, as shown in figure 40. Data presented in this work cannot contribute to this ongoing dispute, as force measurements, biochemical approaches and studies of the atomic structure of involved proteins are better suited for this task. The authors of the elastic ratchet model implicitly integrated side-branches in their model. To address this question I believe electron tomography is the most adequate technique.
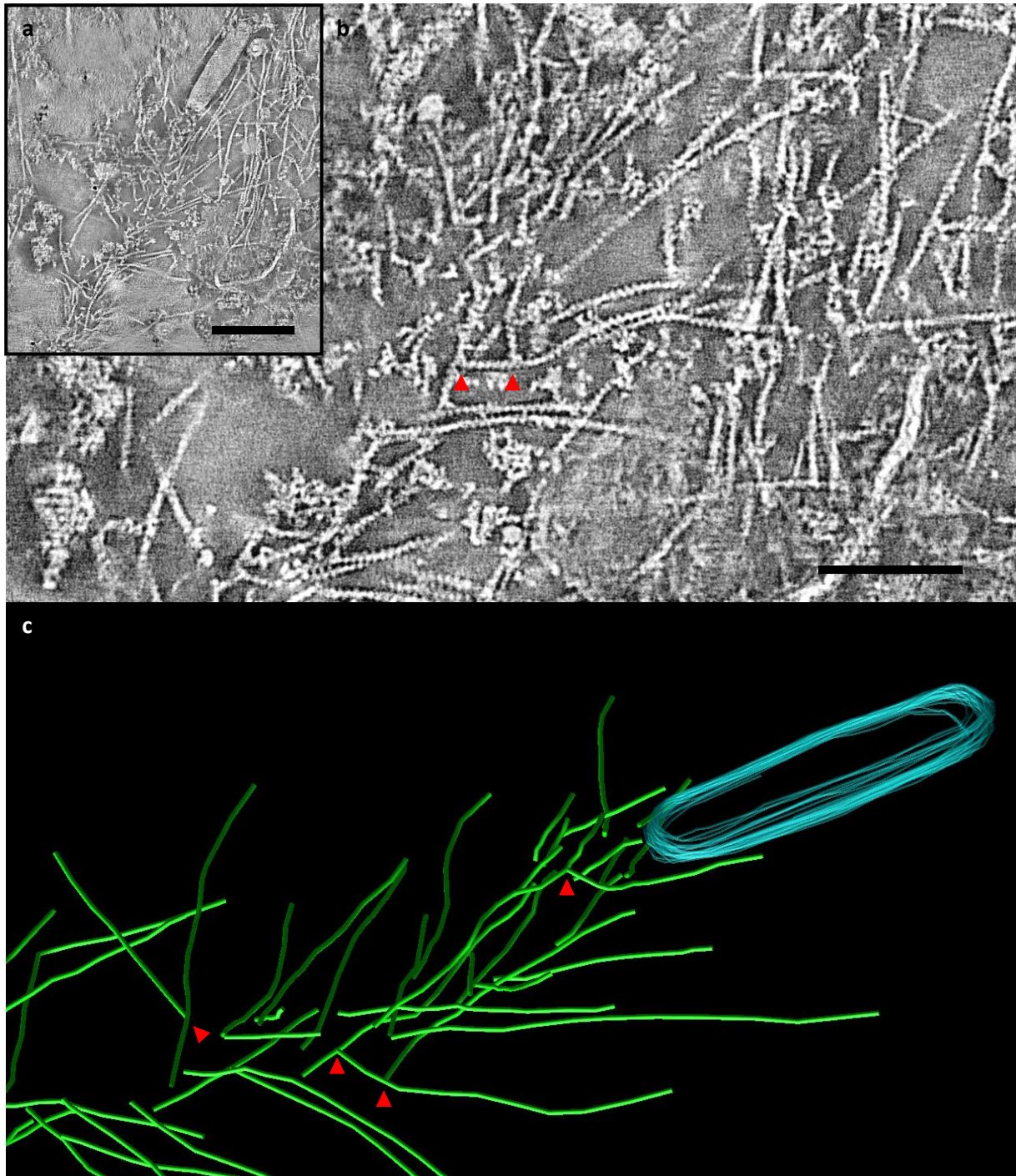
Figure 39 Tomogram section and corresponding model of an *in vivo* baculovirus induced actin comet tail. **(a)** Overview and **(b)** detail of a middle section of the tail with possible branches marked with red arrows. **(c)** The model produced on the basis of the tomogram shows several putative branching points, which are marked with red arrows. Actin filaments are shown in green and the virus in light blue. Three possible models accounting for the observed phenotype are discussed in the text. Magnification: 39,000x. Scale bars: **(a)** 200nm; **(b)** 100nm.

Collapse of the sample and therefore difficulties in detecting individual filaments is the main road block that needs to be overcome to get definitive results. Employing cryo-techniques will hopefully enable us to clarify the structure of baculovirus-induced comet tails. As was
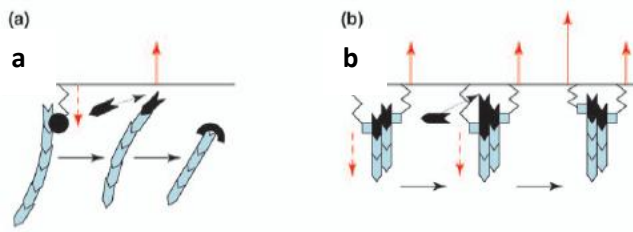
Figure 40 Theoretical, molecular models of actin polymerization at a pathogen surface. **(a)** Elastic ratchet model and **(b)** clamped-filament model were proposed by different autors. Figure taken from Mogilner, 2006 [108].

discussed before, a significant amount of evidence points to extensive homology between baculovirus-induced actin tails and actin tails produced by a range of other pathogens. Thus I think one can bring forward the argument that unraveling the structure of baculovirus tails will help to shed some light on manipulations of the host actin cytoskeleton by other pathogens.
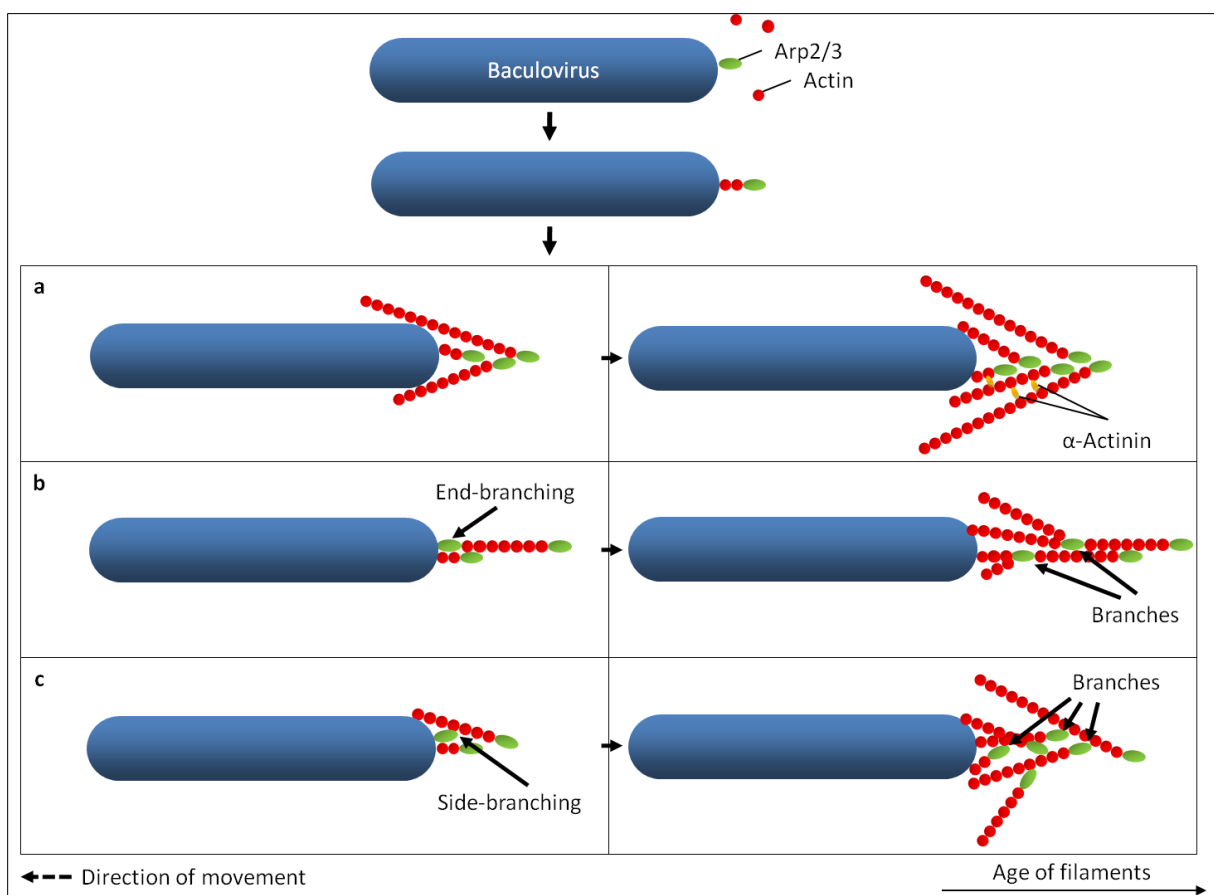
Figure 41 Schematic drawing of three possible models of baculovirus induced actin tails. **(a)** Branching independent, **(b)** end branching and **(c)** side branching model of baculovirus induced actin comet tails. The features and consequences of each model are discussed in the text. Future experiments aim to positively determine, which model reflects reality the closest or point to another mode of polymerizing the propulsion machinery that has not yet been conceived.

ACKNOWLEDGMENTS

REFERENCES

1
Pollard TD, Cooper JA. Actin, a central player in cell shape and movement. Science. 2009 Nov 27;326(5957):1208-12.

2
Tilney LG, Portnoy DA. Actin filaments and the growth, movement, and spread of the intracellular bacterial parasite, Listeria monocytogenes. J Cell Biol. 1989 Oct;109(4 Pt 1):1597-608.

3
Goldberg MB, Theriot JA. Shigella flexneri surface protein IcsA is sufficient to direct actin-based motility. Proc Natl Acad Sci USA 1995, 92:6572-6576.

4
Teysseire N, Chiche-Portiche C, Raoult D. Intracellular movements of Rickettsia conorii and R. typhi based on actin polymerization. Res Microbiol 1992, 143:821-829.

5
Rietdorf J, Ploubidou A, Reckmann I, Holmstrom A, Frischknecht F, Zettl M, Zimmermann T, Way M. Kinesin-dependent movement on microtubules precedes actin-based motility of vaccinia virus. Nat Cell Biol 2001, 3:992-1000.

6

Ohkawa T, Volkman LE, Welch MD. Actin-based motility drives baculovirus transit to the nucleus and cell surface. J Cell Biol. 2010 Jul 26;190(2):187-95.

7

Jarvis DL. Baculovirus-insect cell expression systems. Methods Enzymol. 2009;463:191-222.

8

Kost TA, Condreay JP, Jarvis DL. Baculovirus as versatile vectors for protein expression in insect and mammalian cells. Nat Biotechnol. 2005 May;23(5):567-75.

9

Inceoglu AB, Kamita SG, Hinton AC, Huang Q, Severson TF, Kang K, Hammock BD. Recombinant baculoviruses for insect control. Pest Manag Sci. 2001 Oct;57(10):981-7.

10

Bak XY, Yang J, Wang S. Baculovirus-transduced bone marrow mesenchymal stem cells for systemic cancer therapy. Cancer Gene Ther. 2010 Jun 11.

11

Lanier LM, Volkman LE. Actin binding and nucleation by Autographa california M nucleopolyhedrovirus. Virology. 1998 Mar 30;243(1):167-77.

12

Volkman LE, Goldsmith PA. Mechanism of neutralization of budded Autographa californica nuclear polyhedrosis virus by a monoclonal antibody: Inhibition of entry by adsorptive endocytosis. Virology. 1985 May;143(1):185-95.

13

Goley ED, Ohkawa T, Mancuso J, Woodruff JB, D'Alessio JA, Cande WZ, Volkman LE, Welch MD. Dynamic nuclear actin assembly by Arp2/3 complex and a baculovirus WASP-like protein. Science. 2006 Oct 20;314(5798):464-7.

14

Y.L. Wang. Exchange of actin subunits at the leading edge of living fibroblasts: possible role of treadmilling, J Cell Biol 101 (1985), pp. 597–602.

15

D. Zicha, I.M. Dobbie, M.R. Holt, J. Monypenny, D.Y. Soong, C. Gray and G.A. Dunn, Rapid actin transport during cell protrusion, Science 300 (2003), pp. 142–145.

16

Loisel TP, Boujemaa R, Pantaloni D, Carlier MF. Reconstitution of actin-based motility of Listeria and Shigella using pure proteins. Nature. 1999 Oct 7;401(6753):613-6.

17

Wiesner S, Helfer E, Didry D, Ducouret G, Lafuma F, Carlier MF, Pantaloni D. A biomimetic motility assay provides insight into the mechanism of actin-based motility. J Cell Biol. 2003 Feb 3;160(3):387-98.

18

Pantaloni D, Boujemaa R, Didry D, Gounon P, Carlier MF. The Arp2/3 complex branches filament barbed ends: functional antagonism with capping proteins. Nat Cell Biol. 2000 Jul;2(7):385-91.

19

Delatour V, Helfer E, Didry D, Lê KH, Gaucher JF, Carlier MF, Romet-Lemonne G. Arp2/3 controls the motile behavior of N-WASP-functionalized GUVs and modulates N-WASP surface distribution by mediating transient links with actin filaments. Biophys J. 2008 Jun;94(12):4890-905.

20
Kueh HY, Brieher WM, Mitchison TJ. Quantitative analysis of actin turnover in Listeria comet tails: evidence for catastrophic filament turnover. Biophys J. 2010 Oct 6;99(7):2153-62.

21
Svitkina TM, Verkhovsky AB, McQuade KM, Borisy GG. Analysis of the actin-myosin II system in fish epidermal keratocytes: mechanism of cell body translocation. J Cell Biol. 1997 Oct 20;139(2):397-415.

22
Amann KJ, Pollard TD. Direct real-time observation of actin filament branching mediated by Arp2/3 complex using total internal reflection fluorescence microscopy. Proc Natl Acad Sci U S A. 2001 Dec 18;98(26):15009-13.

23
Urban E, Jacob S, Nemethova M, Resch GP, Small JV. Electron tomography reveals unbranched networks of actin filaments in lamellipodia. Nat Cell Biol. 2010 May;12(5):429-35.

24
Sechi AS, Wehland J, Small JV. The isolated comet tail pseudopodium of Listeria monocytogenes: a tail of two actin filament populations, long and axial and short and random. J Cell Biol. 1997 Apr 7;137(1):155-67.

25
Cameron LA, Svitkina TM, Vignjevic D, Theriot JA, Borisy GG. Dendritic organization of actin comet tails. Curr Biol. 2001 Jan 23;11(2):130-5.

26
Gouin E, Gantelet H, Egile C, Lasa I, Ohayon H, Villiers V, Gounon P, Sansonetti PJ, Cossart P. A comparative study of the actin-based motilities of the pathogenic bacteria Listeria monocytogenes, Shigella flexneri and Rickettsia conorii. J Cell Sci. 1999 Jun;112 (Pt 11):1697-708.

27
Gouin E, Welch MD, Cossart P. Actin-based motility of intracellular pathogens. Curr Opin Microbiol. 2005 Feb;8(1):35-45.

28
Kremer, JR, Mastronarde DN, McIntosh JR. Computer visualization of three-dimensional image data using IMOD. J. Struct. Biol. 116, 71–76 (1996).

29
Islam K, Burns RG. Assembly of microtubules with ATP: evidence that only a fraction of the protein is assembly-competent. FEBS Lett. 1984 Dec 10;178(2):264-70.

30
Iida J, Itoh TJ, Hotani H, Nishiyama K, Murofushi H, Bulinski JC, Hisanaga S. The projection domain of MAP4 suppresses the microtubule-bundling activity of the microtubule-binding domain. J Mol Biol. 2002 Jun 28;320(1):97-106.

31
Machesky LM, Insall RH, Volkman LE. WASP homology sequences in baculoviruses. Trends Cell Biol. 2001 Jul;11(7):286-7.

32
Wang R, Deng F, Hou D, Zhao Y, Guo L, Wang H, Hu Z. Proteomics of the Autographa californica nucleopolyhedrovirus budded virions. J Virol. 2010 Jul;84(14):7233-42.

33
Stamm LM, Morisaki JH, Gao LY, Jeng RL, McDonald KL, Roth R, Takeshita S, Heuser J, Welch MD, Brown EJ. Mycobacterium marinum escapes from phagosomes and is propelled by actin-based motility. J Exp Med. 2003 Nov 3;198(9):1361-8.

34
Smith K, Humphreys D, Hume PJ, Koronakis V. Enteropathogenic Escherichia coli recruits the cellular inositol phosphatase SHIP2 to regulate actin-pedestal formation. Cell Host Microbe. 2010 Jan 21;7(1):13-24.

35
Campellone KG. Cytoskeleton-modulating effectors of enteropathogenic and enterohaemorrhagic Escherichia coli: Tir, EspFU and actin pedestal assembly. FEBS J. 2010 Jun;277(11):2390-402.

36
Weiss SM, Ladwein M, Schmidt D, Ehinger J, Lommel S, Städing K, Beutling U, Disanza A, Frank R, Jänsch L, Scita G, Gunzer F, Rottner K, Stradal TE. IRSp53 links the enterohemorrhagic E. coli effectors Tir and EspFU for actin pedestal formation. Cell Host Microbe. 2009 Mar 19;5(3):244-58.

37
Wu RF, Gu Y, Xu YC, Mitola S, Bussolino F, Terada LS. Human immunodeficiency virus type 1 Tat regulates endothelial cell actin cytoskeletal dynamics through PAK1 activation and oxidant production. J. Virol. 2004;78:779–789.

38
McDonald D, Vodicka MA, Lucero G, Svitkina TM, Borisy GG, Emerman M, Hope TJ. Visualization of the intracellular behavior of HIV in living cells. J. Cell Biol. 2002;159:441–452

39
Jeng RL, Goley ED, D'Alessio JA, Chaga OY, Svitkina TM, Borisy GG, Heinzen RA, Welch MD. A Rickettsia WASP-like protein activates the Arp2/3 complex and mediates actin-based motility. Cell Microbiol. 2004 Aug;6(8):761-9.

40
Blissard GW, Wenz JR. Baculovirus gp64 envelope glycoprotein is sufficient to mediate pH-dependent membrane fusion. J Virol. 1992 Nov;66(11):6829-35.

41
Greber UF, Way M. A superhighway to virus infection. Cell. 2006 Feb 24;124(4):741-54.

42
Abercrombie M, Heaysman JE, Pegrum SM. The locomotion of fibroblasts in culture. I. Movements of the leading edge. Exp Cell Res. 1970 Mar;59(3):393-8.

43
Small JV, Celis JE. Filament arrangements in negatively stained cultured cells: the organization of actin. Cytobiologie. 1978 Feb;16(2):308-25.

44
Wegner A. Head to tail polymerization of actin. J Mol Biol. 1976 Nov;108(1):139-50.

45
Machesky LM, Atkinson SJ, Ampe C, Vandekerckhove J, Pollard TD. Purification of a cortical complex containing two unconventional actins from Acanthamoeba by affinity chromatography on profilin-agarose. J Cell Biol. 1994 Oct;127(1):107-15.

46
Ma L, Rohatgi R, Kirschner MW. The Arp2/3 complex mediates actin polymerization induced by the small GTP-binding protein Cdc42. Proc Natl Acad Sci U S A. 1998 Dec 22;95(26):15362-7.

47
Robinson RC, Turbedsky K, Kaiser DA, Marchand JB, Higgs HN, Choe S, Pollard TD. Crystal structure of Arp2/3 complex. Science. 2001 Nov 23;294(5547):1679-84.

48
Welch MD, Iwamatsu A, Mitchison TJ. Actin polymerization is induced by Arp2/3 protein complex at the surface of Listeria monocytogenes. Nature. 1997 Jan 16;385(6613):265-9.

49
Winter D, Podtelejnikov AV, Mann M, Li R. The complex containing actin-related proteins Arp2 and Arp3 is required for the motility and integrity of yeast actin patches. Curr Biol. 1997 Jul 1;7(7):519-29.

50
Pruyne D, Evangelista M, Yang C, Bi E, Zigmond S, Bretscher A, Boone C. Role of formins in actin assembly: nucleation and barbed-end association. Science. 2002 Jul 26;297(5581):612-5.

51
Schirenbeck A, Arasada R, Bretschneider T, Schleicher M, Faix J. Formins and VASPs may co-operate in the formation of filopodia. Biochem Soc Trans. 2005 Dec;33(Pt 6):1256-9.

52
Quinlan ME, Heuser JE, Kerkhoff E, Mullins RD. Drosophila Spire is an actin nucleation factor. Nature. 2005 Jan 27;433(7024):382-8.

53
Winckler B, Schafer DA. Cordon-bleu: a new taste in actin nucleation. Cell. 2007 Oct 19;131(2):236-8.

54
Symons M, Derry JM, Karlak B, Jiang S, Lemahieu V, Mccormick F, Francke U, Abo A. Wiskott-Aldrich syndrome protein, a novel effector for the GTPase CDC42Hs, is implicated in actin polymerization. Cell. 1996 Mar 8;84(5):723-34.

55
Chen Z, Borek D, Padrick SB, Gomez TS, Metlagel Z, Ismail AM, Umetani J, Billadeau DD, Otwinowski Z, Rosen MK. Structure and control of the actin regulatory WAVE complex. Nature. 2010 Nov 25;468(7323):533-8.

56
Padrick SB, Rosen MK. Physical mechanisms of signal integration by WASP family proteins. Annu Rev Biochem. 2010;79:707-35.

57
Carlier MF, Laurent V, Santolini J, Melki R, Didry D, Xia GX, Hong Y, Chua NH, Pantaloni D. Actin depolymerizing factor (ADF/cofilin) enhances the rate of filament turnover: implication in actin-based motility. J Cell Biol. 1997 Mar 24;136(6):1307-22.

58
Carlsson L, Nyström LE, Sundkvist I, Markey F, Lindberg U. Actin polymerizability is influenced by profilin, a low molecular weight protein in non-muscle cells. J Mol Biol. 1977 Sep 25;115(3):465-83.

59
Didry D, Carlier MF, Pantaloni D. Synergy between actin depolymerizing factor/cofilin and profilin in increasing actin filament turnover. J Biol Chem. 1998 Oct 2;273(40):25602-11.

60
Yin HL, Stossel TP. Control of cytoplasmic actin gel-sol transformation by gelsolin, a calcium-dependent regulatory protein. Nature. 1979 Oct 18;281(5732):583-6.

61
Harris HE, Weeds AG. Plasma gelsolin caps and severs actin filaments. FEBS Lett. 1984 Nov 19;177(2):184-8.

62

Maruyama K, Ebashi S. Alpha-actinin, a new structural protein from striated muscle. Action on actin. J Biochem. 1965 Jul;58(1):13-9.

63

Giardini PA, Fletcher DA, Theriot JA. Compression forces generated by actin comet tails on lipid vesicles. Proc Natl Acad Sci U S A. 2003 May 27;100(11):6493-8.

64

Paluch E, van der Gucht J, Joanny JF, Sykes C. Deformations in actin comets from rocketing beads. Biophys J. 2006 Oct 15;91(8):3113-22.

65

Brieher WM, Coughlin M, Mitchison TJ. Fascin-mediated propulsion of Listeria monocytogenes independent of frequent nucleation by the Arp2/3 complex. J Cell Biol. 2004 Apr 26;165(2):233-42.

66

Marcy Y, Prost J, Carlier MF, Sykes C. Forces generated during actin-based propulsion: a direct measurement by micromanipulation. Proc Natl Acad Sci U S A. 2004 Apr 20;101(16):5992-7.

67

Delatour V, Helfer E, Didry D, Lê KH, Gaucher JF, Carlier MF, Romet-Lemonne G. Arp2/3 controls the motile behavior of N-WASP-functionalized GUVs and modulates N-WASP surface distribution by mediating transient links with actin filaments. Biophys J. 2008 Jun;94(12):4890-905.

68

Streicher P, Nassoy P, Bärmann M, Dif A, Marchi-Artzner V, Brochard-Wyart F, Spatz J, Bassereau P. Integrin reconstituted in GUVs: a biomimetic system to study initial steps of cell spreading. Biochim Biophys Acta. 2009 Oct;1788(10):2291-300.

69

Koestler SA, Auinger S, Vinzenz M, Rottner K, Small JV. Differentially oriented populations of actin filaments generated in lamellipodia collaborate in pushing and pausing at the cell front. Nat Cell Biol. 2008 Mar;10(3):306-13.

70

Pollard TD. Regulation of actin filament assembly by Arp2/3 complex and formins. Annu Rev Biophys Biomol Struct. 2007;36:451-77.

71

Mahaffy RE, Pollard TD. Kinetics of the formation and dissociation of actin filament branches mediated by Arp2/3 complex. Biophys J. 2006 Nov 1;91(9):3519-28.

72

Samarin S, Romero S, Kocks C, Didry D, Pantaloni D, Carlier MF. How VASP enhances actin-based motility. Biochemistry. 2001 Sep 25;40(38):11390-404.

73

Boujemaa-Paterski R, Gouin E, Hansen G, Samarin S, Le Clainche C, Didry D, Dehoux P, Cossart P, Kocks C, Carlier MF, Pantaloni D. Listeria protein ActA mimics WASp family proteins: it activates filament barbed end branching by Arp2/3 complex. J Cell Biol. 2003 Oct 13;163(1):131-42.

74

Egile C, Rouiller I, Xu XP, Volkmann N, Li R, Hanein D. Mechanism of filament nucleation and branch stability revealed by the structure of the Arp2/3 complex at actin branch junctions. PLoS Biol. 2005 Nov;3(11):e383.

75
Rouiller I, Xu XP, Amann KJ, Egile C, Nickell S, Nicastro D, Li R, Pollard TD, Volkmann N, Hanein D. The structural basis of actin filament branching by the Arp2/3 complex. J Cell Biol. 2008 Mar 10;180(5):887-95.

76
Svitkina TM, Borisy GG. Arp2/3 complex and actin depolymerizing factor/cofilin in dendritic organization and treadmilling of actin filament array in lamellipodia. J Cell Biol. 1999 May 31;145(5):1009-26.

77
Breitbach K, Rottner K, Klocke S, Rohde M, Jenzora A, Wehland J, Steinmetz I. Actin-based motility of Burkholderia pseudomallei involves the Arp 2/3 complex, but not N-WASP and Ena/VASP proteins. Cell Microbiol. 2003 Jun;5(6):385-93.

78
Dodding MP, Way M. Nck- and N-WASP-dependent actin-based motility is conserved in divergent vertebrate poxviruses. Cell Host Microbe. 2009 Dec 17;6(6):536-50.

79
Frischknecht F, Moreau V, Röttger S, Gonfloni S, Reckmann I, Superti-Furga G, Way M. Actin-based motility of vaccinia virus mimics receptor tyrosine kinase signalling. Nature. 1999 Oct 28;401(6756):926-9.

80
Van Kirk LS, Hayes SF, Heinzen RA. Ultrastructure of Rickettsia rickettsii actin tails and localization of cytoskeletal proteins. Infect Immun. 2000 Aug;68(8):4706-13.

81
Islam K, Burns RG. Assembly of microtubules with ATP: evidence that only a fraction of the protein is assembly-competent. FEBS Lett. 1984 Dec 10;178(2):264-70.

82
Zabrecky JR, Cole RD. Effect of ATP on the kinetics of microtubule assembly. J Biol Chem. 1982 Apr 25;257(8):4633-8.

83
Duanmu C, Lin CM, Hamel E. Tubulin polymerization with ATP is mediated through the exchangeable GTP site. Biochim Biophys Acta. 1986 Mar 19;881(1):113-23.

84
Iida J, Itoh TJ, Hotani H, Nishiyama K, Murofushi H, Bulinski JC, Hisanaga S. The projection domain of MAP4 suppresses the microtubule-bundling activity of the microtubule-binding domain. J Mol Biol. 2002 Jun 28;320(1):97-106.

85
Van Troys M, Lambrechts A, David V, Demol H, Puype M, Pizarro-Cerda J, Gevaert K, Cossart P, Vandekerckhove J. The actin propulsive machinery: the proteome of Listeria monocytogenes tails. Biochem Biophys Res Commun. 2008 Oct 17;375(2):194-9.

86
Lambrechts A, Gevaert K, Cossart P, Vandekerckhove J, Van Troys M. Listeria comet tails: the actin-based motility machinery at work. Trends Cell Biol. 2008 May;18(5):220-7.

87
Lee HH, Miller LK. Isolation of genotypic variants of Autographa californica nuclear polyhedrosis virus. J Virol. 1978 Sep;27(3):754-67.

88

Hu YC, Tsai CT, Chung YC, Lu JT, Hsu JA. Generation of chimeric baculovirus with histidine-tags displayed on the envelope and its purification using immobilized metal affinity chromatography. Enz and Micro Tech. 2003 Sep;33(4):445-7

89

Chen GY, Chen CY, Chang MD, Matsuura Y, Hu YC. Concanavalin A affinity chromatography for efficient baculovirus purification. Biotechnol Prog. 2009 Nov-Dec;25(6):1669-77.

90

Transfiguracion J, Jorio H, Meghrous J, Jacob D, Kamen A. High yield purification of functional baculovirus vectors by size exclusion chromatography. J Virol Methods. 2007 Jun;142(1-2):21-8.

91

Wu C, Soh KY, Wang S. Ion-exchange membrane chromatography method for rapid and efficient purification of recombinant baculovirus and baculovirus gp64 protein. Hum Gene Ther. 2007 Jul;18(7):665-72.

92

Philipps B, Rotmann D, Wicki M, Mayr LM, Forstner M. Time reduction and process optimization of the baculovirus expression system for more efficient recombinant protein production in insect cells. Protein Expr Purif. 2005 Jul;42(1):211-8.

93

Hofmann C, Sandig V, Jennings G, Rudolph M, Schlag P, Strauss. M. Efficient gene-transfer into human hepatocytes by baculovirus vectors. Proc Natl Acad Sci USA 1995;92:10099–103.

94

Sarkis C, Serguera C, Petres S, Buchet D, Ridet JL, Edelman L. Efficient transduction of neural cells in vitro and in vivo by a baculovirus-derived vector. Proc Natl Acad Sci USA 2000;97:14638–43.

95

Dwarakanath RS, Clark CL, McElroy AK, Spector DH. The use of recombinant baculoviruses for sustained expression of human cytomegalovirus immediate early proteins in fibroblasts. Virology 2001;284:297–307.

96

Lasa I, Gouin E, Goethals M, Vancompernolle K, David V, Vandekerckhove J, Cossart P. Identification of two regions in the N-terminal domain of ActA involved in the actin comet tail formation by Listeria monocytogenes. EMBO J. 1997 Apr 1;16(7):1531-40.

97

Bernheim-Groswasser A, Wiesner S, Golsteyn RM, Carlier MF, Sykes C. The dynamics of actin-based motility depend on surface parameters. Nature. 2002 May 16;417(6886):308-11.

98

Narita A, Maéda Y. Molecular determination by electron microscopy of the actin filament end structure. J Mol Biol. 2007 Jan 12;365(2):480-501.

99

Van der Gucht J, Paluch E, Plastino J, Sykes C. Stress release drives symmetry breaking for actin-based movement. Proc Natl Acad Sci U S A. 2005 May 31;102(22):7847-52.

100

Ishikawa H, Bischoff R, Holtzer H. Formation of arrowhead complexes with heavy meromyosin in a variety of cell types. J Cell Biol. 1969 Nov;43(2):312-28.

101

Tilney LG, Mooseker M. Actin in the brush-border of epithelial cells of the chicken intestine. Proc Natl Acad Sci U S A. 1971 Oct;68(10):2611-5.

102

Blanchoin L, Amann KJ, Higgs HN, Marchand JB, Kaiser DA, Pollard TD. Direct observation of dendritic actin filament networks nucleated by Arp2/3 complex and WASP/Scar proteins. Nature. 2000 Apr 27;404(6781):1007-11.

103

Mullins RD, Heuser JA, Pollard TD. The interaction of Arp2/3 complex with actin: nucleation, high affinity pointed end capping, and formation of branching networks of filaments. Proc Natl Acad Sci U S A. 1998 May 26;95(11):6181-6.

104

Sánchez-Soriano N, Gonçalves-Pimentel C, Beaven R, Haessler U, Ofner-Ziegenfuss L, Ballestrem C, Prokop A. Drosophila growth cones: a genetically tractable platform for the analysis of axonal growth dynamics. Dev Neurobiol. 2010 Jan;70(1):58-71.

105

Campellone KG, Webb NJ, Znameroski EA, Welch MD. WHAMM is an Arp2/3 complex activator that binds microtubules and functions in ER to Golgi transport. Cell. 2008 Jul 11;134(1):148-61.

106

Resch GP, Goldie KN, Hoenger A, Small JV. Pure F-actin networks are distorted and branched by steps in the critical-point drying method. J Struct Biol. 2002 Mar;137(3):305-12.

107

Mogilner A, Oster G. Force generation by actin polymerization II: the elastic ratchet and tethered filaments. Biophys J. 2003 Mar;84(3):1591-605.

108

Mogilner A. On the edge: modeling protrusion. Curr Opin Cell Biol. 2006 Feb;18(1):32-9.

109

Dickinson RB, Purich DL. Clamped-filament elongation model for actin-based motors. Biophys J. 2002 Feb;82(2):605-17.

110

Sachse C, Chen JZ, Coureux PD, Stroupe ME, Fändrich M, Grigorieff N. High-resolution electron microscopy of helical specimens: a fresh look at tobacco mosaic virus. J Mol Biol. 2007 Aug 17;371(3):812-35.

Figures

Figure 1a

Koestler SA, Auinger S, Vinzenz M, Rottner K, Small JV. Differentially oriented populations of actin filaments generated in lamellipodia collaborate in pushing and pausing at the cell front. Nat Cell Biol. 2008 Mar;10(3):306-13.

Figures 1b, 3, 8

Urban E, Jacob S, Nemethova M, Resch GP, Small JV. Electron tomography reveals unbranched networks of actin filaments in lamellipodia. Nat Cell Biol. 2010 May;12(5):429-35.

Figure 2

Padrick SB, Rosen MK. Physical mechanisms of signal integration by WASP family proteins. Annu Rev Biochem. 2010;79:707-35.

Figure 4

Wiesner S, Helfer E, Didry D, Ducouret G, Lafuma F, Carlier MF, Pantaloni D. A biomimetic motility assay provides insight into the mechanism of actin-based motility. J Cell Biol. 2003 Feb 3;160(3):387-98.

Figure 5a

Jeng RL, Goley ED, D'Alessio JA, Chaga OY, Svitkina TM, Borisy GG, Heinzen RA, Welch MD. A Rickettsia WASP-like protein activates the Arp2/3 complex and mediates actin-based motility. Cell Microbiol. 2004 Aug;6(8):761-9.

Figure 5b

Cameron LA, Svitkina TM, Vignjevic D, Theriot JA, Borisy GG. Dendritic organization of actin comet tails. Curr Biol. 2001 Jan 23;11(2):130-5.

Figure 6

Brieher WM, Coughlin M, Mitchison TJ. Fascin-mediated propulsion of Listeria monocytogenes independent of frequent nucleation by the Arp2/3 complex. J Cell Biol. 2004 Apr 26;165(2):233-42.

Figure 7a

Svitkina TM, Verkhovsky AB, McQuade KM, Borisy GG. Analysis of the actin-myosin II system in fish epidermal keratocytes: mechanism of cell body translocation. J Cell Biol. 1997 Oct 20;139(2):397-415.

Figure 7b

Rouiller I, Xu XP, Amann KJ, Egile C, Nickell S, Nicastro D, Li R, Pollard TD, Volkmann N, Hanein D. The structural basis of actin filament branching by the Arp2/3 complex. J Cell Biol. 2008 Mar 10;180(5):887-95.

Figure 10

Machesky LM, Insall RH, Volkman LE. WASP homology sequences in baculoviruses. Trends Cell Biol. 2001 Jul;11(7):286-7.

Figure 11

Gouin E, Welch MD, Cossart P. Actin-based motility of intracellular pathogens. Curr Opin Microbiol. 2005 Feb;8(1):35-45.

Figure 12

Pantaloni D, Boujemaa R, Didry D, Gounon P, Carlier MF. The Arp2/3 complex branches filament barbed ends: functional antagonism with capping proteins. Nat Cell Biol. 2000 Jul;2(7):385-91.

Figure 32

Islam K, Burns RG. Assembly of microtubules with ATP: evidence that only a fraction of the protein is assembly-competent. FEBS Lett. 1984 Dec 10;178(2):264-70.

Figure 33a

Iida J, Itoh TJ, Hotani H, Nishiyama K, Murofushi H, Bulinski JC, Hisanaga S. The projection domain of MAP4 suppresses the microtubule-bundling activity of the microtubule-binding domain. J Mol Biol. 2002 Jun 28;320(1):97-106.

Figure 36

Chen GY, Chen CY, Chang MD, Matsuura Y, Hu YC. Concanavalin A affinity chromatography for efficient baculovirus purification. Biotechnol Prog. 2009 Nov-Dec;25(6):1669-77.

I have tried to find all holders of image copyrights and to obtain their approval to use the images for this work. If copyright infringement occurs nevertheless, I would ask to be notified.

Ich habe mich bemüht, sämtliche Inhaber der Bildrechte ausfindig zu machen und ihre Zustimmung zur Verwendung der Bilder in dieser Arbeit eingeholt. Sollte dennoch eine Urheberrechtsverletzung bekannt werden, ersuche ich um Meldung bei mir.

APPENDIX

German abstract/Deutsche Zusammenfassung

Baculovirus-induzierte actin tails

Jan Müller

Diese Arbeit beschreibt meine Forschung der letzten eineinhalb Jahre in der Arbeitsgruppe von Prof. J. Victor Small am Institut für Molekulare Biotechnologie (IMBA) der Österreichischen Akademie der Wissenschaften. Ziel der Arbeit war es, die strukturelle Organisation des Actin-basierten Antriebssystems aufzuklären. Dafür wurden zwei Ansätze verfolgt: Erstens ein *in vitro* System, das ermöglichte, Actin von Microtubuli ausgehend zu nukleieren. Der zweite Ansatz beschäftigte sich mit den Veränderungen, die Baculovirus, ein Pathogen, das Insekten befällt, im Actinzytoskelett seines Wirten auslöst. Das Ausnützen von Wirtsactin zum Zweck der Fortbewegung ist von mehreren Bakterien und Viren, zum Beispiel *Listeria*, *Rickettsia* und *Vaccinia* bekannt. Diese Pathogene bilden einen Actinschweif – auf Englisch ‚actin comet tail‘ – an ihrer Rückseite aus, von dem sie durch die Wirtszelle befördert werden. Die geringe Größe von Baculoviren, nur etwa 250nm Länge bei 50nm Durchmesser, und ein entsprechend kleinerer Actinschweif ermöglichten ein gänzliches Durchdringen der Probe mit einem Elektronenstrahl und dadurch die Erforschung der Actinstruktur mittels Elektronenmikroskopie. Dafür wurden zwei verschiedene Herangehensweisen gewählt: Zuerst wurden konzentrierte, aufgereinigte Baculoviren mit Actin, dem Arp2/3 Komplex und anderen Actin-regulierenden Proteinen inkubiert und die *in vitro* polymerisierten Actinstrukturen untersucht. Zweitens wurden geeignete Zelllinien wie Fisch-Fibroblasten mit konzentrierten Baculoviren infiziert und die Veränderungen im Zytoskelett *in situ* betrachtet. Fluoreszenzmikroskopie an lebenden Zellen zeigte die Fähigkeit von Baculoviren, viele verschiedene, eukaryotische Zellen in Kultur zu infizieren. Elektronenmikroskopische Aufnahmen der Actinschweife förderten eine sogenannte ‚Fishbone‘-Struktur der ‚comet tails‘ zu Tage, wie sie auch bei *Listeria* und anderen Bakterien in größerem Maßstab beschrieben wurde. Schlussendlich ermöglichte der Einsatz von Elektronentomographie an *in vitro* und *in vivo* polymerisierten Actinkometen die Erstellung von 3D-Modellen. Auf deren Basis werden einige Modelle diskutiert, wie Actin-getriebene Pathogene ihre Antriebsmaschinerie aufbauen.

English abstract

Baculovirus-induced actin tails

Jan Müller

This thesis describes the work I carried out over the last one and a half years as a diploma student in Prof J. Victor Small's lab at the Institute of molecular biotechnology of the Austrian academy of sciences (IMBA). The aim was to elucidate the structural organization of the pushing machineries based on actin filaments, to contribute to an understanding of how actin filament polymerization is harnessed to produce motion. The first part focuses on an *in vitro* system, which allowed observation of actin filaments growing off microtubules. The second part describes our efforts to characterize baculovirus-induced actin tails. Various pathogens, like *Listeria* and *Rickettsia*, as well as *Vaccinia* virus and baculovirus, hijack the actin machinery of cells to propel themselves through the cytoplasm and to move from one cell to another, to propagate their infection. Since baculoviruses are small, around 250 by 50nm in size, the comet tails are correspondingly smaller and filament arrangements more easily resolved by electron microscopy. We used two systems to study the structure of the actin tails: First, an *in vitro* assay, including the isolated virus, Arp2/3 complex, actin and other components. Second, suitable cell types like goldfish fibroblasts and B16 cells were infected with concentrated virus and the tails observed in situ. Fluorescence microscopy enabled us to establish the ability of baculovirus to infect several eukaryotic cell types and analyze new aspects of baculovirus-induced tails. Electron microscopy revealed the 'fishbone'-structure of *in vivo* as well as *in vitro* tails and, finally, electron tomography allowed us to conceive models of how pathogen-induced actin tails are formed.

Curriculum Vitae

Jan Müller

Personal Data

Jan Matthias Müller (Mueller)
Hauerweg 6
2130 Mistelbach
0043 676 9159863
jan.mueller@imba.oeaw.ac.at
Born 24.03.1986 in Vienna, Austria

Education

October 2009 – Present	Diploma work at the Institute of Molecular Biotechnology of the Austrian Academy of Sciences (IMBA) in Vienna in Prof Vic Small's Lab. Work focused on the Actin cytoskeleton structure *in vivo* and using *in vitro* model systems.
January 2009 – July 2009	Research project at the Biochemical department of the University of Leicester in Dr Kayoko Tanaka's lab about proteins involved in meiotic prophase of *S. pombe*
October 2008 – January 2009	Research project at the Biochemical department of the University of Leicester in Dr Mark Pfuhl's group about Structural Analysis of Polycystin-1
October 2008 – May 2009	Erasmus scholarship at the University of Leicester, UK. (Times Higher Education Award UK University of the Year 2008/2009)
August – September 2008	Research project at the Vienna Competence Center in Prof Herbert Strobl's lab about Signal Transduction in Human Dendritic and Langerhans cells
July 2008	Completion of the first part of studies with an average mark of 1,8
September 2005 – June 2008	First part of diploma studies (equivalent to Bachelor) in molecular biology at the University of Vienna
September 2004 – August 2005	Military service in the hospital of Mistelbach
June 2004	A-levels (Matura) with distinction (average mark 1.0)

Conferences

November 22 – November 25 2010	Jan Müller 'Pushing with Actin: New Insights from from Electron Tomography' *International Symposium: 'Protein structure and dynamics – from molecules to assembly'*, Nagoya, Japan. Talk
September 22 – September 25 2010	*UNICA Student Conference 2010: 'Europe through Students' Eyes'*, Rome, Italy. Poster presentation, short talk.
September 15 – September 18 2010	Jan Müller, Edit Urban, Christophe Le Clainche, Taro Ohkawa, Matthew D. Welch, Marie-France Carlier and J. Victor Small. 'Electron Tomography of Baculovirus-induced Actin Comet-Tails'. *International Meeting of the German Society for Cell Biology on Actin Dynamics,* Jena, Germany. Poster presentation
June 1 – July 4 2010	Jan Müller. 'Baculovirus-induced Actin Comet-Tails in vitro'. *Workshop on 'Cellular Morphogenesis: Actin Cytoskeleton and Membrane remodeling'*, Gif-sur-Yvette, France. Short talk
July 7 – July 12 2007	32nd *FEBS Congress 'Molecular Machines'*, Vienna, Austria. Technical assistant

Scientific Experience

Experience in working with viruses, bacteria, yeast and various cell lines using several scientific techniques including Western-, Southern and Northern Blotting, Confocal- and Fluorescence microscopy, FACS, Chromatography techniques, Co-Immunoprecipitation, Electron Microscopy and Tomography (Cryo and Negative Staining)

Skills and Interests

Language skills	German and Polish – Mother tongues English – Fluent French – Intermediate
Hobbies	Plays basketball competitively in the second Austrian league at UKJ Hypo Mistelbach, travelling, reading

Reference

Dr. Kayoko Tanaka
University of Leicester
Department of Biochemistry
Henry Wellcome Building
Lancaster Road, Leicester. LE1 9HN, U.K.
e-mail. kt96@le.ac.uk
Tel. +44 116 229 7126/7025